International Scientific-Technical and Production Journal

The Paton WELDING JOURNAL

March 2010 # 3

English translation of the monthly «Avtomaticheskaya Svarka» (Automatic Welding) journal published in Russian since 1948

Founders: *E.O. Paton Electric Welding Institute of the NAS of Ukraine*
International Association «Welding»

Publisher: *International Association «Welding»*

Address:
E.O. Paton Electric Welding Institute,
International Association «Welding»,
11, Bozhenko str., 03680, Kyiv, Ukraine
Tel.: (38044) 287 67 57
Fax: (38044) 528 04 86
E-mail: journal@paton.kiev.ua
http://www.nas.gov.ua/pwj

State Registration Certificate
KV 4790 of 09.01.2001

Subscriptions:
$324, 12 issues per year,
postage and packaging included.
Back issues available.

CONTENTS

140th anniversary of the birthday

Evgeny Oskarovich Paton

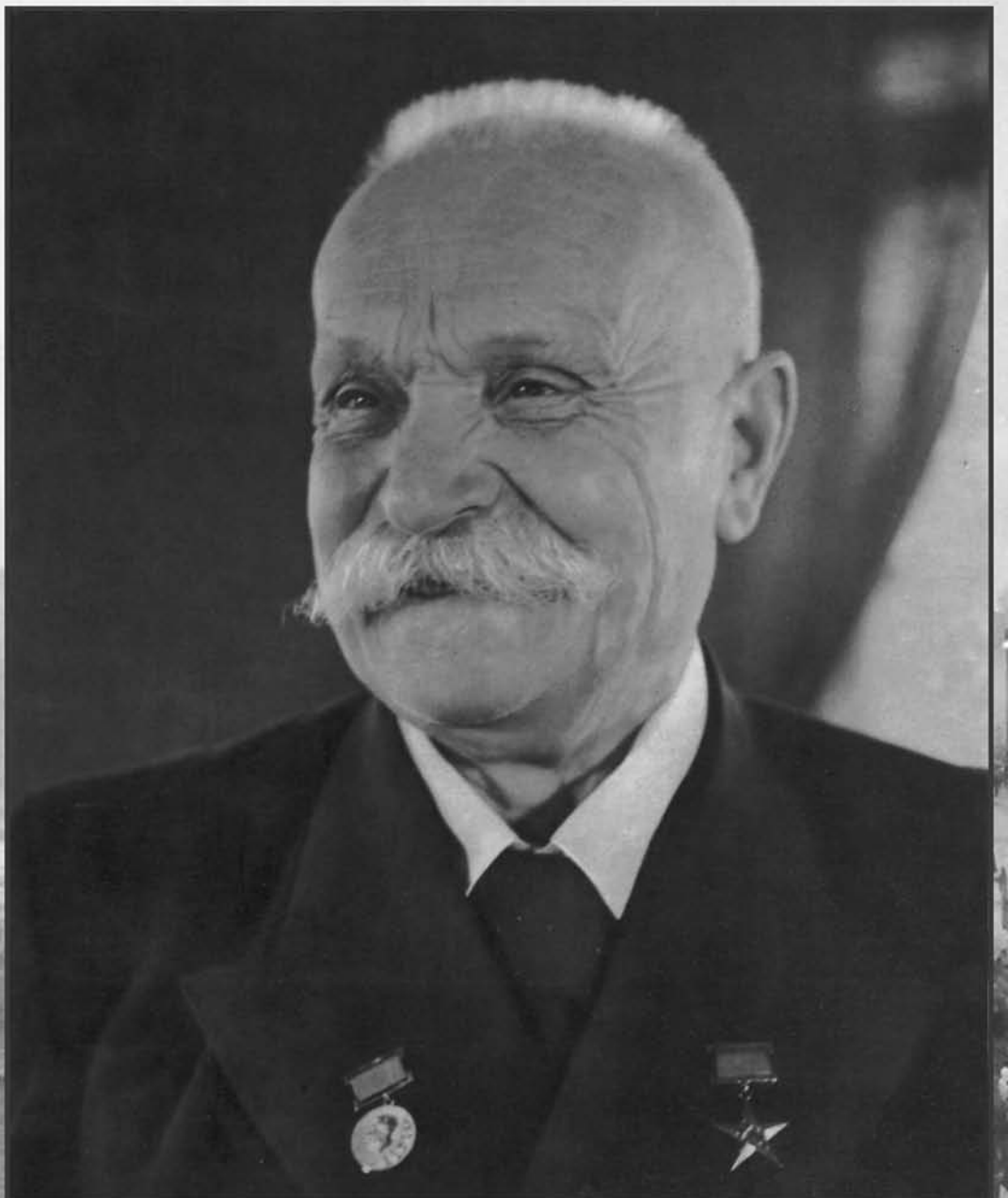

Founder of the Electric Welding Institute

E.O. PATON — OUTSTANDING SCIENTIST, TEACHER AND ORGANISER OF SCIENCE AND MANUFACTURING (140th anniversary of the birthday)

Evgeny Oskarovich Paton was born on the 5th of March 1870 in Nice (France) in the family of the Russian consul. He received his secondary education in a gymnasium in Breslau (Germany), where along with a fundamental training in exact sciences he also acquired a perfect knowledge of the German, French and English languages. In 1888 he entered the Engineering Department of the Royal Saxon School of Technology of Dresden (now the Dresden Polytechnic Institute), which he brilliantly finished in 1894. After the graduation, he was offered a post of a junior member of the research staff of the Institute. But, brought up by the family in the patriotic spirit, the young engineer firmly resolved to devote himself to serving his Motherland, and in 1895 he moved forever to Russia.

To have the right for engineering activity in Russia, in that same year E.O. Paton entered the fifth year of the St. Petersburg Road Engineers Institute, within eight months passed 12 exams, completed several projects, and already in May 1896 received the diploma of a Russian engineer. Upon graduating from the Institute, Evgeny Paton started working as a scientific assistant under the supervision of Prof. F.S. Yasinsky at the Institute and at the Technical Department of Track Maintenance of the Nikolaevskaya Railroad Administration. The talented professor had a great and beneficial influence on the young specialist. Next year, 1897, Evgeny Paton started his teaching work at the just arranged Moscow Engineering School of Communications. Here he met professors L.D. Proskuryakov, L.F. Nikolai, N.A. Belelyubsky and M.N. Gersevanov, the joint work with whom exerted a beneficial effect on formation of the young scientist.

In the age of 31 he defended his thesis, received the degree of a junior scientific assistant and was appointed a professor of the School. Evgeny Paton devoted seven years of his life to the Moscow Engineering School of Communications. During those years he worked out his own teaching principles, and commenced his many years' work on writing manuals and preparing teaching aids on bridge construction. He developed a very strict order of day for himself, beginning at 6 a.m., and meticulously followed it all his life.

E.O. Paton was continuously working at self-improvement, thoroughly prepared his lectures, and was very exacting and demanding to students. He tensely worked on development of the courses of bridges, carefully processed a large amount of reference sources, and verified and checked designs over and over again. Two volumes of manuals on railway bridges, and examples of designs of wood, iron and stone bridges were published within a short space of time. The name of E.O. Paton — a young bridge construction professor — became widely known, and his books were quickly sold out.

In 1904, the young professor was invited to run the Chair of Bridges at the Kiev Polytechnic Institute (KPI). Soon Evgeny Paton was elected a dean of the Engineering Department of the Institute. He leaped vigorously into foundation of a museum and laboratory of bridges with a special library. In addition to teaching, Evgeny Paton gave much consideration to writing of manuals, designing and constructing of bridges. The Mukhransky bridge in Tbilisi, two bridges across the Ros River, the Kiev Footbridge over the Petrovskaya alley, ceilings of the KPI halls and «Metropol» hotel in Moscow, etc. were built under his leadership.

During the First World War, Evgeny Oskarovich energetically started designing bridges by an assignment of the Military Department. He developed an original design of sectional bridges, called the Paton bridges, which found wide application for the military needs.

In 1918 Evgeny Paton published the «Restoration of Bridges» manual, and worked on designs of new bridges. In 1920 he founded the Kiev Bridge Testing Station at the People's Commissariat of Communications, and was running it for ten years. About 150 bridges of dif-

ferent systems in Ukraine, Belarus, Volga region and Kazakhstan were inspected and tested under his leadership and with his personal participation during those years. E.O. Paton collected extensive factual data, which he used in his teaching and design work.

In 1920, the White Poles, while retreating, blew up a very beautiful structure — the chain bridge across the Dnieper River in Kiev. In 1922, E.O. Paton undertook to restore the bridge, contributing all his indomitable energy to that deed. Evgeny Oskarovich was not only the author of the original design, but also an organiser of the building activity. Owing to his inventiveness, ability to resolve the most complicated problems and persistently overcome difficulties, the bridge named after Evgeniya Bosh started functioning in June 1925.

In 1925–1929, E.O. Paton was intensively working on designs of new bridges. He participated in All-Union and international competitions, justly winning appreciations and first prizes. As a whole, Evgeny Oskarovich devoted 35 years of his scientific, engineering and teaching activities to bridge construction, designed 40 bridges, and published over 160 studies dedicated to various aspects of bridge construction. Many of his students became famous scientists, engineers and production managers. His election a full member (academician) of the All-Ukrainian Academy of Sciences (VUAN) in 1929 was well deserved. E.O. Paton with a good reason is considered the founder of the bridge construction school in Ukraine.

Much success had been achieved by that time in design of iron bridges, but the process of their construction remained very labour-consuming and imperfect. That prompted him to look for new technologies. While preparing a new edition of the «Iron Bridges» manual, Evgeny Oskarovich included into it a section on the use of welding for construction of bridges.

He saw the ways of radically improving fabrication of bridge spans in a new method for joining metals, i.e. electric welding. And E.O. Paton made a bold and far-sighted decision — to study welding by involving the fundamentals of metallurgy, metal science, electrical engineering and physics, i.e. new issues for a bridge constructor.

He had to start out of nowhere: no equipment, no qualified people and no premises were available. Four workers and three rooms in basement — this is what the electric welding laboratory of VUAN was initially. Then the Electric Welding Committee was founded on a voluntary basis at VUAN, where E.O. Paton was the organiser and permanent chairman. The intensive work was deployed on this spare base, aimed at investigation of strength of welded structures, popularisation and application of electric welding in manufacturing, transport and building. At that early stage E.O. Paton put forward an idea of establishing a specialised research institution to address all the problems arising in development of the welding industry. The Presidium of VUAN approved establishment of such an institution in 1933, and on the 3rd of January 1934 the official status of the Electric Welding Institute was determined by a resolution of the Government.

From the very beginning E.O. Paton provided for such an organisational structure of the Institute that should consist of research and experimental production departments, design bureau and workshops. That was the origin of the world-first specialised welding research and engineering centre, the activities of which, in contrast to classical academic organisations, were not limited to conducting purely fundamental research, but from the very outset were aimed at finding end-to-end solutions for real problems of the national economy: from in-depth theoretical research to commercial application of the research and development results.

The Institute was widening the area of research. First of all, the comprehensive investigations were conducted to study welded structures, their strength under various service conditions, stresses and strains.

Unlike the majority of the research efforts in the Western Europe, which were conducted on small laboratory-scale samples (which is much simpler and less expensive), the Electric Welding Institute tried to carry out experiments on welded assemblies, beams and girders close to the full-scale ones. That required building of big testing facilities, but, in return, gave more accurate and reliable results.

Investigations of welded structures conducted by the Institute immediately attracted much attention and were positively assessed.

The second important area of research appeared soon — mechanisation and automation of arc welding. Based on a wide life, scientific and industrial experience, E.O. Paton came to

a conclusion that success in a new cause could be achieved only through making a very difficult, but essential step — mechanisation and automation of welding, replacement of a hand and skill of an electric welding operator by an automatic welding device. This task is still of high importance.

The targeted fundamental research launched by E.O. Paton and his disciples became a theoretical base of the welding science and transformed it into a powerful source of technical progress, which led to revolutionary fulfilments in many industries. Monographs and articles of associates of the Institute also contributed to that. A demand arose for qualified welding engineers, and in 1935 Evgeny Oskarovich arranged a Welding Chair at the Kiev Polytechnic Institute.

In the pre-war years the Electric Welding Institute was active in development of reliable equipment for automatic open-arc welding. However, manual welders-stakhanovites first left behind sophisticated and expensive automatic arc welding devices both in the quality of welding and productivity. By comprehensively studying the problem and concentrating the scientific potential of the Institute, together with the Institute's team, Evgeny Oskarovich developed a new method for submerged-arc welding. It provided a several times increase in productivity and dramatic improvement of the quality of the welds. Submerged-arc welding became a commercially reliable and economically advantageous process, and was widely recognised as early as in 1940. To externsively apply the new method, it was necessary to develop automatic devices, fluxes and wires, and arrange their production within the shortest possible period.

Evgeny Paton requested assistance from the Government. At the end of 1940 he was summoned to Moscow. As a result, the resolution on wide application of submerged-arc welding was prepared and then approved by the Government in a short space of time. The resolution provided for introduction of the new method at 20 largest factories, arrangement of production of the required equipment, fluxes and wire, and expansion of the Electric Welding Institute. E.O. Paton was appointed the State Councillor and a member of the Board for Machine Building at the USSR Council of People's Commissars. The resolution became a historical event in development of the Soviet welding technology.

In March 1941, E.O. Paton was awarded the Stalin Prize of the USSR of the first degree for the development of the method and equipment for high-speed submerged-arc welding. An enormous energy of E.O. Paton and of the entire team of the Electric Welding Institute ensured successful implementation of the resolution of the Government. The scales of application of submerged-arc welding were rapidly growing.

The Great Patriotic War that began on the 22nd of June 1941 was a real ordeal for the entire Soviet Union.

The Academy of Sciences of the Ukrainian SSR and most of its institutes were evacuated to Ufa. E.O. Paton requested the Evacuation Commission to evacuate the Electric Welding Institute to the Urals. The Institute moved to the Urals Wagon Building Factory (Uralvagonzavod) in Nizhny Tagil, which became an arsenal of weapon and ammunition for the front. At the urgent request of E.O. Paton, the Institute took a direct part in arrangement of manufacture of armoured tank bodies by focusing its efforts on application of submerged-arc welding in production of weapon and ammunition.

The activity of E.O. Paton during the war years was especially fruitful. Under the most difficult conditions he deployed the exploration and design work aimed mainly at development of high-speed automatic welding of amour steels to manufacture the armoured bodies of tanks. Under severe condition of the war time, associates of the Institute led by E.O. Paton were the first in the world to solve the most complicated scientific and technical problems associated with automatic welding of armour: they elaborated the reliable technology (V.I. Dyatlov, T.M. Slutskaya, B.I. Ivanov), investigated the processes occurring in the high-power welding arc burning under a flux (A.M. Makara, B.E. Paton), and developed new welding fluxes.

The output of tanks was arranged within the record-breaking terms at the Factory, and the first threatening machines T-34 went out from its gates in January 1942.

At the end of 1942, the Institute developed automatic devices with a constant wire feed speed. The principle of self-adjustment of the welding arc underlying these automatic devices made it possible to simplify design and facilitate manufacture and maintenance of the automatic devices, as well as widen their capabilities in application. In addition to the tank manufac-

turing plants, the Electric Welding Institute introduced automatic welding at other defence enterprises as well. Line production of high-explosive air bombs, missiles for Katyushas, as well as other weapon and ammunition for the needs of the front by using high-speed automatic submerged-arc welding was arranged for the first time in the world. By the end of 1944, automatic submerged-arc welding had been applied at 52 factories.

Evgeny Oskarovich and a number of associates of the Institute were awarded the orders of the USSR for successful application of automatic submerged-arc welding in industry.

On the 2nd of March 1943, E.O. Paton, the first of the Ukrainian academicians, was awarded the title of the Hero of Socialist Labour of the USSR for the outstanding achievements in ensuring a rapid manufacture of tanks.

In summer 1944, Evgeny Oskarovich returned to his home city Kiev liberated from fascist occupants by the Soviet Army.

That was the beginning of the second life of the Electric Welding Institute. The Institute was given a building in Gorky Street.

The war years hardened and strengthened the team of the Institute, which retained its capacity and enthusiasm for work. By using developments of the Urals period, before the end of 1945 the Institute introduced automatic submerged-arc welding at 12 major enterprises. In that year the Institute was named after its founder and leader.

The Institute was rapidly growing and developing under the leadership of E.O. Paton. Profound scientific investigations were expanded, multiple developments appeared, books and monographs on various problems of welding were published.

The range of issues addressed by Evgeny Oskarovich in those years was continuously widening. New and new social and state responsibilities were added to his duties on managing the Institute. Evgeny Paton was elected a Vice President of the Academy of Sciences of the Ukrainian SSR, giving up much effort to its activities. He was twice elected a Deputy of the Supreme Soviet of the USSR. E.O. Paton actively participated in addressing the state matters, and gave much concern to his voters. The high authority and reputation of Evgeny Oskarovich and of the Institute he headed were continuously growing not only in the USSR, but also abroad. The Electric Welding Institute by right took up a leading position in the world among research institutions involved in welding. None of the countries, even such a rich and developed country as the USA, had such a research and development centre.

Welded bridges remained a subject that was particularly close to Evgeny Oskarovich. Despite a very busy schedule, he never stopped dealing with them by developing and realising the ideas hatched out for many years.

The acme of many years' activities of Evgeny Paton was construction of the all-welded road bridge across the Dnieper River in Kiev instead of the Evgeniya Bosh Bridge ruined in the war time. He did not live only about three months to see realisation of his dream. The grand opening of the bridge named after E.O. Paton took place on the 5th of November 1953. The bridge is a structure with a long span, all its elements welded with the automatic devices being joined on site by using automatic submerged-arc welding. The E.O. Paton Bridge is still one of the biggest all-welded bridges in the world. The fiftieth anniversary of the Bridge was celebrated in 2003.

Evgeny Oskarovich Paton lived a long life filled up with continuous and incessant creative work. He had a rare diligence and extraordinary energy. The major part of his life he was busy working for 12–14 hours a day.

The contribution of E.O. Paton to the scientific and technical progress, training of engineering staff and formation of the scientific school was marked with the orders of the Russian Empire and orders of the USSR, namely: order of St. Stanislav, order of St. Anna, two orders of Lenin, Gold Star of the Hero of the Socialist Labour, two orders of the Red Banner of Labour, order of the Patriotic War of the 1st Degree, and order of the Red Star. He was awarded the title of the Honoured Scientist.

Editorial Board

PECULIARITIES OF FLASH BUTT WELDING OF HIGH-STRENGTH ALUMINIUM ALLOY 2219

S.I. KUCHUK-YATSENKO, P.N. CHVERTKO, L.A. SEMYONOV, S.M. SAMOTRYASOV and **K.V. GUSHCHIN**
E.O. Paton Electric Welding Institute, NASU, Kiev, Ukraine

Peculiarities of flash butt welding of high-strength heat-hardening alloy 2219 were studied. It was shown that welded joint have no defects of the type of oxide films and delaminations. Optimal conditions for heating of the plastic deformation zone in upsetting were determined. A 15–20 % weakening of the heat-affected zone in the welded joints can be fully eliminated by postweld heat treatment (hardening and subsequent artificial ageing). Tensile strength of the welded joints is at a level of 93–95 % of that of the base metal.

Keywords: *flash butt welding, high-strength aluminium alloy, heating, defects of joints, mechanical properties, weakening, heat treatment of joints*

High-strength aluminium-base alloys have found wide application in aerospace engineering for manufacture of different-purpose parts and structures used in aircraft. In particular, many load-carrying elements of structures are produced from high-strength heat-hardening alloy 2219 of the Al–Cu alloying system. They are manufactured by using various welding methods (arc, electron beam, flash butt, friction, etc.), which determine to a considerable degree the welded joint performance [1].

Continuous flash butt welding is one of the most economically and technically viable methods for manufacture of straight-lined and annular billets. This method provides a high and consistent quality of the joints, combines assembly and welding operations in one cycle, and requires no consumables (electrodes, wires, fluxes, shielding gases, etc.) [2].

In this connection, it was of interest to study weldability of high-strength aluminium alloy 2219 in continuous flash butt welding, degree of weakening of the joints and probability of formation of defects in them.

Investigations and development of the technology for continuous flash butt welding of parts of alloy 2219 (composition, wt.%: 6.45 Cu, 0.31 Mn, 0.14 Zr) were carried out on samples with a cross section of 20 × 100 mm in the T851 state (hardening, cold deformation and artificial ageing). It was taken into account that in continuous flash butt welding of parts of aluminium-base alloys the joints are usually formed during upsetting (Figure 1). Considering thermal-physical properties of this alloy and its thickness, resistance preheating was used prior to continuous flashing to achieve optimal heating of the plastic deformation zone in upsetting.

High sensitivity of alloy 2219 to thermal cycles required that comprehensive investigations be performed to identify heating parameters to be used in welding.

Optimal conditions of formation of a welded joint in upsetting can be created provided that the material to be welded has equal yield stress and tensile strength values in the deformation zone. In this case, the resulting welded joints have minimal internal stresses and are free from cracks or other defects.

In flash butt welding with formation, the intensive deformation zone is almost equal to the upsetting allowance. Mechanical characteristics (tensile strength σ_t and yield stress σ_y) of alloy 2219 at increased temperatures were studied to identify optimal heating prior to upsetting (Figure 2).

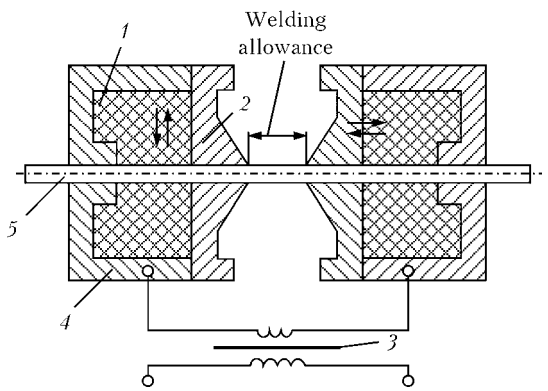

Figure 1. Flow diagram of the continuous flash butt welding process: *1* — heat-insulating insert; *2* — forming knives; *3* — welding transformer; *4* — current conductor; *5* — workpiece

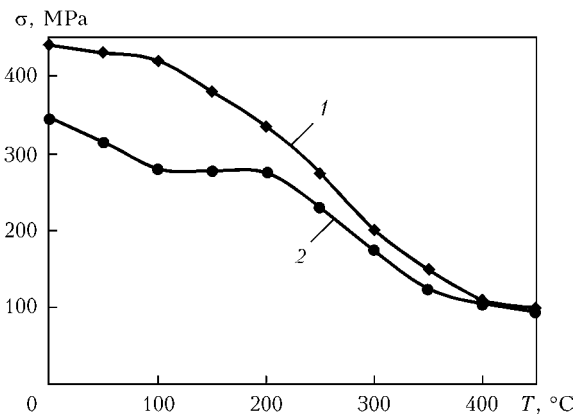

Figure 2. Mechanical properties of alloy 2219 at increased temperatures: *1* — σ_t; *2* — σ_y

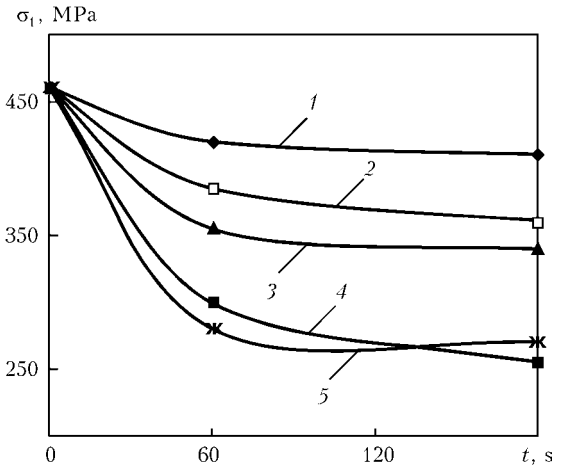

Figure 3. Tensile strength versus heating temperature and holding at this temperature: *1* — 250; *2* — 300; *3* — 350; *4* — 400; *5* — 450 °C

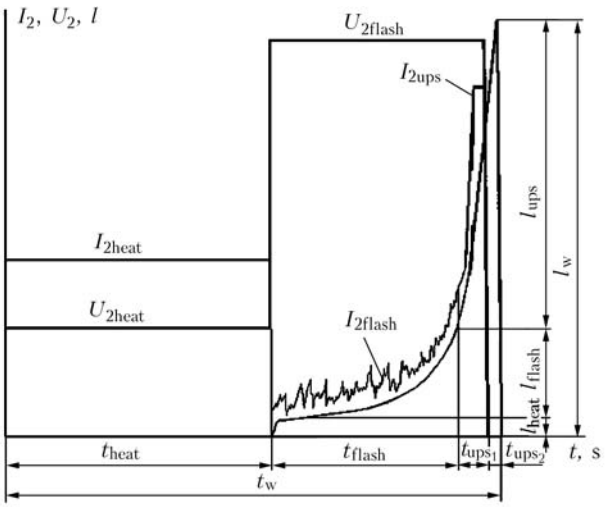

Figure 4. Cyclogram of the flash butt welding process with preheating: I_{2heat}, I_{2flash}, I_{2usp} — current in welding circuit for heating, flashing and upsetting; U_{2heat}, U_{2flash} — voltage in welding circuit for heating and flashing; l_w, l_{heat}, l_{flash}, l_{ups} — welding, heating, flashing and upsetting allowances; t_w, t_{heat}, t_{flash}, t_{ups} — welding, heating, flashing and upsetting times

It can be seen from the Figure that the optimal conditions for deformation can be created at a temperature of about 400 °C. These data allow a conclusion that to produce sound welded joints it is necessary to provide heating of the near-contact zone in the intensive deformation region to a temperature above 400 °C.

The effect of the heating temperature and time of dwelling at this temperature on mechanical properties

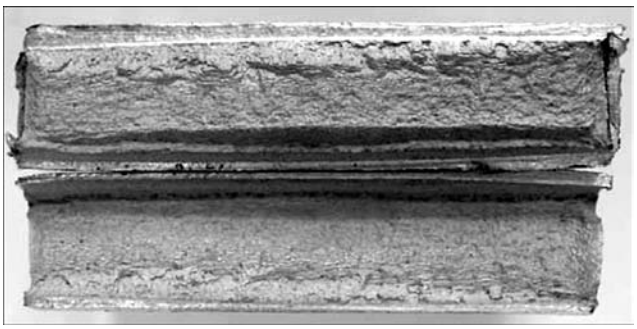

Figure 5. Appearance of fractures in welded samples with notch along the joining line

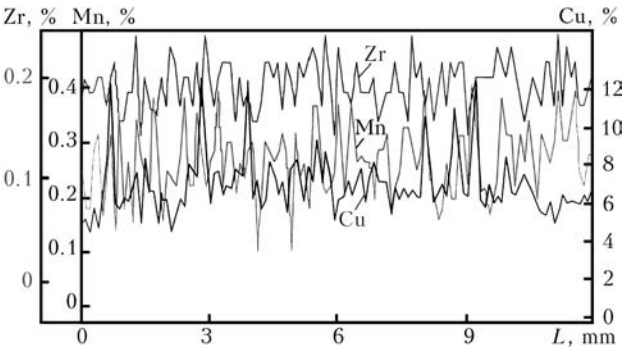

Figure 6. Distribution of alloying elements in welded joint (base metal HAZ–joint–base metal HAZ)

of the alloy was investigated to identify the optimal thermal cycle of flash butt welding.

The base metal samples were resistance heated in a laboratory welding machine to a preset temperature and held for a certain time. After heating, holding at the preset temperature and air cooling, the samples were subjected to tensile tests (Figure 3).

Analysis of the test results shows that mechanical properties of the samples greatly depend upon the heating temperature and time of holding at this temperature. Even a relatively short holding for 20–30 s at a temperature of 400–450 °C leads to a 15–25 % decrease in strength values.

This high sensitivity of the alloy to heating requires that the welding parameters be as rigid as possible, ensuring a minimal heating time. Such parameters provide the sound welded joints (almost without weakening) only on small thicknesses (up to 12 mm). Welding of larger thicknesses at the above parameters fails to ensure the required heating, this leading not only to formation of defects in the welded joints and HAZ metal (e.g. the required deformation in upsetting is not achieved, and probability of formation of oxide films grows), but also to a 20–30 % decrease in the strength values. The above defects can be avoided by increasing the heating time in welding, this causing an increased weakening of the weld and HAZ metals.

In such cases it is necessary to use postweld heat treatment to improve strength of the welded joints.

Welding was performed by using the laboratory flash butt welding machine with a modified secondary

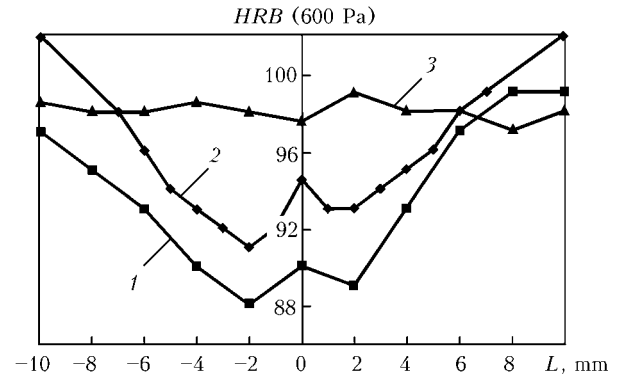

Figure 7. Distribution of hardness in welded joint after welding (*1*), ageing (*2*) and heat treatment (*3*)

Results of mechanical tensile tests of base metal and welded joints before and after heat treatment

Specimens	Mechanical properties			
	$\sigma_{0.2}$, MPa	σ_t, MPa	δ, %	ψ, %
Base metal	339	430.5	11.2	21
Welded joint	200–214 / 208	347.4–350.8 / 350.0	4.7–5.8 / 5.2	13–17 / 14
Welded joint after heat treatment	266–297 / 278	380–422 / 402	4.7–8.4 / 6.4	5.2–15.6 / 8.6

circuit at a power of 75 kV·A under the following conditions: flashing voltage U_{2flash} = 6.5–8.0 V, initial flashing speed — 2 mm/s, final flashing speed — 16 mm/s, welding time t_w — up to 60 s, including flashing time t_{flash} — up to 15 s. Total welding allowance l_w is 60 mm. The process cyclogram is shown in Figure 4.

After welding, part of the samples was heat treated under the following conditions: hardening (heating to 535 °C, holding at this temperature for 2 h, water cooling) and subsequent artificial ageing (heating to 180 °C, holding at this temperature for 24 h).

Fractures of the welded samples with a notch along the joining line exhibit no defects (Figure 5).

Mechanical tensile tests of the base metal and welded joints before and after heat treatment were conducted on flat specimens. Results of the tests are given in the Table.

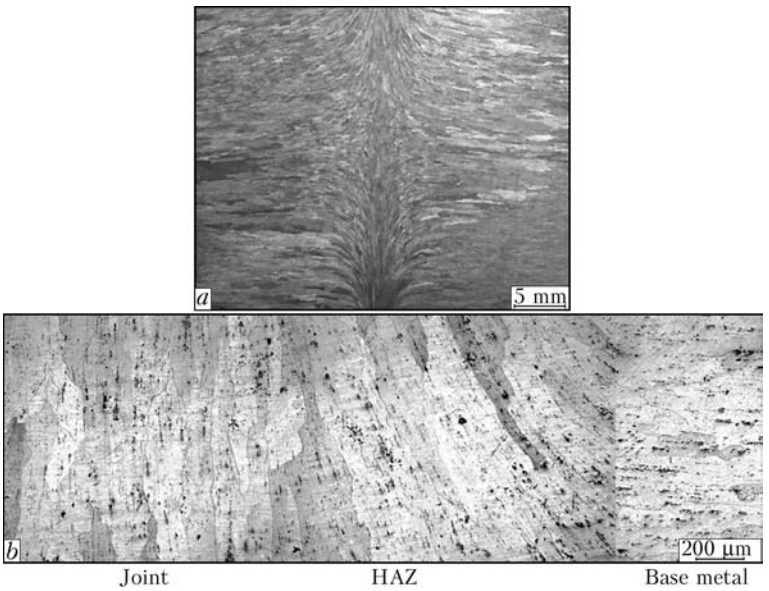

Figure 8. Macrostructure (*a*) and microstructure (*b*) of welded joint after heat treatment

No substantial redistribution of main alloying elements along the joining line and in the HAZ metal is seen in flash butt welding of alloy 2219. In the majority of the welded joint the content of alloying elements is almost identical to that in the base metal (Figure 6).

As shown by the Rockwell hardness measurements, the length of HAZ is 20–25 mm. A considerable decrease in hardness is detected in the joining zone after welding (Figure 7, curve *1*), which is an indirect indication of weakening of this zone. Artificial ageing allowed increasing hardness of the weld and HAZ metals, although leaving the anneal regions located symmetrically about the joining line (Figure 7, curve *2*). Postweld heat treatment performed under the above conditions provides the distribution of hardness in the HAZ metal close to that in the base metal (Figure 7, curve *3*).

Metallographic examinations show that the welded joints are fully free from such defects as oxide films, delaminations, etc. (Figure 8, *a*). Microstructure of the base metal contains different-size oriented grains of solid solution of copper in aluminium. Structure of the alloy also contains intermediate phases formed during the heat treatment process (Figure 8, *b*).

Orientation of grains in the weld metal and adjoining HAZ regions gradually changes by 90° relative to the initial orientation of grains of the base metal, and coincides with orientation of deformation of metal in upsetting. Intermetallic phases are also oriented to a direction of metal flow in upsetting.

CONCLUSIONS

1. The flash butt welded joints on alloy 2219 are free from defects of the type of oxide films, delaminations, etc.

2. The minimal temperature of the deformation zone in alloy 2219 should be about 400 °C. Short-time heating to this temperature within 20–30 s leads to a 15–25 % decrease in strength characteristics.

3. Decrease in hardness accompanied by a 15–20 % weakening takes place in the HAZ metal of the welded joints.

4. Ageing provides increase in hardness of the weld and HAZ metals, leaving the weakening regions.

5. Postweld heat treatment (hardening and subsequent artificial ageing) provides the distribution of hardness close to that in the base metal, as well as strength at a level of 93–95 %.

1. (1984) *Commercial aluminium alloys*: Refer. Book. Ed. by F.I. Kvasov, I.N. Fridlyander. Moscow: Metallurgiya.
2. Kuchuk-Yatsenko, S.I. (1992) *Flash butt welding*. Kiev: Naukova Dumka.

EFFECT OF ELECTRIC PULSE TREATMENT ON RESIDUAL CHANGE IN SHAPE OF THIN-SHEET WELDED STRUCTURES (Review)

L.M. LOBANOV, N.A. PASHCHIN, V.P. LOGINOV and **A.G. POKLYATSKY**
E.O. Paton Electric Welding Institute, NASU, Kiev, Ukraine

It is shown that treatment of thin-sheet welded joints by electric current pulses is an efficient method for regulation of residual deformations of welded structures. With electric pulse treatment of butt welded joints on steel 30KhGSA and aluminium alloy AMg6, the values of sags of plates are decreased from 3 to 9 times. An advantage of this treatment consists in mobility of the equipment used, thus allowing its application for straightening of separate elements of large-sized thin-sheet welded structures, including those in service.

Keywords: *arc welding, high-strength steel, aluminium alloy, welded structures, butt joints, straightening of welded joints, residual change in shape, sagging, preliminary tension, forming, pressing, electroplastic effect, current pulse treatment, plastic deformation*

One of the urgent problems of welding manufacturing is need in regulation of residual change in shape of welded structures. In manufacture of new types of structures the advanced consumables and welding technologies are applied, for which the conventional methods of providing preset accuracy of manufacture are not always suitable.

The purpose of the present work is generalization of modern conceptions about the ways of control of change in shape of metallic products under the influence of electric current pulses. The possibility of use of such effect for straightening of thin-sheet metallic structures is offered and experimentally checked.

The conventional ways of control of residual change in shape of structures can be divided into thermal and mechanical ones depending on the character of effect on the structure in the process of its welding or postweld treatment.

Nowadays the application of thermal methods of treatment considering the expenses for energy carriers increases greatly the cost of manufacture of metallic structures, especially of large-size bridge [1] and ship hull [2] ones, as well as products of light alloys with high heat conductivity. At the same time the automation of process [3] in combination with modern calculation methods, optimizing heat effect on the structure, allows successful use of this method of treatment in modern production. The mathematic models of heat straightening have been developed for such types of structures as thin-wall shells, shafts [4], ship-building panels [5–7], allowing minimizing the heating of product at maximum efficiency of straightening operation.

In heat treatment by tempering in clamping fixtures [1], based on heating of workpiece together with assembly outfit, the high heat energy is consumed for heating of massive assembly devices, applied for fixation of a workpiece. Taking into account that efficiency of tempering is proportional to specific amount of heat per 1 t of a mass of structure (considering the outfit), the application of different heating schemes for treatment of large-size welded structures becomes not profitable. The compromise solution is local tempering of separate assemblies of welded structure, however it is limited in application and not efficient for the products of metals with high heat conductivity.

The force methods of straightening are based on applying the mechanical loads to the structure at different stages of its manufacture compensating its residual change in shape caused by welding.

The reverse bending is an efficient method of compensation of welding deformations in the products with a relatively small bending rigidity, for example, in welding-in of flanges into thin-sheet shell structures [8]. It complicates the welding technology, but in a number of cases it is the more rational solution than postweld treatment. Here, the application of the above-mentioned method is not rational due to high cost of assembly fixture.

Welding with a preliminary tension is one of methods of reducing the welding deformations of thin-sheet structures, which is used in manufacture of large-size panels of light alloys [9, 10]. Its drawback is high cost of a special equipment for tension of elements being welded.

The main drawbacks of the above described methods of straightening is the high level of power and metal consumption. In this connection the need is appeared in search for the new approaches to the assurance of a preset accuracy of manufacture of welded structures.

The promising approach, characterized by the simplicity of application, low power consumption and not requiring the metal-intensive equipment is the pulsed method of treatment realizing the shock-wave effects applied to metal structures in the process of their manufacture.

Thus, the traditional method of peening of welded joints found its development as far back as the 1980s by application of ultrasonic impact tool [11, 12], possessing large capabilities of control.

Fundamental and applied investigations, carried out since the 1960s [13], allowed stating the abrupt increase in ductility and decrease in metal resistance to deformation due to simultaneous effect of mechanical stresses and electric current of high density. This phenomenon was called electroplasticity [14]. Its practical application has opened the new possibilities for deforming metals and alloys, including refractory metals, and also for improving their properties after mechanical shaping.

This regularity of current effect is differed from the known heat effect, being a basis of an electric contact heating, by the fact that it is manifested only in the metal being deformed, i.e. in specimens under the effect of elastic mechanical stresses [15, 16] or under load of higher than yield strength [17]. In this case, at the moment of current pulse effect the material is characterized by a non-stationary stress-strain state influencing the change in geometric characteristics of part being treated [18].

The common feature of all these methods of pulsed treatment of metals is the supply of high-density currents directly into the zone of metal deforming and localizing the area of current effect. These types of treatment based on electroplastic effect (EPE) are differed from electric contact heating used in drawing and rolling. In advanced technologies of shaping the structural materials the processes of intensification of deforming the semi-products are used by using the non-thermal effect of pulsed current, namely the realization of EPE. Here, the expenses are decreased for heating in operations of forging, stamping and drawing and also the heating of technological fixture is eliminated.

Basing on EPE the technologies of producing super-conducting wires, strips and stamped parts of brittle materials (cast iron, beryllium, rhenium) with a minimum level of technological residual stresses by applying high-density currents in the zones of drawing, rolling, stamping and after pressure treatment of parts are realized [19]. The mentioned methods of shaping the metallic materials have a number of common regularities which should be taken into account in use of electric pulse treatment for straightening of deformations caused by welding.

The results of investigations on electric plastic drawing of structural steels [19] showed that the current effect allows increasing the rate of deformation in drawing. The electric pulse effect on deforming steel 08G2S leads to the increase of homogeneity of fragmented structure of metal, and plastic deforming of metal is manifested at earlier stages of loading at concurrent increase of a volume fraction of a plastic component. This is confirmed by data obtained in electric dynamic treatment under the conditions of an uniaxial tension of specimens of carbon steel and its welded joints [20]. In this case the intensive plastic yielding of metal, which is expressed by the formation of Chernov–Luders bands, began in the elastic region of deformation of specimens.

Results of investigations [19, 21] showed that EPE can be applied for intensification of the process of metal forming in manufacture of parts of vehicles. The current effect makes it also possible to prevent the fatigue cracks and to extend the service life of parts operating at cyclic loading.

The thermal intensification and also the electric contact heating, used in technological operations of forming thin-walled parts of a load-carrying structure and lining of vehicles, have a number of disadvantages, such as high power consumption, high temperature of forming leading to the growth of a grain and deterioration of service characteristics of produced parts, need in post operation heat treatment. These drawbacks are eliminated by using the electric pulse effects during forming. Single- and multi-pulse effect was used at different stages of forming of vehicle parts. Here, the definite level of specific electric power supplied to the semi-product, number of current pulses, degree of preliminary deformation of semi-product and rate of cooling after forming finishing were preset.

It was found that at optimum electric pulse effect the ultimate strength of product material, the fatigue limit and service life are increased without decrease in ductile properties of the material. The electric pulse effect allows in many cases increasing in service life of vehicles by increasing their corrosion resistance. It was determined that the time before the corrosion cracking of specimens of aluminium alloy D16 is 3 times increased, and the rate of corrosion of aluminium alloy AMg3M is reduced by one order. It was found that the electric pulse effect influences the anisotropy of mechanical properties of semi-products for vehicle parts which is taken into account in designing of products of aeronautical engineering.

To study the influence of electric pulse effects on ductile properties of semi-products used for forming of vehicle parts, the specimens were subjected to tensile tests at different degree of relative deformation [22]. It was determined that multiple electric pulse effect in the process of forming leads to 3.5–4 times increase in ductility of alloys at the expense of combined effect of EPE and heat effect. Here, the single effect by current pulses after deformation (instead of post operational heat treatment) contributes to a complete recovery of ductility margin that cannot be attained using traditional furnace heat treatment. The single electric pulse effect before the deformation beginning leads to increase of elongation up to 45 %.

The evaluation of technological capabilities of electric pulse effect in change of shape was made in rolling-out and rolling-up, flanging, sheet bending for

small radii and also in operations of cut-off and bending of profiles, specific for aircraft manufacture, using tension, longitudinal and transverse stretch-wrap forming of a sheet. It was found on the basis of results obtained [22] that the electroplastic effect can be used for intensification of processes of sheet forming of metals and alloys. At different stages of forming it is rational to use the single- and multi-pulse effect at which the definite level of electric power, supplied to the semi-product, and number of current pulses, as well as degree of preliminary semi-product deformation is preset. At optimum electric pulse effect the static strength of product material and fatigue strength without deterioration of its ductile properties are increased in the process of forming, while the level of residual technological stresses of the product is decreased. Specific features of an electric pulse effect were tested on steels of grades 12Kh18N10T, 30KhGSA, titanium alloys VT8, OT4, VT20 and aluminium alloys D16, 1420, V95T, AMg6.

Basing on the analysis of studied processes of shaping the structural steels, the presence of common regularities in them such as change in parameters of technological stresses or plastic deformations due to EPE stimulation under the current pulses effect can be noted. Here, the deforming forces at concurrent increase of ductility of the material treated are decreased.

Coming from works [13–23] on plastic shaping and regulation of stressed state of metals under conditions of current effects, it can be concluded that the technology of shaping on the basis of treatment by current pulses can be realized for straightening of welded structures.

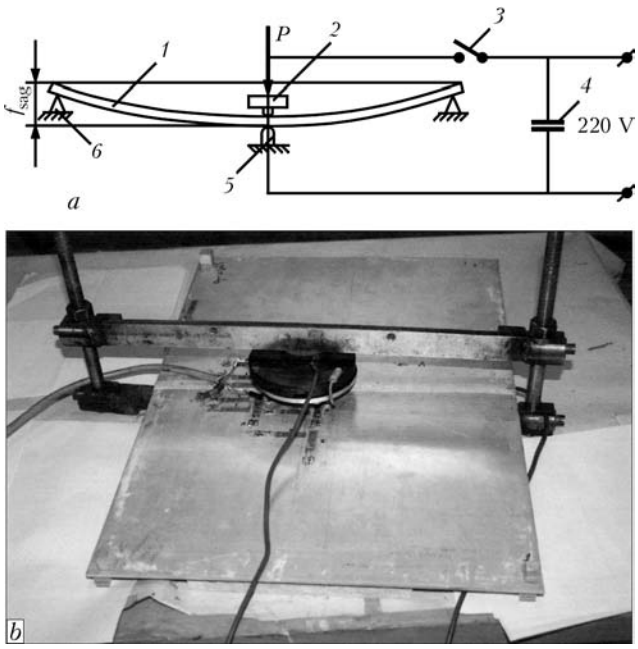

Figure 1. Electric pulse treatment of specimens of welded joints: *a* — scheme of current supply and three-point bending of plates (*1* — specimen; *2* — electrode; *3* — electric switch; *4* — bank of capacitors; *5* — current connector; *6* — support); *b* — specimen of butt joint of alloy AMg6 fixed in a loading device

In treatment of the welded joint by current pulses the elastic component of residual deformation of shaping is transformed into plastic component that has a positive effect on geometric characteristics of metal structures.

The electric pulse treatment can increase the efficiency of such methods of preliminary force effect as the rigid fixing [1] or preliminary elastic tension [9, 10] of elements being welded. At force schemes realized in listed methods of treatment the external loads are applied to the welded structure, at which the treatment of welded joints by current pulses gives the maximum effect. This is due to the EPE realization by transformation of elastic deformations in structure elements into plastic ones in their treatment in fixture. Here, the assembly force contours used for realization of these methods provide geometric characteristics of product, fixed in them, at a sufficient accuracy.

To treat the specimens of welded joints by current pulses, a laboratory equipment was designed and manufactured, where the main element was a bank of capacitors, completed with a charge and discharge devices and also a recording equipment.

List and purpose of devices included into the laboratory equipment, as well as a principle of its operation are described in detail in [23].

The investigations of effect of current pulses on the regulation of residual change in shape of welded joints were carried out on specimens of butt joints of steel 30KhGSA and aluminium alloy AMg6. External loading was realized by the scheme of a three-point bending of plates along the weld line (Figure 1). Sagging of plates f_{sag} was preset to provide the level of preliminary stresses in specimens in the zone of treatment within the 10–30 MPa range. The bending was performed in contact of electrode tip of a capacitor machine with a plate surface. After reaching the preset values of sagging the batteries discharged and then the parameters of treatment condition were recorded and discharge energy was determined. After completion of current pulse effect the changes in geometric characteristics of plates as a result of treatment were defined.

The measure of sagging was made along the longitudinal and transverse edges of welded plates of steel 30KhGSA of 200 × 200 size and 3.5 mm thickness, treated with current pulses. Before the treatment, the initial sags were measured, then a single effect of current pulse at energy $E = 300$ J was made and sagging was measured again. Figure 2, *a, b* shows the change in shape of welded plates after welding and electric pulse treatment. It is seen from the Figure that before the treatment the plate had longitudinal sags of a typical saddle with 4.3–6.5 mm sag at edges and 6.7 mm sag on the weld. After treatment the residual sags along the longitudinal edges 3–5 times decreased (to 1.2–1.3 mm) and on weld — 8–9 times decreased (to 1.1–1.4 mm). Here, the deviations from plane along one diagonal of the plate reached zero values, while along the second diagonal they 2–3 times de-

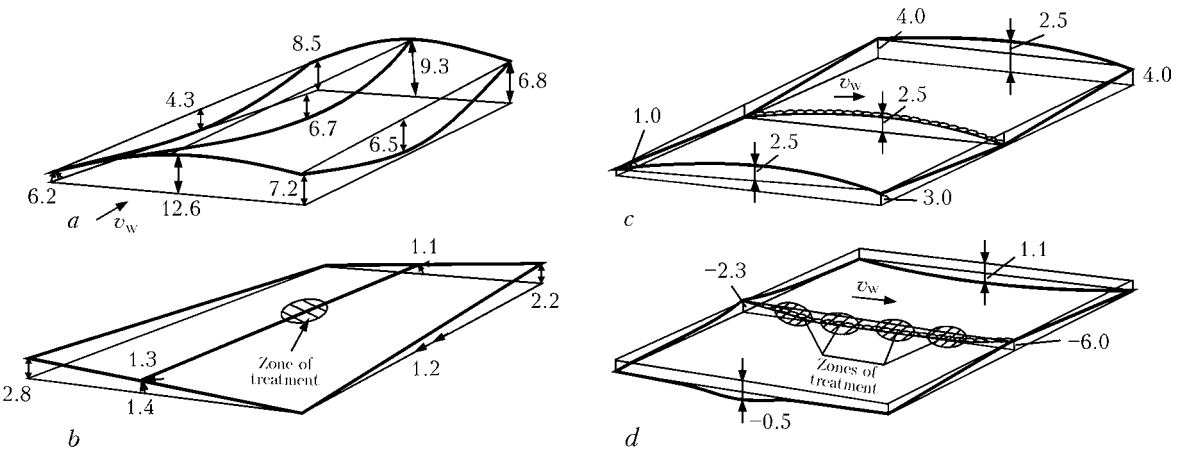

Figure 2. Residual changes in shape of butt joints of steel 30KhGSA (*a, b*) and aluminium alloy AMg6 (*c, d*) after welding (*a, c*) and electric pulse treatment (*b, d*)

creased (from 6.2–6.8 to 2.2–2.8). This proves that maximum effect of treatment due to EPE is attained at that weld area, where the values of residual welding stresses are maximum, that is confirmed by data of works [20] on electric stimulation of low-carbon steel.

To evaluate the efficiency of process of electric pulse treatment, the measurements were made of general sags of plate of alloy AMg6 of 400 × 350 mm size and 4 mm thickness with a butt weld, treated by a series of current pulses consisting of four electric discharges at E = 300 J in the direction from its middle to edges. It is seen from Figure 2, *c, d* that after current pulse effect the sign of sagging is changed for opposite one, and a sag is decreased by 4–5 times (from 2.5 to –0.5 mm). Here, the treatment by a series of current pulses is more effective than by a single electric discharge.

The advantage of electric pulse treatment consists in mobility of used equipment that makes this method suitable for straightening of separate elements of large-size thin-sheet welded structures including also those in service. To perform the electric pulse treatment there is no need in powerful units as the electric discharges of 0.005–1 s are used, and the used element base provides the following operation parameters: pulse current is $I_p \le 10$ kA, voltage is $U_p \le 3$ kV.

Thus, the analysis of advanced technologies of change in shape of metal structures under conditions of electric pulse effect gives premises for application of current pulse treatment for straightening thin-sheet welded structures.

After pulse current treatment of specimens of butt joints of steel 30KhGSA the longitudinal sags along weld decreased by 8–9 times, along the edge — by 3–5 times, the deviation from plane — by 2–3 times.

In treatment of specimens of butt joints of alloy AMg6 by a series of current pulses the values of longitudinal sags along the weld line 4–5 times decreased with a change of sign.

1. Lobanov, L.M., Makhnenko, V.I., Trufyakov, V.I. et al. (1993, 1997) *Welded building structures*. Vol. 1, 2. Kiev: Naukova Dumka.
2. Kuzminov, S.A. (1974) *Welding deformations of ship hull structures*. Leningrad: Sudostroenie.
3. Paton, B.E., Lobanov, L.M., Tsybulkin, G.A. et al. (2003) Automated thermal straightening of welded thin-sheet structures. *The Paton Welding J.*, **7**, 2–6.
4. Makhnenko, O.V., Muzhichenko, A.F. (2007) Mathematical modeling of thermal straightening of cylindrical shells and shafts with distortions along their longitudinal axis. *Ibid.*, **9**, 17–22.
5. Makhnenko, O.V. (2008) Increase of efficiency of thermal straightening of welded thin-sheet structures on basis of mathematical modeling. *Ibid.*, **9**, 6–10.
6. Makhnenko, O.V. (2008) Combined application of thermoplasticity and shrink function methods for examination of thermal straightening of shipbuilding panels. *Matem. Metody ta Fizyko-Mekhanichni Polya*, 51(**4**), 193–201.
7. Makhnenko, O.V., Muzhichenko, A.F., Seyffarth, P. (2009) Application of mathematical modeling in thermal straightening of shipbuilding panels. *The Paton Welding J.*, **1**, 6–11.
8. Lobanov, L.M., Makhnenko, V.I., Velikoivanenko, E.A. et al. (1988) About parameters of preliminary elastic bending as applied to spherical shells. *Avtomatich. Svarka*, **9**, 1–4.
9. Pavlovsky, V.I., Pashchin, N.A. (1988) Regulation of stress-strain state in welding of thin-wall large-size panels of high-strength aluminium alloys. In: *Proc. of 3rd All-Union Symp. on Technological Residual Stresses* (Kutaisi, Sept. 1988). Moscow.
10. Paton, B.E., Utkin, V.F., Lobanov, L.M. et al. (1989) Fabrication of welded large-size thin-wall panels of high-strength aluminium alloys. *Avtomatich. Svarka*, **10**, 10–18.
11. Kravtsov, T.G., Ryzhkov, I.F., Statnikov, E.Sh. (1981) Increase in fatigue resistance of deposited shafts using the ultrasonic treatment. *Ibid.*, **10**, 35–38.
12. Makhnenko, V.I., Kravtsov, T.G. (1986) Thickness of plastically deformed layer in ultrasonic peening of deposited products. *Ibid.*, **8**, 98–110.
13. Spitsyn, V.I., Troitsky, O.A. (1985) *Electroplastic deformation of metal*. Moscow: Nauka.
14. Troitsky, O.A., Rozno, A.G. (1970) Electroplastic deformation of metal. *Fizika Tv. Tela*, 12(**1**), 203–210.
15. Lobanov, L.M., Pashchin, N.A., Loginov, V.P. et al. (2007) Change of the stress-strain state of welded joints of aluminium alloy AMg6 after electrodynamic treatment. *The Paton Welding J.*, **6**, 7–14.
16. Lobanov, L.M., Pashchin, N.A., Loginov, V.P. et al. (2007) Effect of electrodynamic treatment on stressed state of welded joints on steel St3. *Ibid.*, **7**, 6–8.
17. Baranov, Yu.V., Troitsky, O.A., Avramov, Yu.S. et al. (2001) *Physical principles of electropulse and electroplastic treatment and new materials*. Moscow: MGIU.
18. Stepanov, G.V., Babutsky, A.I., Mameev, I.A. (2004) Nonstationary stress-strain state in long rod caused by high density current pulse. *Problemy Prochnosti*, **4**, 60–67.
19. Gromov, V.E. (1992) *Principles of electrostimulation of plasticity of metals and alloys*: Syn. of Thesis for Dr. of Techn. Sci. Degree. Tomsk.
20. Lobanov, L.M., Makhnenko, V.I., Pashchin, N.A. et al. (2007) Features of formation of plastic deformations at electrodynamic treatment of welded joints of St3 steel. *The Paton Welding J.*, **10**, 7–11.
21. Veprev, A.A., Popov, O.V. (1992) Intensification of forming processes under action of pulse electric current. *Aviats. Promyshlennost*, **7**, 9–10.
22. Semashko, N.A., Krupsky, R.F., Kupov, A.V. et al. (2004) Acoustic emission in electric pulse deformation of titanium alloys. *Materialovedenie*, Special Issue, **7**, 29–33.
23. Lobanov, L.M., Pashchin, N.A., Skulsky, V.Yu. et al. (2006) Influence of electrodynamic treatment on the stress-strain state of heat-resistant steels. *The Paton Welding J.*, **5**, 8–11.

STUDY OF RESIDUAL STRESS AND MECHANICAL PROPERTIES OF 2Cr13 STAINLESS STEEL STEAM TURBINE BLADES BY DIFFERENT LASER SURFACE MODIFICATIONS

JIANHUA YAO[1], **LIANG WANG**[1], **QUNLI ZHANG**[1], **ZHIJUN CHEN**[1] and **V.S. KOVALENKO**[2]
[1]Zhejiang University of Technology, Zhejiang, China
[2]Laser Technology Research Institute of the NTUU «Kiev Polytechnic Institute», Kiev, Ukraine

As the key part of steam turbine, the blades work under the impact of high-speed steam and water droplet. Water droplet erosion on the inlet edge area is considered as the common failure pattern. In this paper, three laser surface modification ways including quenching, remelting and alloying were used to avoid water droplet erosion on the 2Cr13 stainless steel turbine blades. Residual stress and mechanical properties of the three modification methods were compared respectively. The result shows that the surface microhardness of blades increases after laser surface modifications. The tensile strength of the material is improved and meanwhile both the elongation percentage and reduction in cross sectional area are decreased. The impact fractures were all brittle fractures. The laser hardening zone presents residual compressive stress, and the heat-affected zone presents small transverse tensile stress.

Keywords: *laser surface modification, turbine blade, residual stress, mechanical properties*

Steam turbine blades are critical components in power plants, which convert the linear motion of high temperature and high pressure steam flowing down a pressure gradient into rotary motion of the turbine shaft [1, 2]. Water droplet erosion is a well-known phenomenon on the moving blades operating at the low-pressure end of steam turbines. It is initiated by «small», primary droplet condensate in bulk of the supercooled steam in the flow, and then gets separated on the blade surface and generates secondary «large» droplets, which causes erosion [3].

To improve the water droplet erosion resistance of low-pressure blades, laser cladding of stellite alloy has been applied, which resulted in generation of residual stresses in the cladding region [4]. The reason is that the difference in thermal expansion between the stellite alloy and parent metal during cooling, thermal strain caused by the differences in heating/cooling at differing locations and the directional stiffness within the sections present [5].

In order to overcome the above disadvantage of high residual stress after laser cladding and to obtain dense bonding hardening layer, laser quenching, laser remelting and laser alloying techniques were introduced to strengthen steam turbine blades and to maintain high surface hardness as well [6, 7]. As a kind of hardenable, chromium stainless steels 2Cr13 combines the superior wear resistance of high carbon alloy with the excellent corrosion resistance of chromium stainless steel. Adding sufficient amounts of carbon to chromium stainless steel, the microstructure of the alloy has the capability to transform into something featured excellent strength, hardness, edge retention, and wear resistance through proper heat treatment (hardening) process. The presence of sufficient chromium will impart the necessary corrosion resistance and form chromium carbide particles to enhance the wear resistance of the given alloy. Due to the virtues mentioned above, 2Cr13 is applied in the area of dental, surgical instruments and nozzles, as well as steam turbine blades.

In this article, the techniques of laser quenching, laser remelting and laser alloying were applied on the 2Cr13 steam turbine blades because of their high surface hardness and low residual stress. Laser quenching is a technology which using the laser heating and self-cooling to complete the quenching processing. Laser remelting is a material surface rapid melting and solidifying processing. By adding alloying material to the substrate surface, laser alloying technique could acquire outstanding surface quality while maintaining the bulk material properties. The three techniques should be applied in different type of blades under different operating environments, substituting for the traditional hardening techniques on blades. Then the blades service life will be extended and the units high efficiency operating will be maintained. The microstructure, microhardness, mechanical properties and residual stress of strengthened layer by different techniques were researched and discussed.

Experimental procedure. The substrate material is 2Cr13 which has been processed by hardening and tempering (heating to 980–1035 °C, followed by quenching in oil, then tempering at 220–300 °C). The chemical composition of the 2Cr13 stainless steel is as follows, wt.%: 0.16–0.21 C; 12 Cr; <1 Si; <0.8 Mn; <0.03 S; <0.04 P; balance — Fe.

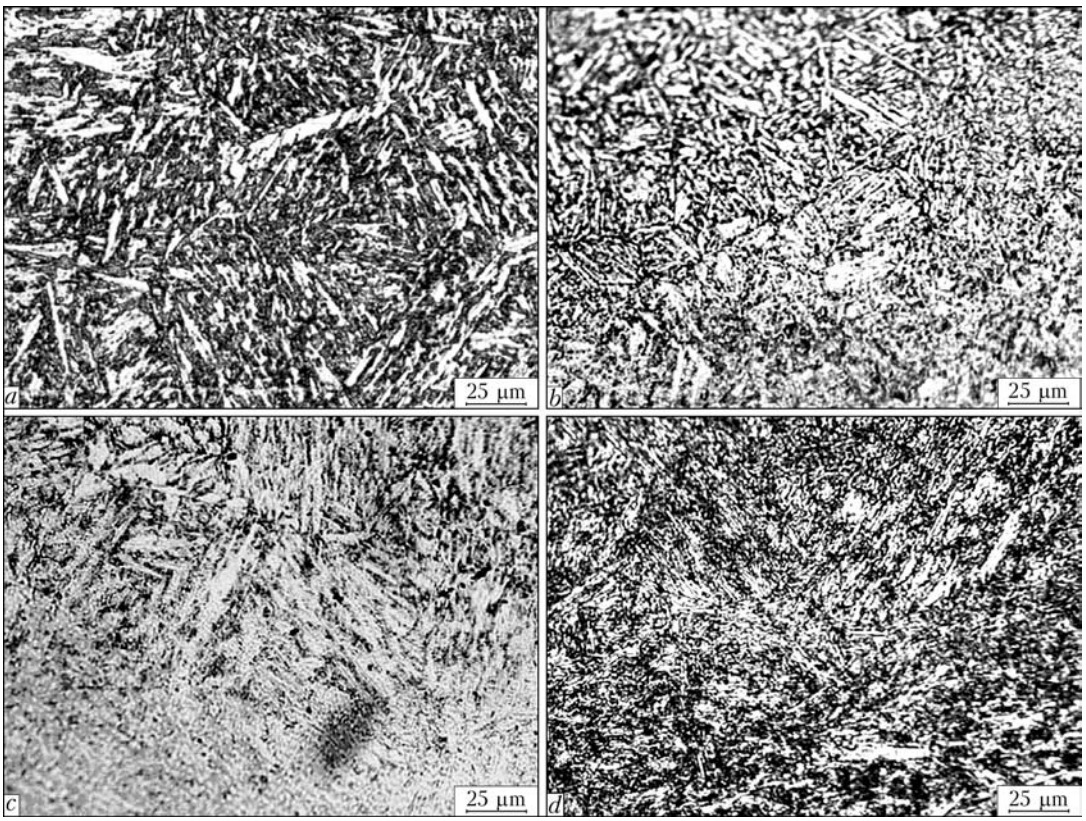

Figure 1. Microstructure of the middle part of laser hardening layer: *a* — substrate; *b* — laser quenching (sample 1); *c* — laser remelting (sample 2); *d* — laser alloying (sample 3)

Figure 1, *a* shows the microstructure of 2Cr13 stainless steel with tempered sorbite. The surface was cleaned by sonication in acetone or alcohol. When the surface of the sample was clean and dry, the alloying powder mixed with some binder was smeared on the surface. The experiments were carried out by a 7 kW rated power CW CO_2 laser system with a CNC controlled working table. Three different optimized laser processing parameters were used to strengthen the 2Cr13 steam turbine blades (Table 1). Samples 1, 2 and 3 were processed by laser quenching, remelting and alloying respectively. The chemical composition of laser surface alloying material for the three samples was as follows, wt.%: 1.3 Si; 2.86 Cr; 3.29 Ni; 0.98 Fe; 40.24 W; 51.33 Co.

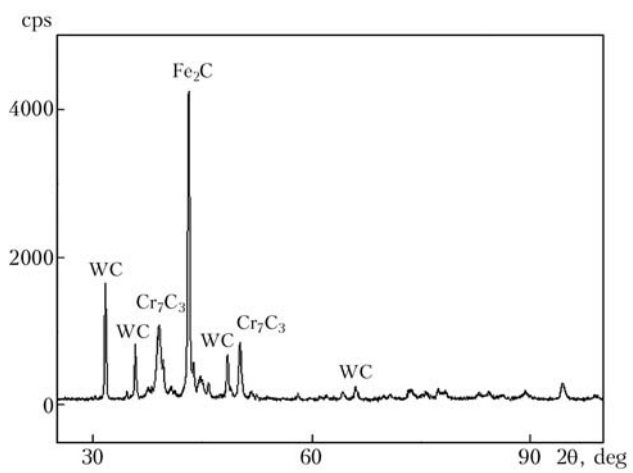

Figure 2. XRD pattern of the top of alloyed layer surface

The mechanical properties were tested by WE-30 hydraulic universal test machine. The microstructure and composition were observed using the FEI-SIRION100 scanning electronic microscope (SEM) equipped with Thermo NORAN energy diffraction spectrometer (EDS). The XRD patterns of the alloyed surface were measured on Thermo SCINTAG X" TRA. The microhardness was tested by the HDX100 microhardness tester with the load of 200 g and the action time of 15 s. The residual stress was tested by X-350A residual stress tester.

Results and discussion. *Microstructure and microhardness*. After laser quenching (sample 1), the fine martensites with staggered distributing are found in strengthened layer (Figure 1, *b*). During the rapid heating and rapid cooling process of laser hardening, the growth of austenite is restrained, and the high degree refined microstructure forms, which results in the increase of the surface hardness. After laser remelting (sample 2), the surface of the remelting layer appears to be as-cast structure, and the martensite in

Table 1. Optimized laser parameters at laser beam size of 2 × × 8 mm^2

Sample No.	Power, kW	Scanning speed, mm/min	Added alloying material
1	1.2	300	No
2	1.6	500	Same
3	1.6	500	Yes

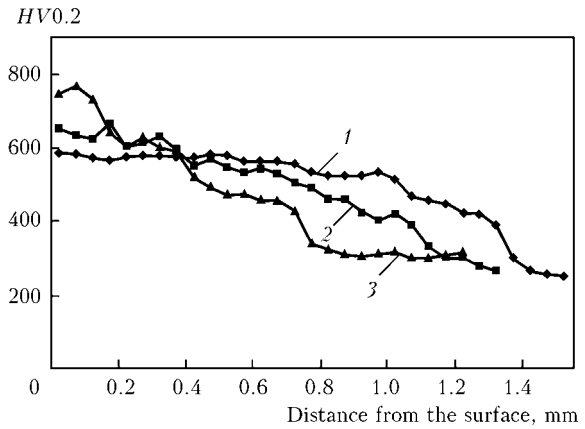

Figure 3. Cross-section hardness after laser hardening of samples 1–3 (*1–3*)

HAZ is bigger than in substrate (Figure 1, *c*). Compared with laser remelting, the microstructure after laser alloying is much finer (Figure 1, *d*). During the laser alloying process, under the high laser power irradiating, the surface of the sample is molten and the alloying materials are fusing into the melting layer simultaneity, which can be proved by the EDS results (wt.%: 0.29 Si; 13.78 Cr; 10.59 W; 0.47 Ni; 0.46 V; 1.32 Mo; Fe and C — balance). According to XRD results (Figure 2) the phases of the alloyed layer include WC, Fe_2C and Cr_7C_3. The highly decentralized WC hard phases will be the main reason for the microhardness improvement (Figure 3). The hardenability of the materials is enhanced because of the existence of chromium. Meanwhile, the hardness is increased due to the formed Cr_7C_3 hard phases. As an element to expand the austenite region, the added nickel prevents the formation of the second-phase particles and improves the surface erosion resistance performance.

Table 2. Tensile test results after laser processing

Sample No.	Tensile strength, MPa	Elongation, %	Reduction in area, %
1	881.51	15.93	39.40
2	860.14	13.88	33.43
3	863.88	13.47	32.77
Substrate	850.65	15.97	41.50

Table 3. Impact test results after laser processing

Sample No.	Impact energy, J	Toughness, J/cm^2
1	37.3	46.67
2	37.4	46.83
3	37.0	46.25
Substrate	37.7	47.08

The cross-section hardness after laser hardening was tested from surface to substrate (see Figure 3). Indicated from this Figure, the thickness of laser quenching layer (sample 1) is about 1.2 mm, the thickness of laser remelting layer (sample 2) is about 0.9 mm, and the thickness of laser alloying layer (sample 3) is about 0.4 mm. The hardness is declined from the surface to substrate with gradient. The hardening layer hardness of sample 1 is lower than that of both sample 2 and sample 3. However, the depth of quenching layer is greater than in sample 2 and sample 3. The lower speed results in thicker heating depth and the finer martensites with staggered distribution are transformed, which is the primary hardening mechanism of laser quenching (see Figure 2). Because of higher laser scanning speed and rapid cooling speed,

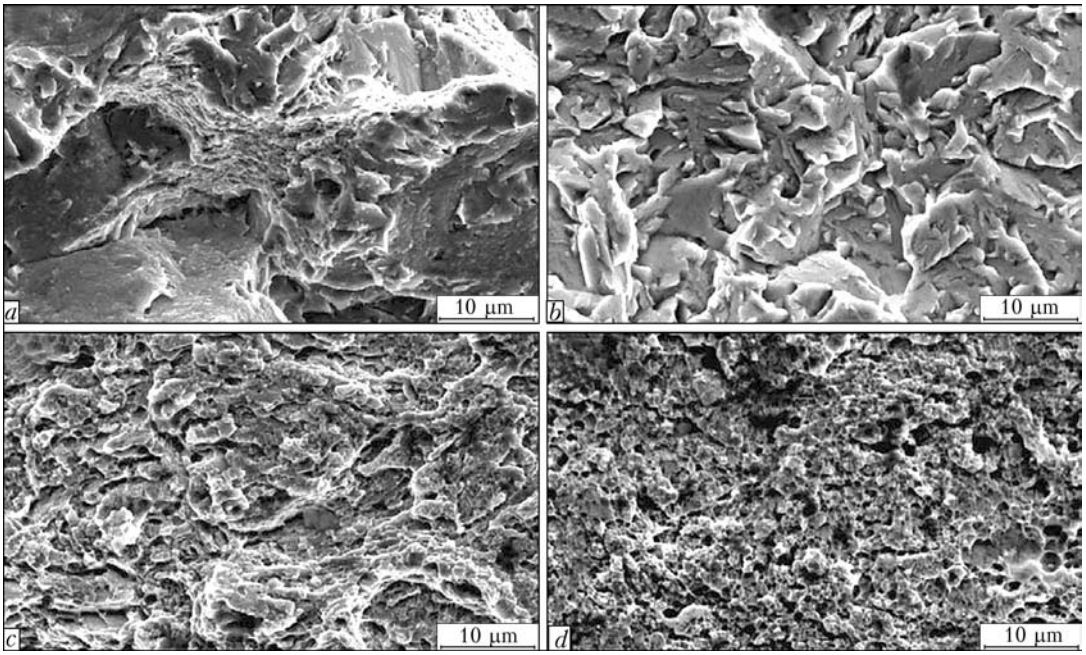

Figure 4. Impact fracture pattern after laser hardening: *a* — substrate; *b* — laser quenching (sample 1); *c* — laser remelting (sample 2); *d* — laser alloying (sample 3)

the hardening layer of sample 2 and 3 is thinner than in sample 1. The largest hardness value is found in sample 3 due to the added alloying material and hardness phases (WC, Fe_2C and Cr_7C_3) after laser processing.

Mechanical properties. The tensile test results after laser processing are shown in Table 2. After laser processing, the tensile strength of the samples are improved, but the elongation and the reduction in cross-sectional area are reduced. After laser quenching (sample 1), the grains are refined, so that the tensile strength improves a little. Compared with the laser quenching technology, laser remelting and alloying need higher laser power density to melt the surface. Because of the as-cast microstructure, the microscopic mechanical properties decline, resulting in the reduction of elongation.

The impact results after laser processing are shown in Table 3. After laser processing, the impact toughness of the samples are all reduced because of the residual stress and brittle martensite after laser radiating.

Figure 4 shows the impact fracture pattern of the substrate and the three samples. The plentiful cleavage planes are found in substrate, but there are partial dimples. After laser quenching (sample 1), the cleavage planes are a bit smaller. The pattern of samples 2 and 3 (after laser remelting and laser alloying) are also cleavage planes. Because of the higher laser power and higher cooling speed, the grains are much finer than those of sample 1, so the cleavage planes are smaller than those of the substrate and sample 1.

Residual stress. Figure 5 shows the sketch map of laser hardening section. The laser hardening section is the convex surface of blades, which section would be suffered a number of water droplets impact in the last-stage of steam turbines. To avoid the integral distortion and reduce the cost, only local section was chosen to strengthen. Residual stress test points of the laser hardening section are also shown in Figure 5. Points *1*, *3–8* are in the laser hardening section, points

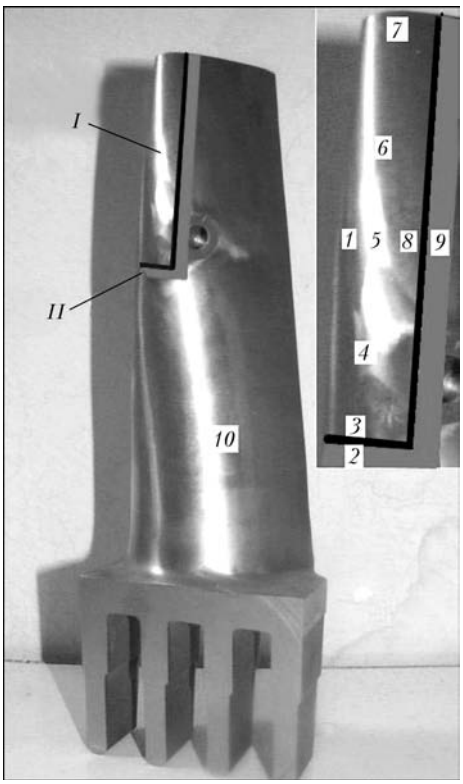

Figure 5. Sketch map of residual stress test points distribution in laser hardening section: *I* — laser strengthening section; *II* — HAZ

2 and *9* — in the HAZ and point *10* — in the substrate for comparison.

The residual stress distributions of the blades after laser quenching and laser alloying are shown in Figure 6, *a*, *b*. The processing parameters of laser remelting is the same with laser alloying, so that the residual stress test result of laser remelting is approximately considered as the same with the laser alloying. The transverse stress and longitudinal stress of original blade surface (see point *10* in Figure 5) are –231 and –212 MPa respectively. The transverse residual stress in HAZ presents tensile stress, and the longitudinal residual compressive stress in HAZ is much lower than in laser processing section (points *2* and *9*). The re-

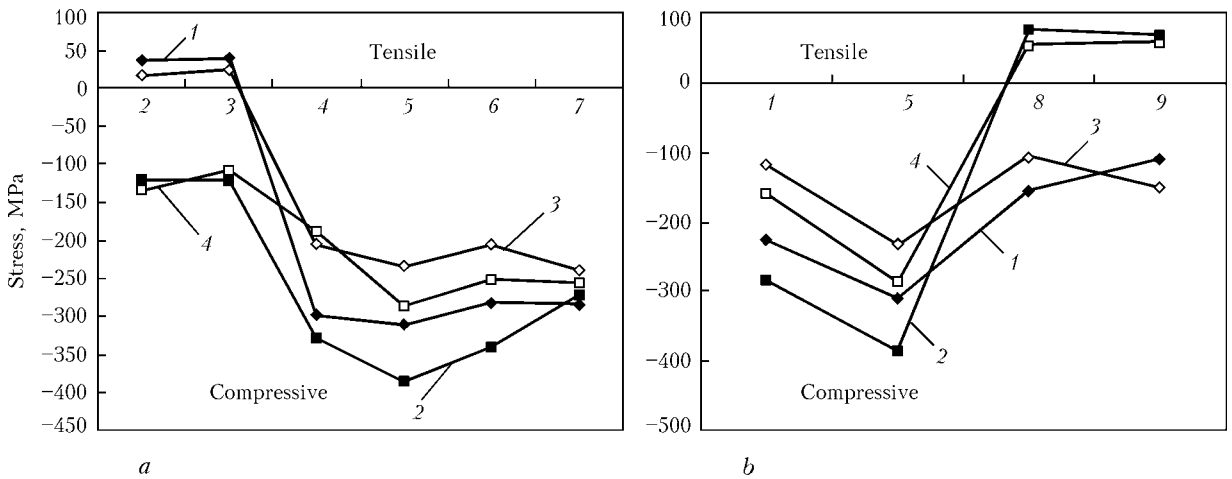

Figure 6. Residual stress distributions of the blades after laser quenching (points *2–7*) (*a*) and laser alloying (points *1, 5, 8, 9*) in transverse (*1, 3*) and longitudinal (*2, 4*) directions

sidual stress state of points *2* and *3* are similar to the points *8* and *9*. These points are all beside the laser scanning initial position with lower laser energy, so the effect of relief annealing under laser lower irradiating energy results in different residual stress state from the section under laser high irradiating energy. The residual stresses in high energy section of laser processing are all present compressive stress. It is obvious that the residual compressive stress after laser alloying is larger than that of laser quenching, whether the transverse direction or longitudinal direction. On the effect of laser fast heating and rapid cooling, the material occurs phase-change, transforming into the martensite during laser quenching processing, which results in the volume expanding. Therefore the material surface presents residual compressive stress. The laser alloying needs higher laser power, so the blade surface processing section is melted. Under the short processing of rapid cooling after laser heating, the molten material is solidified instantly and the original stress state is changed simultaneously [8]. In the practical applications, the appropriate compressive stress is favorable, while the tensile stress will reduce the fatigue life of the blades.

CONCLUSIONS

1. The thickest hardening layer is found after laser quenching, but its hardness is lower than in laser remelting and laser alloying. The martensites with staggered distributing are the main microstructure of strengthened layer after laser quenching. The microstructure in laser remelting is finer than in laser quenching. The laser alloying has the highest hardness (*HV*0.2-780) but thin harden layer. The WC, Fe_2C and Cr_7C_3 are the main hardening phases in the alloyed layer.

2. After three laser techniques processing, the tensile strength of the material is improved and meanwhile both the elongation percentage and reduction in cross sectional area are decreased. The impact resistance of material is not declined after laser hardening. From the impact fracture SEM analysis, the impact fractures of hardening layers are plentiful brittle fractures. With the increasing of laser scanning speed and laser power, the grains of cleavage planes are getting smaller gradually. The smallest grain of cleavage plane is present to the sample of laser alloying.

3. After laser processing, the laser hardening zone presents high residual compressive stress in both directions. But the edge of laser scanning zone and HAZ presents transverse tensile stress and lower longitudinal compressive stress. Compared with the surface residual stress after laser quenching, the residual compressive stress of laser alloying is increased more than 35 %.

The contrast and discussion of the three different laser hardening techniques on steam turbine blades will be the favorable reference to choose proper laser processing technique to harden turbine blades surface.

Acknowledgements. *The authors would like to appreciate financial support from International Cooperation Project of Ministry of Science and Technology (JG-JD-2008001) and the Open Foundation of Provincial Key Discipline of Advanced Manufacturing Technology (AMT200506-009).*

1. Wei-Ze, W., Fu-Zhen, X., Kui-Long, Z. et al. (2006) Failure analysis of the final stage blade in steam turbine. *Mater. Sci. Eng. A*, **437**, 70–74.
2. Mazur, Z., Garcia-Illescas, R., Aguirre-Romano, J. (2008) Steam turbine blade failure analysis. *Eng. Fail. Anal.*, **15**, 129–141.
3. Mann, B.S., Arya, V. (2003) HVOF coating and surface treatment for enhancing droplet erosion resistance of steam turbine blades. *Wear*, **254**, 652–667.
4. Kathuria, Y.P. (2000) Some aspects of laser surface cladding in the turbine industry. *Surf. Coat. Technol.*, **132**, 262–269.
5. Bendeich, P., Alamb, N., Brandt, M. et al. (2006) Residual stress measurements in laser clad repaired low pressure turbine blades for the power industry. *Mater. Sci. Eng. A*, **437**, 70–74.
6. de Camargo, J.A.M., Cornelis, H.J., Cioffi, V.M.O. et al. (2007) Coating residual stress effects on fatigue performance of 7050-T7451 aluminum alloy. *Surf. Coat. Technol.*, **201**, 9448–9455.
7. Borrego, L.P., Pires, J.T.B., Costa, J.M. et al. (2007) Fatigue behaviour of laser repairing welded joints. *Eng. Fail. Anal.*, **14**, 1586–1593.
8. Frenka, A., Marsdena, C.F., Wagnie'rea, J.-D. et al. (1991) Influence of an intermediate layer on the residual stress field in a laser clad. *Surf. Coat. Technol.*, **45**, 435–441.

COMPARATIVE EVALUATION OF METHODS FOR DETERMINATION OF FRACTURE TOUGHNESS OF HAZ METAL OF LOW-ALLOY STEEL WELDED JOINTS

V.S. BUT
E.O. Paton Electric Welding Institute, NASU, Kiev, Ukraine

The article presents results of experimental studies of fracture toughness of the HAZ metal of low-alloy steel welded joints with different schemes of formation of a notch. Currently available methods for preparation of specimens and results of testing them to crack tip opening displacement under three-point loading were evaluated.

Keywords: *manual arc welding, welded joints, fracture toughness, crack tip opening displacement fracture diagram, metallographic examinations, structure, test temperature*

At present, the special consideration in evaluation of performance of critical structures and constructions, pressure vessels and pipelines operating under severe conditions is given to resistance of welded joints to brittle fracture.

As shown in study [1], the key factors leading to formation of brittle fracture of a welded joint include stress concentration caused by a notch (dramatic change in cross section, technological defects of welds and base metal), tensile residual stresses at the notch root, decreased ductile properties in the above region, and low temperature.

Criterion of non-linear fracture mechanics, i.e. the value of crack tip opening displacement (CTOD) δ_c [2] finds an increasingly wide application, along with traditional criteria (impact toughness, fracture character), for evaluation of sensitivity of welded joints to brittle fracture. Quantitatively reflecting fracture resistance of materials and welded joints with crack-like defects of a technological and operational origin, this indicator makes it possible to find values of critical temperatures that separate regions of tough, quasi-brittle and brittle fractures for structural materials. This is of practical importance for the welded joints in view of the probability of local embrittlement of metal in the weld zone and, therefore, the need to limit working temperature ranges by a tough state [3].

Advantages of the crack opening displacement (COD) test method are covered in detail in studies [1–4]. Moreover, welded joints of some repaired structures inevitably contain stress raisers, which may affect not only formation of cold cracks, but also resistance to brittle fracture.

As a rule, embrittlement of metal in welding of structural steels takes place in a coarse-grained region of the heat-affected zone (HAZ). In this connection, evaluation of resistance of welded joints to brittle fracture is usually performed proceeding from the results of tests of the notched specimens within the said zone under three-point slow loading [5].

As proved by the world experience, when using the CTOD method for determination of permissible sizes of crack-like defects in the welded joints, the most reliable results are exhibited by the specimens with incomplete root face penetration (IRFP) in groove of a joint, which are made according to the Japanese procedure [6] (Figure 1, *a*). Welding of such specimens is performed in a special fixture (Figure 1, *b*), which limits angular deformations and allows free deformation to occur in a direction that is transverse to the weld. However, this procedure is labour-consuming. It is meant only for welding with stick electrodes, as it requires that the fusion interface of the multilayer weld be parallel to a slot gap.

Manufacture of specimens and method for making notches, according to study [7], allows using the CTOD procedure for other welding methods as well. In this case, specimens with a V-groove are advantageous over the other ones owing to simplicity and labour intensiveness of their manufacture.

To establish adequacy of the said procedures and correlation of the results, in this study the joints on steels X60 and 17G1S with different groove shapes (Figure 2) were welded under identical welding conditions by using stick electrodes. Chemical compositions of the steels are given in the Table.

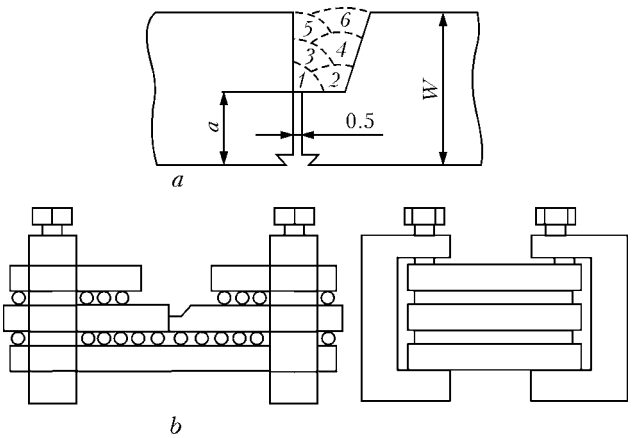

Figure 1. Schematics of welded specimen with IRFP in edge (*a*) and device for its welding (*b*): *1–6* — groove filling sequence

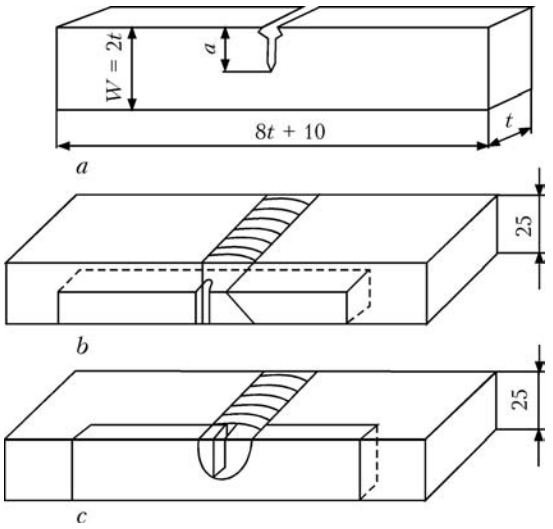

Figure 2. Schematics of specimens cut out from welded joints for CTOD with different shapes of notches

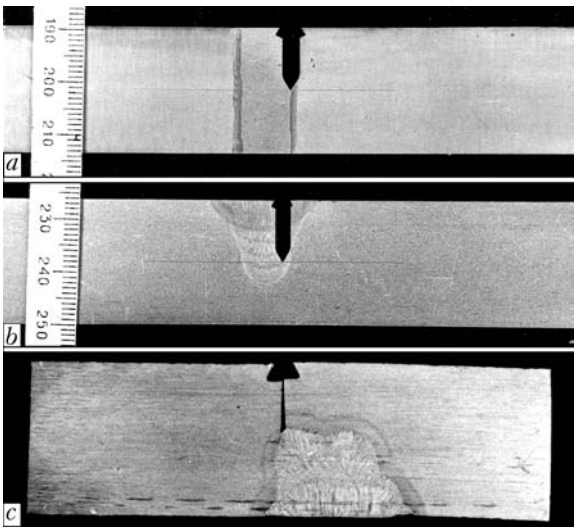

Figure 3. Macrosections with artifical (mechanical) and natural notches in HAZ: *1* — notch located parallel to fusion interface; *b* — notch made at angle to joining interface; *c* — natural notch with IRFP

Notches were made by the mechanical method in the said specimens at an angle normal and parallel to the fusion interface (Figure 2). In all the cases the tip of a notch with a curvature radius of 0.1 mm was located at a distance of 0–0.3 mm from the fusion interface. In addition, specimens with a natural stress raiser, i.e. IRFP in a groove of the welded joint, were also welded. In this case, a gap between the weld edges (Figure 1, *a*) was chosen according to recommendations [7].

Macrosections of welded specimens for the CTOD tests with different schemes of formation of a notch are shown in Figure 3. Specimens with IRFP were bend tested using the same procedure as specimens with mechanical notches according to the recommendations of British Standard BS5762–79 and procedure [8]. In this case, the COD tests were carried out at a controlled and relatively low speed of rise of a load, v_c, by simultaneously fixing it and COD with an X–Y recorder. The tests were ended when the uncontrolled crack propagation was achieved and fracture took place. A set of three specimens of each welded joint at the same temperature was used for the tests. Schematics and sizes of the specimens for evaluation of CTOD are shown in Figure 2, *a*. The CTOD tests are performed by plotting the load–COD diagram. As a rule, the curves obtained correspond to one of the fracture types shown in Figure 4 [9].

Special fixture was made for tests by the CTOD procedure (Figure 5). Main components of the fixture are a load-bearing clamp and clip with a movable load bearing base, this allowing testing of specimens over a wide range of thicknesses (5–30 mm) under three-point loading. Strain gages that monitor the level of loading were attached to the surface of side plates of the load bearing clamp at points of maximal bending stresses formed in loading of a specimen. This increases the sensitivity of a strain gage and provides proportionality on coordinate y in recording the load–COD diagram. Furthermore, placing of the strain gages outside the cooling environment allows extending their service life and improving reliability in multiple tests under low temperature conditions.

Specimens of the said sizes were tested to three-point bending at a controlled loading speed (2 mm/min) and temperature of –30 to –110 °C using the hydraulic machine with a load of 300 kN, equipped with a strain intensifier, adjustable power unit and two-coordinate recording flat-bed potentiometer. A down to –70 °C temperature of the specimens was provided using a petrol solution of carbonic acid snow. Nitrogen vapours were used to cool specimens to a lower temperature. Temperature of the specimens was monitored with chromel-alumel thermocouples and millivoltmeter. Calibration temperature–stress diagram was preliminarily plotted, and temperature of the specimens was controlled during the tests on the basis of this diagram.

Three types of load–COD diagrams, i.e. A, C and E, were fixed during the tests (Figure 4). At a tem-

Chemical composition of steels under investigation

Steel grade	C	Mn	Si	Ni	S	P	V	Nb	Al	C_{eq}
X60	0.12	1.60	0.48	0.20	0.01	0.025	0.08	0.06	0.01	0.42
17G1S	0.18	1.48	0.39	0.10	0.03	0.022	–	–	–	0.43

Note. C_{eq} was determined by using the International Institute of Welding formula.

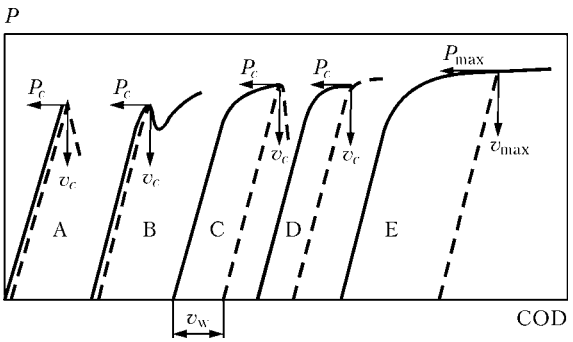

Figure 4. Types of load–COD diagrams: P_c — critical load

perature of −70 °C, specimens with an artificial notch fractured by the C and E type, and specimens with IRFP — by the A type. When temperature was decreased to −90 °C, the 17G1S steel specimens with a mechanical notch fractured by the A type, and the X60 specimens — by the C type. At −110 °C, all the specimens fractured by the A type.

At a temperature increased to −50 °C or higher, specimens with IRFP fractured by the C type. Curves of variation in δ_c for specimens of the investigated steels versus test temperature and type of notch in HAZ were plotted on the basis of minimal values of δ_c (Figure 6). It can be seen from the Figure that the scheme of making a notch by the mechanical method in the coarse-grained region of HAZ does not affect CTOD. Comparative evaluation of brittle fracture resistance of the HAZ metal can and must be performed on specimens made by the simplest and least labour-consuming procedure described in study [7], according to which it is possible to evaluate HAZ of any type of the welded joints produced by different welding methods. Specimens with IRFP have a much lower CTOD value than specimens with an artificial (mechanical) notch tested at a temperature of −70 °C, this value reaching that of the specimens with a notch at a higher (−40 °C) test temperature.

The X60 steel specimens with an artificial notch have a sufficiently high CTOD value (0.22–0.31 mm) within a range of −70 to −80 °C, whereas the 17G1S steel specimens have a much lower CTOD value, $\delta_c \approx$ $\approx$ 0.1 mm at −80 °C. At a temperature decreased to −110 °C, different steel specimens with an artificial notch have almost identical (minimal) CTOD values in HAZ of the welded joints. Using the material evaluation criteria ($\delta_c \approx 0.12$ mm) given in study [8], it can be assumed that the HAZ metal (coarse-grained region) of the X60 steel welded joints will have a brittle fracture at a temperature below −90 °C, and that of the 17G1S welded joints — at a higher temperature (−80 °C). Using the CTOD values obtained on specimens with IRFP, we can see that the temperature range of brittle fracture of the said zone regions is below −60 and −45 °C for steels X60 and 17G1S, respectively.

Comparison of the temperature dependencies of δ_c in HAZ of the welded joints on steels X60 and 17G1S

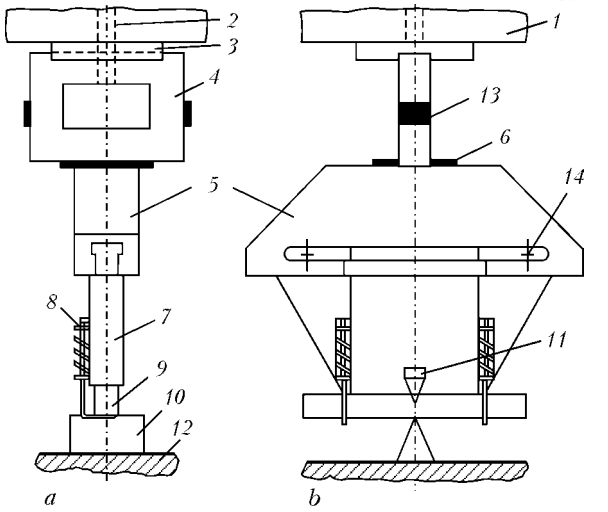

Figure 5. Schematic of fixture for testing specimens by the CTOD procedure: *1* — upper cross-arm; *2* — fixing rod; *3* — bearing foot; *4* — load-bearing clamp; *5* — clip with movable bearings; *6* — heat insulating gasket; *8* — hold-down; *9* — specimen; *10* — fixed bearing; *11* — COD sensor; *12* — testing machine platform; *13* — load sensor; *14* — retainer

(tensile strength 540–600 MPa), derived on specimens with IRFP and artificial notch, showed that for steels of the investigated grades both dependencies corresponded to each other very well. However, the δ_c values of specimens with IRFP were much lower, and the threshold of brittle fracture of HAZ shifted towards the positive temperature by 30–35 °C, compared with specimens with an artificial notch in HAZ. This can be explained by the following reasons. Firstly, tip of a natural notch in specimens with IRFP is on the fusion line, therefore, it should be sharper compared with specimens with the artificial notch; secondly, concentration of plastic strains and residual stresses takes place at the notch tip during welding. Hence, it can be concluded that for an accurate and

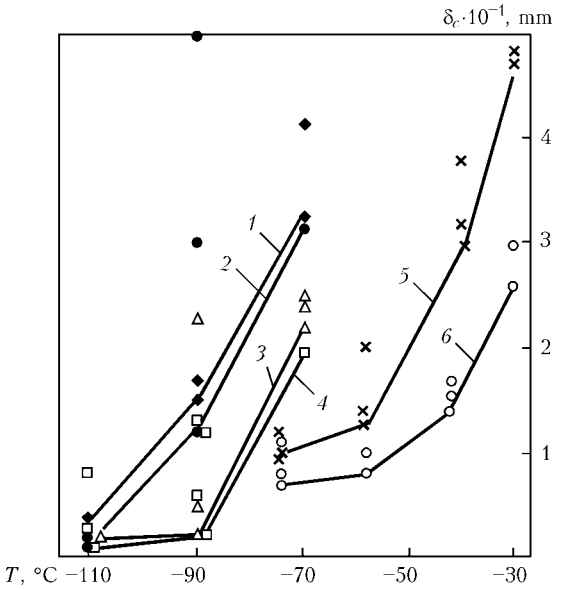

Figure 6. CTOD versus test temperature and notch type in HAZ of X60 (*1, 2, 5*) and 17G1S (*3, 4, 6*) steel specimens: *1, 3* — notch parallel to fusion interface; *2, 4* — notch normal to fusion interface; *5, 6* — specimens with IRFP

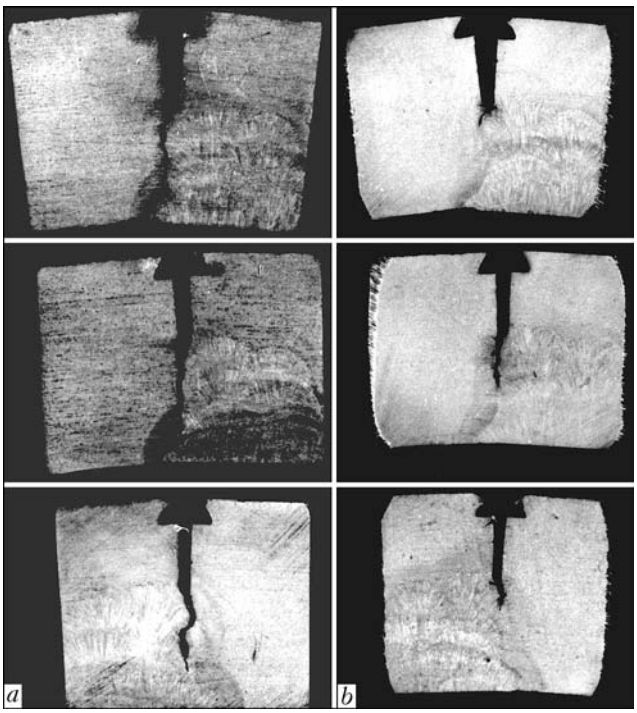

Figure 7. Character of fractures of 17G1S (*a*) and X60 (*b*) steel specimens

reliable evaluation of resistance of a welded joint to brittle fracture the notch tip should be located in a coarse-grained region of HAZ. However, such a notch is hard to make by the mechanical method. Specimens with IRFP make it possible to simply and reliably obtain the required characteristics, as in this case the natural notch tip is located exactly on the fusion interface. The δ_c values of specimens with IRFP can be used to determine permissible sizes of crack-like defects in the welded joints by the calculation method, according to [10]. At the same time, as shown by investigations, satisfactory results in determination of fracture toughness can be obtained by carefully marking and accurately making an artificial notch in the required region of HAZ. However, it should be noted that the temperature range of tough fracture widens towards decrease in temperature by 30–35 °C.

The δ_c criterion, whose values are 0.20–0.25 mm (the latter value applies to welds), has been used abroad for quite a long time in design critical structures to establish requirements to toughness of metal and welded joints. Imposing higher requirements to welded joints is attributable to the probability of appearance of additional factors, such as a higher probability of formation of defects in the joints, compared to base metal [11].

Considering the above specification levels of crack resistance of the welded joints, it can be concluded that the range of tough fracture of the HAZ metal on steel X60 is above −45 °C, and that on steel 17G1S — above −30 °C. As the lowest temperature for northern gas pipelines [12] is only −15 °C (for oil pipelines even higher), the said steels can be recommended for manufacture of repair sleeves and split welded T-joints [13, 14]. At the same time, steel X60 allows reducing the probability of brittle fracture of the welded joints, which seems to be related to metallurgical peculiarities of melting and rolling.

Sections were cut out to investigate the character of crack propagation and microstructure of individual regions of the welded joints on specimens with IRFP. As indicated by analysis, cracks propagate mostly along the fusion interface in a coarse-grained region (Figure 7, *a*), and in some cases they initiate in the coarse-grained region and propagate to the weld metal. It should be noted that cases of propagation of cracks into the weld metal of both 17G1S and X60 steel welded joints were fixed at the lowest test temperature (−75 °C). Apparently, this is related to substantial embrittlement of the weld metal and metal of the coarse-grained region. Moreover, cracks in specimens of steel 17G1S propagate to a lower depth than in specimens of steel X60. Figure 8 shows a typical picture of crack propagations in specimens of steel 17G1S with IRFP. Investigations of structure of the welded joint metal showed the following. Structure of the base metal was ferritic-pearlitic in all the cases. Hardness of steel 17G1S was *HV* 190, and hardness of steel X60 was *HV* 170. The weld metal of a welded joint was a cast mixture of hypoeutectoid ferrite, pearlite and regions of bainite. Structure of the HAZ metal in the overheated region (coarse-grained) on steel X60 was bainitic-pearlitic with hypoeutectoid ferrite precipitated mostly along the grain boundaries, and that on steel 17G1S consisted mainly of upper bainite, acicular ferrite and an insignificant portion of pearlite and hypoeutectoid ferrite.

Investigations of the character of propagation of cracks showed that the latter propagated primarily

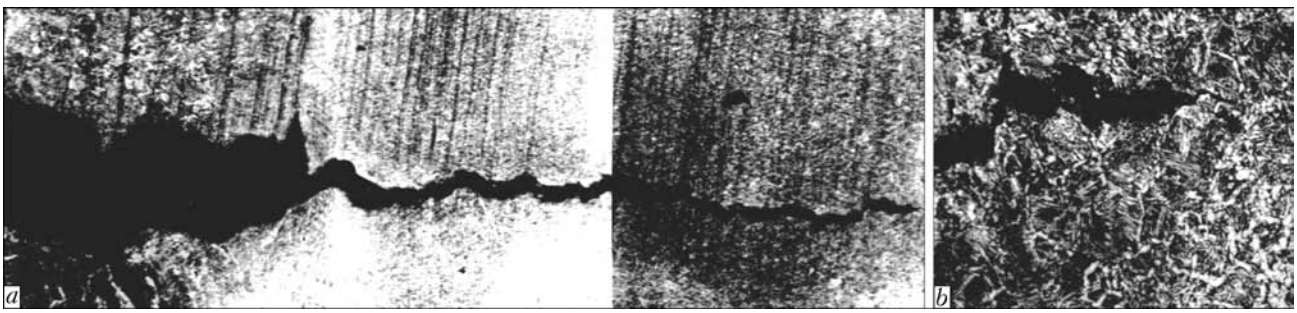

Figure 8. Panoramic view of typical propagation of cracks in 17G1S specimen with IRFP (*a* — ×63), and fragments of crack in its arrest region (*b* — ×200)

through the regions of upper bainite and acicular ferrite, and in rare cases — through the regions of hypoeutectoid ferrite. As a rule, the cracks stopped in the zones of locations of tough components.

At the same time, investigations were carried out to study peculiarities of fracture of the HAZ metal in specimens with an artificial notch by the common procedure using electron microscopes JEM-120 and JEM-200CX.

The X60 steel specimens tested at a temperature of −70 °C were characterised by a tough type of fracture. The fracture surface was mainly of a cellular type with a high degree of plastic flow prior to the fracture. Fracture centres initiated in a region of coarse phase precipitates. The regions of tough fracture, having a lower degree of plastic flow prior to the fracture (flatter facets), and regions of intergranular fracture could also be seen. The intergranular character of fracture is indicative of embrittlement in some regions of the grain boundaries. Fracture of a 17G1S steel specimen also had a tough character. However, boundaries of the tearing facets indicate to a lower degree of plastic flow prior to the fracture. Brittle fracture zones (lath pattern) were also detected. However, their share was insignificant.

Fractures of the 17G1S steel specimens at a test temperature of −90 °C were mostly of a tough character with flat facets or facets with a higher plastic flow prior to the fracture. Regions of a quasi-tough and brittle fracture were detected. Similar tests of specimens of the X60 steel welded joints showed that their fracture surface in HAZ had a tougher character of fracture, compared to the 17G1S steel welded joints, which is in agreement with data of mechanical tests of specimens of the investigated grades of steels. Tough fracture with a substantial plastic flow prior to the fracture took place both in the bulk and along the boundaries of grains.

Fractographic examinations of fractures of the 17G1S steel specimens at a temperature of −110 °C showed that fracture was mostly of a brittle character with clearly defined lath pattern and tearing ridges. It should be noted that intercrystalline fracture most often takes place at the above temperature. The fracture character of the X60 steel specimens was the same as that of the 17G1S steel specimens tested at the same temperature. Fractures occurring because of brittle cleavage and an insignificant share of the quasi-tough fracture regions were also detected. Given that fractures in HAZ of the welded joints on the investigated steels at a test temperature of −110 °C were identical, it can be concluded that the effect of alloying elements on fracture toughness is levelled at a low test temperature.

Fractures of specimens with mechanical notches made normal and parallel to the fusion interface were also investigated. Based on the results of fractographic examinations, the character of fracture of the welded joints was found to be identical even with different schemes used to make a notch in the coarse-grained region of HAZ. It was established that the δ_c values do not depend upon the method for making of a mechanical notch, and are considered reliable if the notch tip is at a distance of no more than 0.3 mm from the fusion interafce.

Metallographic examinations fully confirmed the CTOD test results. Temperature dependencies of δ_c of the HAZ metal of welded joints on the steels investigated, derived on specimens with IRFP and artificial (mechanical) notch, were in good agreement with each other. In this case, resistance of metal in the coarse-grained region of HAZ was higher for steel X60, compared with steel 17G1S.

Therefore, the simplest and least labour-consuming procedure for making a mechanical notch in HAZ is that at an angle to the fusion interface, which allows evaluation of brittle fracture resistance of the HAZ metal of the welded joints made over a wide range of welding heat inputs, compared with the deposited and base metal.

The CTOD values in testing of specimens with IRFP and mechanical notch show good correlation. However, in the first case the brittle fracture threshold shifted towards a positive temperature by 30–35 °C. This should be taken into account in defining a temperature range of brittle fracture of the HAZ metal by the results of testing of specimens with a mechanical notch.

1. Krasovsky, A.Ya., Krasiko, V.N. (1990) *Crack resistance of main pipeline steels*. Kiev: Naukova Dumka.
2. Broek, D. (1980) *Principles of fracture mechanics*. Moscow: Vysshaya Shkola.
3. (1988) *Fracture mechanics and strength of materials*: Refer. Book. Vol. 1. Ed. by V.V. Panasyuk. Kiev: Naukova Dumka.
4. Gray, T.G., McCombe, A.A., Shanks, W.A. (1985) CTOD testing to BS 5762. *Metals and Mater.*, **4**, 223–285.
5. Krasovsky, A.Ya. (1980) *Brittleness of metals at low temperatures*. Kiev: Naukova Dumka.
6. Ando, K. (1979) Evaluation of fracture toughness in heat-affected zone using the three point method for bend testing of notched specimens. *Yosetsu Gakkaishi*, **5**, 55–60.
7. Dolby, R.E. (1971) Welding and fracture initiation in QT low alloy steels. *Metal Constr. and Brit. Welding J.*, **3**, 99–103.
8. Kirian, V.I. (1984) Procedure for evaluation of resistance of structural steels to tough fracture. *Avtomatich. Svarka*, **11**, 1–6.
9. Fletcher, L. (1979) Practical COD fracture toughness measurement and evaluation. *Australian Welding J.*, **7**, 51–56.
10. Koshelev, P.R., Egorov, Yu.I. (1985) Application of fracture mechanics for evaluation of load-bearing capacity of main pipelines. In: *Strength of structures being in service in low temperature conditions*. Moscow: Metallurgiya.
11. Girenko, V.S., Dyadin, V.P. (1986) Relationships between impact toughness and fracture mechanics criteria of structural materials and their welded joints. *Avtomatich. Svarka*, **10**, 61–62.
12. Paton, B.E., Trufyakov, V.I., Kirian, V.I. (1982) Requirements to toughness of steel of main pipelines with extended fracture arresters. *Ibid.*, **12**, 5–9.
13. Makhnenko, V.I., But, V.S., Velikoivanenko, E.A. et al. (2003) Estimation of permissible sizes of welds for mounting T-joints and sleeves on active main pipelines. *The Paton Welding J.*, **8**, 6–11.
14. But, V.S., Olejnik, O.I. (2007) Main trends in technology for repair of active pressurized main pipelines. *Ibid.*, **5**, 30–35.

CONTROL OF SENSORLESS DC DRIVES OF WELDING MACHINES

Yu.N. LANKIN, V.F. SEMIKIN and **L.F. SUSHY**
E.O. Paton Electric Welding Institute, NASU, Kiev, Ukraine

Control circuits for reversible DC motors with speed stabilization by the electromotive force are described. Microprocessor-based transistor sensorless drive was developed, characterized by flat loading characteristics, absence of switching contacts for reversal, and possibility of precise setting of speed prior to starting the motor.

Keywords: *arc welding, DC motor, speed stabilization, sensorless drive, thyristor regulator, transistor regulator, micrprocessor, digital control*

Electric drives are an integral part of practically all the arc welding machines. This primarily is the electrode wire feed drive, drives of welding carriage displacement, transverse oscillations of welding head, welding head positioning, etc. DC motors became the most widely accepted in controlled electric drives. Compared to AC asynchronous motors they have much simpler speed control and considerably smaller overall dimensions. In addition, AC asynchronous motors are manufactured, as a rule, for 220 V and higher power voltage, which, according to safety rules [1] allows them to be used both in stationary and mobile automatic machines. Modern contactless synchronous machines feature excellent mass and size and adjustment characteristics. However, both they and their control systems are highly expensive.

The following requirements are made of electrode wire feed drives of semi-automatic welding machines: not less that 1:10 range of rotation frequency adjustment; stability of established rotation frequency irrespective of mains voltage fluctuations of +5 – +10 % and shaft load moment of 0–100 % not worse than ±10 % [2]. Drives for welding with pulsed wire feed, periodical transverse movement of the welding head, systems of automatic adjustment of nonconsumable electrode welding voltage and systems of automatic seam tracking should feature an essentially larger range of speed adjustment and limit speed.

Such characteristics can only be achieved at application of control systems with negative feedback by the motor rotation frequency. The best results were obtained in systems with the sensor of electric motor speed — DC or AC tachogenerator, pulsed optical sensor or Hall sensor. Unfortunately, speed transducers are complex, expensive and it is not always physically possible to install them. For instance, popular D90 and D25 motors of Kiev OJSC «Artyom-kontakt» do not allow connecting a speed transducer to the shaft from the motor side opposite to the reducer.

In the simplest drives tachometer bridge voltage is used as feedback signal [3, 4], its main disadvantage being its low accuracy. In reality, tachometer bridge voltage is proportional not to motor speed, but to motor power voltage and current. Such a system is equivalent to the system with negative feedback by motor supply voltage and positive feedback by load (current). The most negative characteristic of the system is the fact that current feedback is positive and its increase to improve the motor load characteristic rigidity leads to system instability. As a result, in the drives with feedback by the signal of tachometer bridge it is never possible to achieve flat drive characteristics, as in systems with speed transducers. The range of motor speed adjustment is also narrowed.

Sensorless systems with feedback by electromotive force (emf) of motor armature windings demonstrate much better results [5]. As is known, emf is equal to [6]

$$E_a = C_e n \Phi,$$

where C_e is the motor design parameter; Φ is the excitation flux; n is the motor shaft rotary speed. Thus, motor emf $/$ characterizes motor speed not worse than machine tachometer does. The problem consists in being able to measure emf.

Value of emf can be measured, if we switch the motor into generator mode, disconnecting it from the power source. At short-time power cut-off, the motor continues rotating by inertia, and, therefore, the emf is the armature voltage. If the motor is powered from an adjustable DC source, the control system should periodically cut-off the power supply, and measure the motor voltage during the formed pause. When the motor is powered from rectified single-phase mains voltage, the motor runs in generator mode for a considerable part of mains voltage half-period. This occurs when motor emf is greater than the power source instantaneous voltage (Figure 1).

Thyristor sensorless drive. To check the principle of speed adjustment by thyristor drive motor emf a mock-up of an analog control system was made, the block diagram of which is shown in Figure 2.

The regulator was tested with DC commutator motor M of D90 type of 130 W power. The motor is

powered from a controllable two-stage rectifier on optronic thyristors *VD*1, *VD*2. The rectifier is powered by step-down transformer *T*1.

After resistive divider *R*1, *R*2, motor armature voltage comes to repeater *DA*2, and from its output it comes to analog switch *DA*4, which is controlled by output voltage of comparator *DA*3. Voltage proportional to armature current of motor *M* is applied to comparator inverting input from shunt *R*3 connected into motor armature circuit. As a result, when no current flows through the motor armature, and the motor operates in generator mode, switch *DA*4 is closed and capacitor *C*2 is charged up to voltage proportional to motor emf. When the motor armature voltage is greater than emf, current flows through motor armature and switch *DA*4 is opened by a command from *DA*3. As a result, voltage on capacitor *C*2 stays proportional to motor emf all the time. After repeater *DA*5, this voltage is applied to regulator *DA*1, the output of which is connected to regulator of thyristor phase control on uni-junction transistor *VT*2. Circuit of synchronization of *VT*2 operation with the mains is assembled of transistor *VT*1 and rectifier *VD*3. Speed is assigned by potentiometer *R*4.

Testing of regulator mock-up demonstrated a high accuracy of stabilization of motor speed in a broad range of variation of mains voltage and motor shaft load. An indubitable advantage of thyristor regulator is its ultimate simplicity and reliability, it practically does not apply any limitations on motor power and supply voltage. It has the disadvantage of a low power factor, particularly at a high motor speed due to pulsed nature of motor armature current. As a result, the root-mean-square value of motor current determining its heating, is essentially higher than the average value of current determining the motor shaft moment.

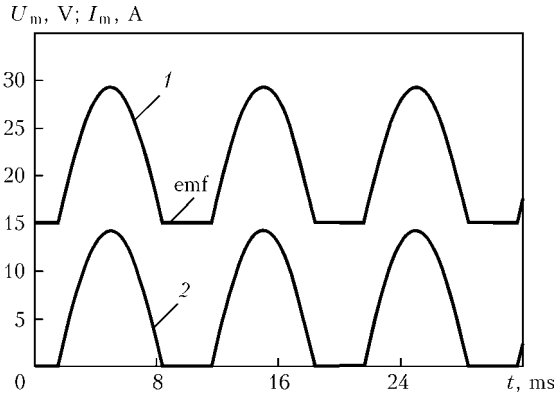

Figure 1. Oscillograms of voltage U_m (*1*) and current I_m (*2*) of the motor powered from full-wave AC voltage rectifier of 50 Hz frequency

Microprocessor-based thyristor sensorless drive. Application of microprocessors in a thyristor drive allows simplification of the device circuit, while using more perfect control algorithms. Figure 3 gives the block-diagram of microcontroller thyristor sensorless DC drive.

Application of a microcontroller allowed changing the algorithm of the motor reversal control, combining in one system, alongside the control function also the function of representation of the assigned and actual motor speed in the digital form.

Used as controller *DD*1 is this development was a single-crystal microcontroller PIC16F873 of Microchip, USA.

Potentiometer *R*1 sets motor speed v_{set}. Potentiometer output voltage is applied to one of the inputs of microcontroller analog-digital converter (ADC). Voltage from dividers *R*4 and *R*5, which are connected to armature of motor *M*, is applied to ADC other input. Microprocessor processing of this voltage allows extracting the value of motor emf from it.

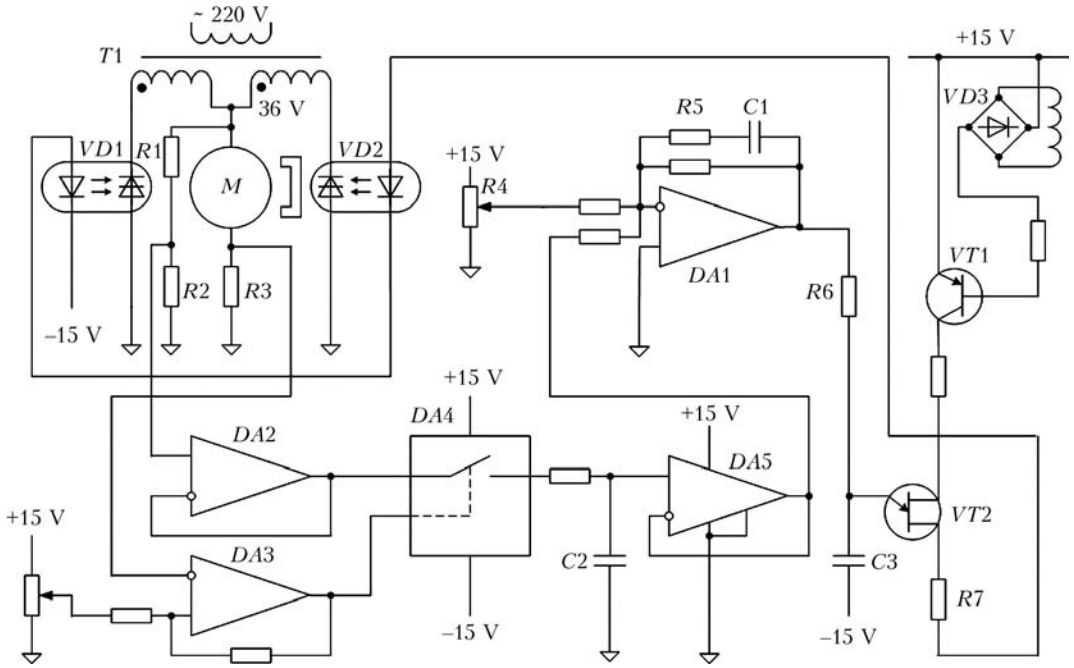

Figure 2. Block diagram of speed adjustment of non-reversible thyristor drive with negative feedback by DC motor emf

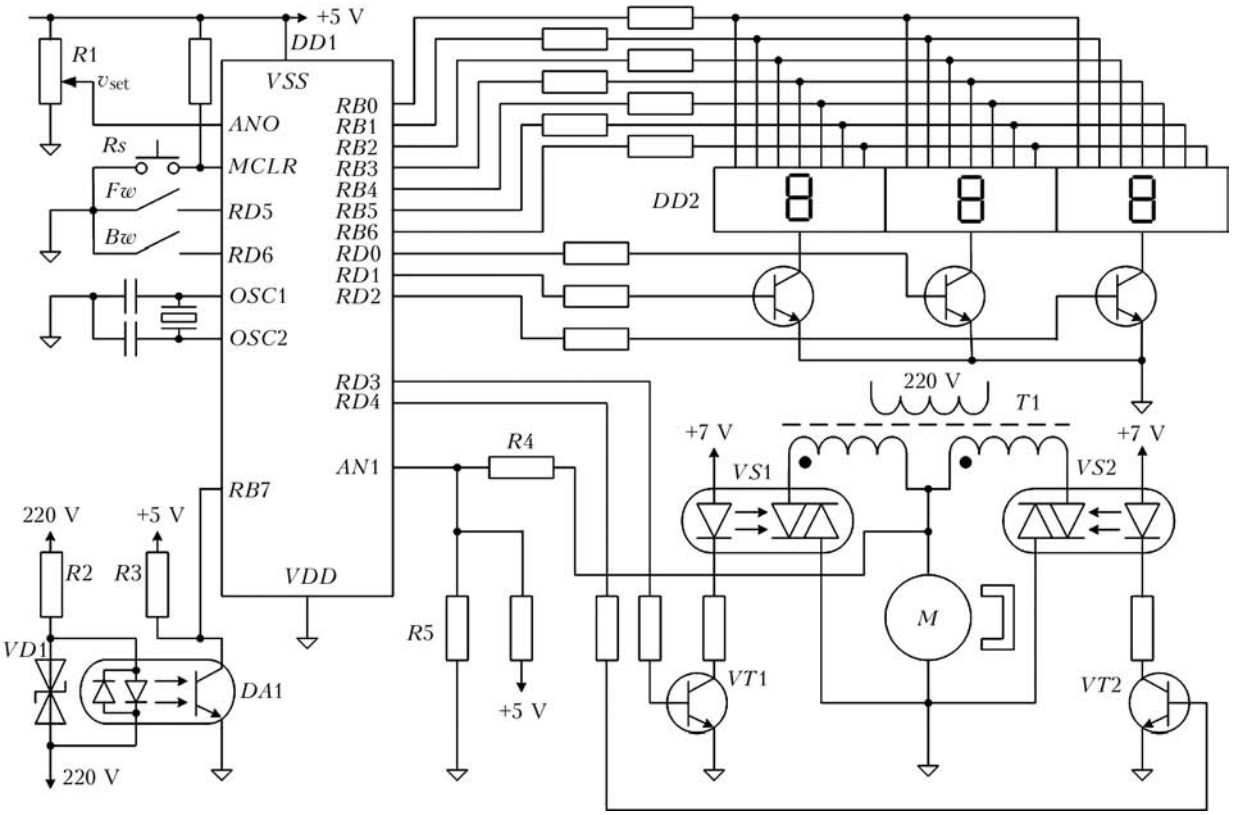

Figure 3. Block diagram of microprocessor-based reversing thyristor sensorless drive

Synchronization with mains voltage is performed by a circuit assembled of *R*2, *R*3, *VD*1, *DA*1. This results in formation at input *RB*7 of controller *DD*1 of pulses of synchronization with the mains, starting the interrupt-driven subroutine of drive control at the start of each half-period of mains voltage.

Switches *Fw* (forward) and *Bw* (backwards) generate commands for motor shaft revolution in the respective direction. *Rs* button is used for controller hand reset.

Pulses of switching on opto-triacs *VS*1 and *VS*2 are generated at controller outputs *RD*3 and *RD*4. These pulses are applied to bases of transistors *VT*1, *VT*2, to the collectors of which the opto-triac emitting diodes are connected. At switching on of transistors *VT*1, *VT*2 the respective opto-triac is switched on in the direction determined by switches *Fw* and *Bw*.

Opto-triacs are connected in single-phase circuit of full-wave reversible rectifier powered from transformer *T*1, in which the secondary winding has a center tap. The rectifier is loaded on the armature of DC commutator motor *M* with excitation from permanent magnets.

A large number of output registers of PIC16F873 microcontroller, in addition to control and adjustment devices, allows connecting to it a three-digit seven-segment LED indicator *DD*2 in the dynamic control mode. At open switches *Fw* and *Bw* the indicator shows value of set motor speed, and at switching on of motor rotation, the indicator shows the value of measured motor speed. Static error of speed adjustment is absent, due to application of discrete proportional-integral control algorithm, and motor speed is equal to the set value, thus allowing the speed value to be assigned with high accuracy before starting the motor.

Microprocessor transistor sensorless drive. For power supply to low-power low-voltage DC motors the most rational is application of transistorized pulse-width converters. A typical solution is a bridge circuit based on power field transistors with insulated gate (MOSFET). High frequency of pulse-width conversion results in low ripple of motor armature current, and transistor operation in the switching mode ensures their minimum heating, compared to operation in the linear mode. Microcontroller PIC16F684, ideally suited for such purposes, was selected for transistor control. It has built-in functions of pulse-width modulation (PWM) of transistor bridge control, current protection in each PWM period, function of protection from bridge through-currents at motor reversal, and it incorporates flash-memory, thus simplifying system debugging. The above-mentioned microcontroller is manufactured in 14-leg DIP case. A simplified schematic of microprocessor sensorless transistor reversible DC drive is given in Figure 4.

The drive power components are based on powerful complementary field-effect transistors *VT*2–*VT*5. Transistors *VT*3, *VT*5 have logic level control inputs, and are directly controlled by microcontroller. Transistors *VT*2, *VT*4, live with high voltage, are connected to microcontroller control outputs through

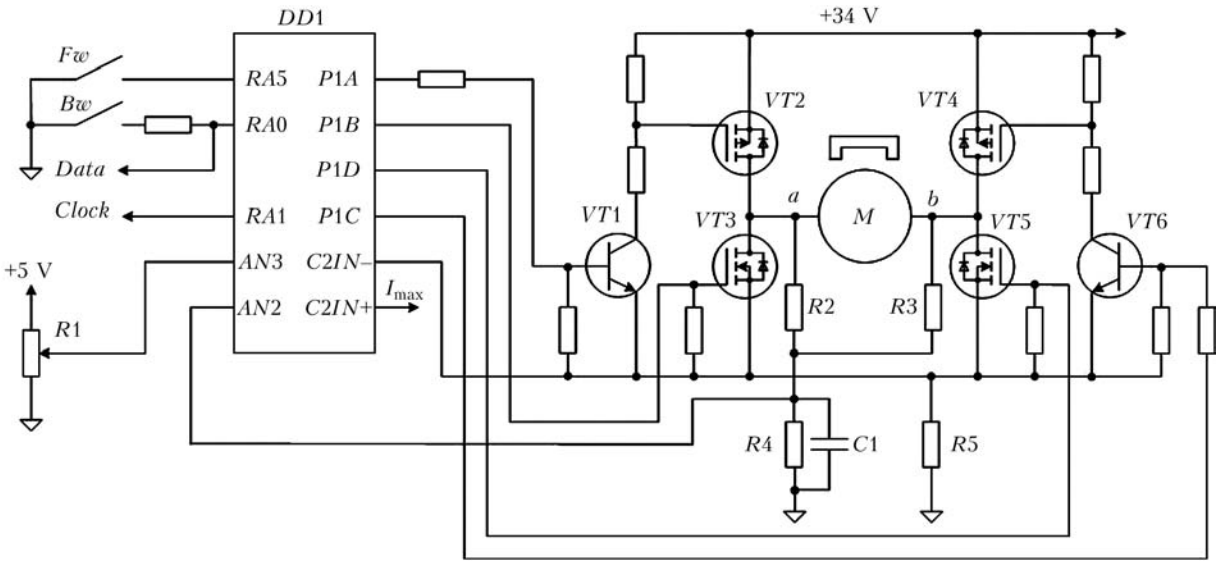

Figure 4. Simplified block diagram of microprocessor-based sensorless reversible transistor drive

low-power matching transistors *VT*1, *VT*6. Direction of motor rotation is assigned by *Fw* and *Bw* switches.

PWM control is used for adjustment of motor revolutions, in which the mean value of voltage applied to the motor, determines its revolutions, while changing according to the power pulse ratio. A signal from *Fw* switch switches on transistors *VT*1 and *VT*2, and PWM signal is applied to the gate of transistor *VT*5. As a result, the motor rotates in the working direction at the set speed. At reversal transistors *VT*3, *VT*4, *VT*6 switch on.

As was noted above emf of motor armature winding can be measured at the moment, when no power is applied to the armature, and the motor rotating by inertia runs in generator mode. Power switching off is performed in each PWM period, and, therefore, theoretically, emf can be measured with PWM frequency. In reality it is only possible at comparatively low PWM frequency, as the electric circuit of motor armature has a quite considerable inductance. At switching off of the supply voltage the armature current starts decreasing, thus causing self-induced emf, which is subtracted from armature winding emf. If during the supply voltage pause, armature current drops to zero, armature emf can be observed in the winding after that. Thus, measurement of motor emf values with maximum frequency, i.e. in each PWM period, requires its relatively low frequency, ensuring an intermittent current of motor armature. In addition, the maximum range of relative duration of PWM pulse should be limited so that the duration of mandatory PWM pause were sufficient for emf measurement. In this connection, a method of periodical short-term interruption of motor power supply at high PWM frequency was applied.

Motor power supply interruption was performed during a time interval equal approximately to units of milliseconds, which is sufficient for measurement and processing of emf values by the controller. Measured emf value is read from points *a* and *b* of the bridge (see Figure 4) and applied to input AN2 (ADC) of microcontroller through dividers R2–R4. Figure 5 shows oscillograms of emf of electric motor of D90 type during its power supply interruption periods. This voltage is reduced to the range of input voltage values of microcontroller ADC (0–5 V).

Motor speed is assigned by potentiometer *R*1, its output voltage being applied to microcontroller *AN*3 input (ADC).

Microcontroller operation cycle is 10 ms. In this case control signal is applied to bridge transistors for 7.5 ms, and for 2.5 ms bridge transistors are switched off, and the motor, rotating by inertia, runs in generator mode. During this time controller takes several

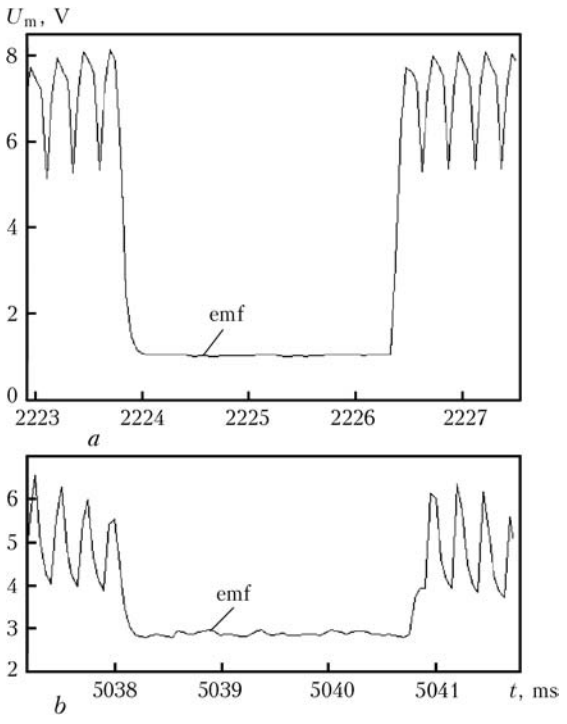

Figure 5. Oscillograms of electric motor armature voltage at low (*a*) and high (*b*) rotary speed

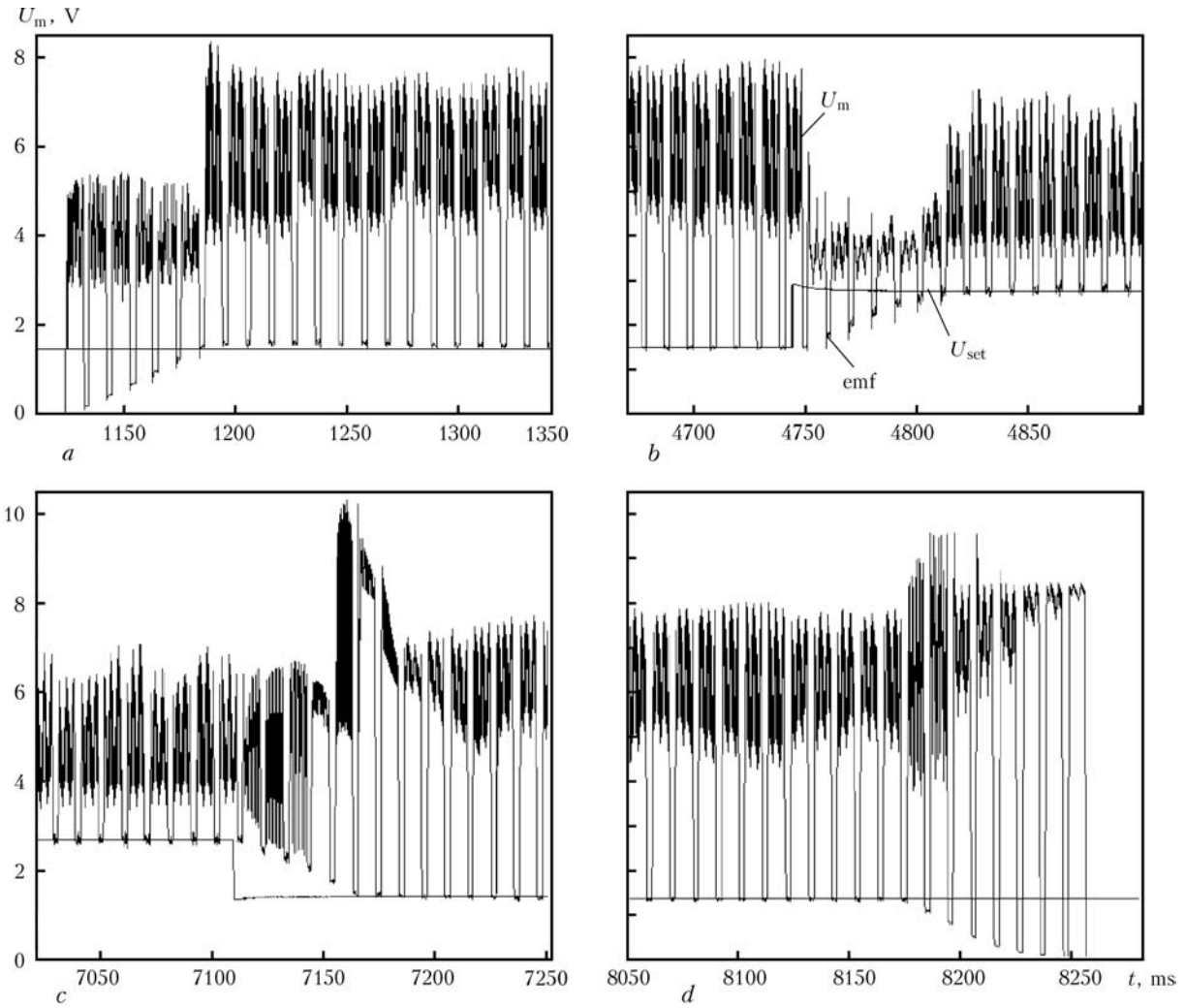

Figure 6. Transient processes in the closed adjustment system at starting (*a*), step-like increase (*b*) and decrease (*c*) of motor speed setting, as well as its stopping (*d*)

emf, measurements, averages them and calculates the control actions, namely PWM pulse duration. PWM frequencies are equal to 4 kHz.

Recurrent discrete law of proportional-integral (PI) control was used for stabilization of motor speed [6]. In order to reduce the time of executing the programmed speed lowering, the negative value of control action is implemented by reversal of motor supply voltage through appropriate control of bridge thyristors.

Figure 6 shows the transient processes with a closed feedback by motor armature emf at step-like change of assigned revolutions. As is seen from the Figure, the drive executes 30 % changes of assigned speed in 50–60 ms. Without feedback, the acceleration time is equal to 300 ms, and that of deceleration is 750 ms.

Due to application of PI-regulator, static error of speed adjustment is zero, at variation of both motor load, and mains voltage fluctuations. As a result, adjustment range is equal to not less than 1:50, which is more than enough for welding equipment.

Voltage, proportional to armature current, is read from shunt *R*5, and is applied to inverting input *C*2*IN*$^-$ of microcontroller built-in comparator. Voltage proportional to the assigned maximum armature current I_{max} is applied to non-inverting input. If motor current is higher than I_{max}, motor power is cut-off till the next PWM period. This way instant protection of bridge transistors by current is achieved practically without any additional equipment or programming costs. It results in effective limiting of armature current during transient processes at motor starting, reversal and abrupt load change, etc.

Connection to speed/setter digital indicator is performed through series interface I^2C by transfer of *Data* and *Clock* signals through microcontroller outputs *RA*0 and *RA*1. Indicator data is updated with 0.32 s interval. In the stopping mode the indicator displays the set speed, and in the rotation mode it shows the measured speed value averaged over data updating interval.

Thus, DC motors became the most widely accepted for drives of non-stationary welding machines. Application of negative feedback by motor speed greatly improves drive stability, its static and dynamic characteristics. Application of motor armature emf as signal of negative feedback by speed provides an essential cost reduction and improvement of the reliability of

motor automatic control system. The developed microprocessor transistor sensorless drive features flat load characteristics, absence of switch contacts for reversal, high reliability, small overall dimensions and low cost, and ability of precise setting of motor speed before its starting.

1. *GOST 12.2.007.8–75*: Electric welding systems for plasma treatment. Safety specification. Introd. 01.01.78.
2. (1986) *Arc welding equipment*: Refer. Book. Ed. by V.V. Smirnov. Leningrad: Energoatomizdat.
3. (1986) *Automation of welding processes*. Ed. by V.K. Lebedev, V.P. Chernysh. Kiev: Vyshcha Shkola.
4. Lankin, Yu.N., Masalov, Yu.A., Bajshtruk, E.N. (2006) Schematic for control of welding machine drives. *The Paton Welding J.*, **7**, 50–51.
5. *AN 893*: Low-cost bidirectional brushed DC motor control using the PIC16F684. www.microchip.com.
6. Piotrovsky, L.M. (1956) *Electric machines*. Vol. 1. Moscow; Leningrad: Gosenergoizdat.
7. Izerman, R. (1984) *Digital control systems*. Moscow: Mir.

PRODUCTION OF POWDER OF THE Ni–Cr–Al–Y SYSTEM ALLOY DOPED WITH SILICON BY THE POWDER METALLURGY METHOD

E.A. ASTAKHOV[1], **I.V. KUD**[2], **L.S. LIKHODED**[2], **D.P. ZYATKEVICH**[2], **M.S. YAKOVLEVA**[2] and **L.I. ERYOMENKO**[2]
[1]E.O. Paton Electric Welding Institute, NASU, Kiev, Ukraine
[2]I.N. Frantsevich Institute of Problems of Materials Science (IPM), NASU, Kiev, Ukraine

The influence of solid-phase interaction of Ni–Cr–Al–Y alloy with silicon at up to 1100 °C temperature was studied. It was established that to produce the Ni–Cr–Al–Y + Si alloy it is expedient to use nickel mechanically doped with silicon as one of the initial intermetallic components of the alloy, this preventing presence of free silicon in the alloy and ensuring uniform distribution of silicon through the powder volume.

Keywords: *detonation spraying, powders, heat-resistant alloy Ni–Cr–Al–Y, mechanical doping with silicon, solid-phase interaction, phase composition, distribution of doping elements*

Heat-resistant nickel-base alloys are widely applied to manufacture parts operating under extreme conditions of high temperatures and aggressive environments [1]. Development of new materials for protective coatings by adding doping elements to compositions of standard alloys in order to improve their service characteristics, such as heat and corrosion resistance, is of high current importance.

According to the diagram of dependence of heat and corrosion resistance of coatings upon the content of chromium in them [2], the chosen alloy for the investigations (composition, wt.%: 79 Ni, 15 Cr, 5.8 Al, 0.2 Y) is classed with the most heat-resistant ones, and doping with active additions is one of the ways of increasing its functional characteristics of heat and corrosion resistance. Silicon is not often referred to as belonging to the doping elements (boron, magnesium, zirconium, hafnium, etc.), although it should play an important role as a coating element that forms a strong and dense self-passivating oxide film during oxidation. Some researchers studied the effect of silicon on resistance of alloys at increased temperatures [3, 4]. However, these studies are of a contradictory character and contain no generalisations on the protection mechanism of the coatings to be used as a basis to select certain amounts of doping additions or compounds containing the required elements and set the method for adding them to an alloy.

The purpose of this study was to investigate solid-phase interaction of initial components of the Ni–Cr–Al–Y alloys with silicon within a service temperature range (up to 1100 °C). The alloys were produced by the powder metallurgy method. Several methods are available for adding doping impurities [5]. Silicon can be added to the initial mixture of nickel, chromium and aluminium powders, followed by powder metallurgy operations (mixing, crushing or mechanical activation, heat treatment, etc.), or it is possible to first produce a silicon compound with one or several initial components and then mix it with other components of the alloy. The doping method is determined by technological peculiarities of subsequent processes. This study considered several methods for adding silicon.

One of methods for adding a silicon impurity to a complex nickel-base alloy is adding it together with yttrium oxide during the process of production of a standard alloy powder. Yttrium oxide and silicon (up to 4 wt.%) are added at a stage of mixing to a mixture of Ni_3Al and Cr(Ni) powders preliminarily produced by solid-phase synthesis in vacuum. Then, following the flow diagram of the process developed by the authors, the diffusion processes of interaction of silicon with main phases of the alloy, i.e. Ni_3Al and Cr(Ni), should take place during vacuum heat treatment.

The interaction products after vacuum heat treatment at a temperature of 1000 °C for 2 h were investigated by X-ray analysis and scanning electron mi-

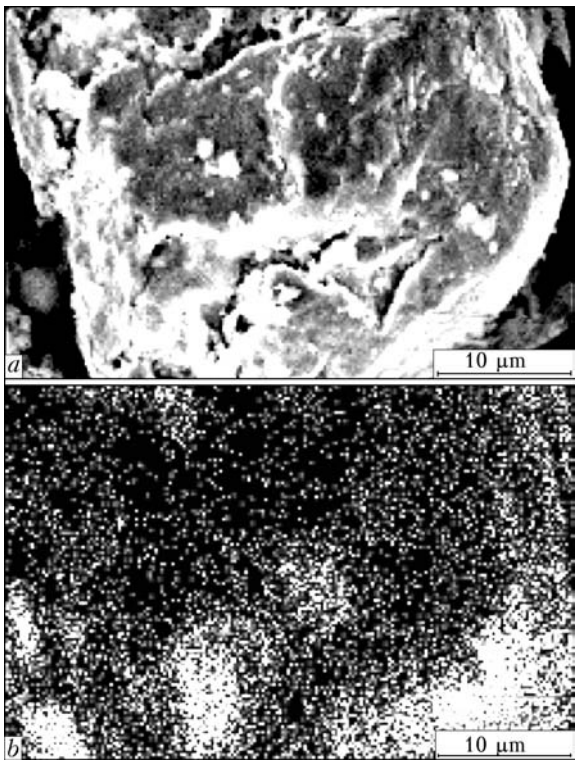

Figure 1. Microstructure of particle of IPM synthesised powder (*a*) and distribution of silicon in it (in reflected electrons) (*b*)

croscopy. According to the X-ray analysis data, the synthesised material consists of a mixture of the main phases, i.e. Ni_3Al and Cr(Ni), and silicon, which is in a free state. The data of scanning electron microscopy and energy-dispersive method given in Figure 1 and in Table 1 are indicative of a non-uniform distribution of silicon through the volume. It can be seen that the maximal amount of silicon is concentrated on surfaces of the particle.

Elemental composition of the produced powder is as close as possible to that of the chosen standard powder.

Investigations show that adding the doping impurity at a stage of mixing of the preliminarily synthesised powders of Ni_3Al, Ni(Cr) and Y_2O_3, followed by heat treatment in vacuum at a temperature of 1000 °C, does not provide completeness of the diffusion processes, and does not yield the products containing no free silicon. This gives no way of fully

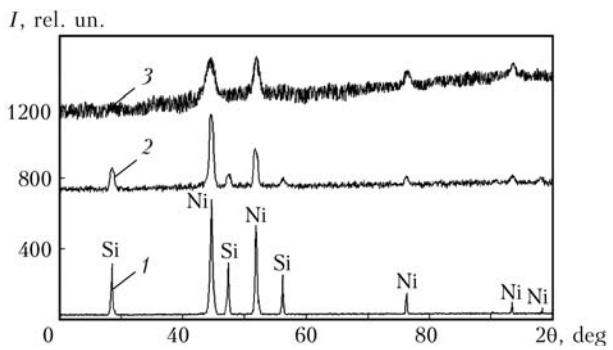

Figure 2. Diffraction patterns of mechanical synthesis products of the Ni–Si system as a function of weight ratio at process duration of 60 min: *1* — 1:5; *2* — 1:10; *3* — 1:20

Table 1. Chemical composition of powder of Ni–Cr–Al–Y alloy, wt.%

Manufacturer of powder	O	Al	Si	Cr	Ni	Y
IPM	0.15	5.38	3.60	14.90	76.15	0.21
Commercial (India)	0	11.54	0	31.91	55.73	0.82

reproducing the elemental composition of a material in detonation sprayed coatings due to fractionation. Because of the above-said, as well as considering the data on substantial solubility of silicon in nickel (5 %) at room temperature to form solid solution, it was expedient to use nickel doped with silicon during mechanical synthesis as one of the initial components of the alloy. In study [6] this solution is identified as α-solution, and in study [7] — as γ-solution. In our investigations we designate it as γ-Ni, in analogy with solid solutions of the austenitic class.

Investigations of the process of solid-phase interaction of nickel and silicon in mechanical synthesis (mechanical doping) included evaluation of the process on the basis of technological factors, such as weight ratio (ratio of powder weight to weight of milling bodies) and duration of the process.

To study mechanical synthesis, the nickel and silicon powders (in amounts to yield 4 wt.% Si in nickel) were preliminarily mixed in a planetary-type mill in the reversal mode for 2 h in alcohol to homogenise the reaction mixture. After drying, the mixture was subjected to high-energy treatment.

Mechanical synthesis is a high-energy crushing that induces internal stresses in a solid body, this causing deformation of atomic bonds, formation of defects of a crystalline structure and excitation of electron sub-system of a crystal. At that, each particular case is characterised by predominance of certain channels of relaxation of the stored energy. Thus, in formation of new boundary surfaces the energy consumption for restructuring is minimal, and atoms in the surface layer have a high margin of the excessive energy, this creating favourable conditions for chemical transformations of contacting materials.

Table 2. Characteristics of mechanical synthesis products of Ni–Si system

Weight ratio — powder to spheres weight ratio	Duration, min	Phase composition	Lattice spacing of nickel, nm
1:5	30	Ni, Si	0.352
	60	Ni, Si	0.353
1:10	30	Ni, Si	0.352
	60	γ-Ni, Si	0.350
1:20	30	γ-Ni, Si	0.349
	60	γ-Ni	0.347

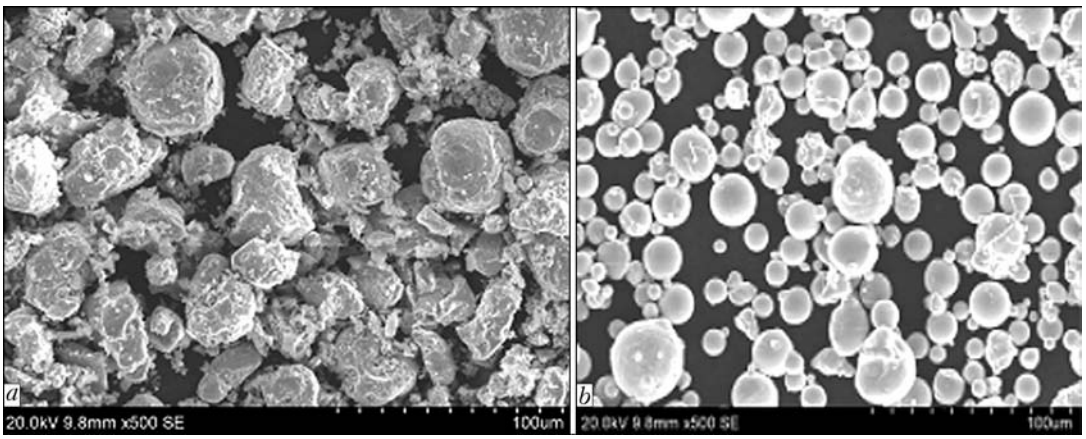

Figure 3. Morphology of powders produced by IPM (*a*) and «Stark» Company (*b*)

The process was carried out in a pulse mode, which led to a change in the crystalline lattice energy due to formation of different structural defects (dislocations, vacancies). This resulted in stimulation of the diffusion processes in the system by the stored energy at certain technological parameters.

The mechanical synthesis products were examined by X-ray phase analysis (Table 2, Figure 2).

Analysis of the obtained experimental data indicates to a substantial effect of the energy intensity of the process, which is a function of the technological parameters at a constant speed of rotation of the reactor. At a weight ratio of 1:5, the milling products are a mixture of initial components, independently of the process duration.

A slight change in the character of diffraction maxima of nickel and silicon is indicative of occurrence of the first stage of deformation of the powder (Figure 2, curve *1*). Increase of weight ratio to 1:10 is accompanied by partial amorphisation of silicon, this being evidenced by lowering and broadening of its diffraction maxima. Increase in imperfection and stress level of nickel shows up in broadening at high angles of its diffraction images (Figure 2, curve *2*). Increase of the process duration to 60 min leads to the beginning of formation of solid solution of silicon in nickel (γ-Ni), this being evidenced by a change in the lattice spacing of nickel.

A weight ratio of 1:20 is accompanied by an even more pronounced intensification of the process. According to the X-ray analysis data, not only the quantitative composition of the interaction products changes, but also a distortion of the pattern of diffraction maxima of γ-Ni takes place, which is indicative of a stressed and non-equilibrium state of the system

Table 3. Chemical composition of powders, wt.%

Manufacturer of powder	O	Al	Si	Cr	Ni	Y
IPM	0.15	5.38	2.6	15.40	76.26	0.21
«Stark» Company	–	9.54	–	21.91	67.73	0.82

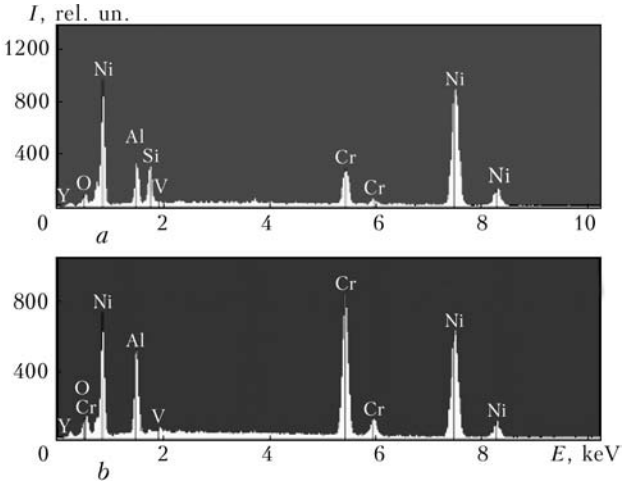

Figure 4. Elemental composition of powders produced by IPM (Ni–Cr–Al–Y + Si) (*a*) and by «Stark» Company (Ni–Cr–Al–Y) (*b*)

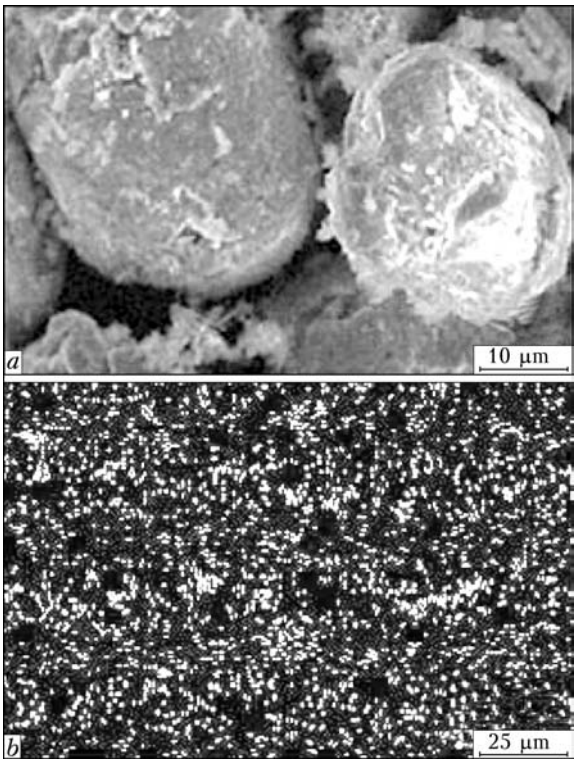

Figure 5. Microstructure of particles of the powder of mechanically synthesised alloy Ni–Cr–Al–Y (*a*) and distribution of silicon in them (in reflected electrons) (*b*)

(Figure 2, curve *3*). At the 60 min duration of the process, the product of mechanical synthesis is solid solution of silicon in nickel.

Therefore, the investigations conducted made it possible to identify the technological parameters of mechanical synthesis, the product of which is a powder of solid solution of silicon in nickel (γ-Ni).

According to the technological process, production of the Ni–Cr–Al–Y + Si alloy powder provides for the use of individual intermetallics Ni_3Al and Ni(Cr) after the low-temperature solid-phase synthesis, followed by their mixing with yttrium oxide, granulation and vacuum heat treatment. The mechanically synthesised powder of solid solution of silicon in nickel is used as one of the initial components at a stage of production of the intermetallic powders. The special consideration was given to investigation of the effect of doped nickel on temperature-time parameters of synthesis of intermetallic phases Ni_3Al and Ni(Cr).

The data of X-ray analysis of intermetallics Ni_3Al and Ni(Cr) synthesised in vacuum, which make the base of the Ni–Cr–Al–Y + Si alloy, indicate to the absence of free silicon in them.

The phase and elemental composition, as well as morphology of the produced powder were determined by the methods of X-ray analysis and scanning electron microscopy with energy-dispersive analysis.

As can be seen from Figure 3, *a*, the produced powder consists of equiaxed particles with a mean diameter of about 60 μm, which meet requirements to the detonation spraying powders.

X-ray microanalysis of the experimental powder (Figure 4, *a*; Table 3) confirmed the presence of silicon in it. Energy-dispersive scanning of the produced powder of the Ni–Cr–Al–Y alloy doped with silicon reveals a non-uniform distribution of all elements through the volume (Figure 5).

Therefore, the work done to evaluate solid-phase interaction of initial components of the Ni–Cr–Al–Y alloy with silicon in a service temperature range (up to 1100 °C) made it possible to establish that direct doping of intermetallic components Ni_3Al and Ni(Cr) of the Ni–Cr–Al–Y alloy with silicon in vacuum heat treatment at a temperature of 1100 °C leads to the undesirable presence of free silicon in the solid-phase interaction products, as well as to the non-uniform distribution of silicon in the alloy. To produce the Ni–Cr–Al–Y–Si alloy, it is expedient to use nickel mechanically doped with silicon as one of the initial intermetallic components of the alloy, since this allows avoiding the undesirable presence of free silicon in the alloy and ensures the uniform distribution of silicon through the powder volume.

1. (1995) *Superalloys II: High-temperature materials for aerospace and industrial power units*. Book 1. Moscow: Metallurgiya.
2. Li, W.Z., Yao, Y., Wang, Q.M. et al. (2008) Improvement of oxidation resistance of NiCrAlY coatings by application of CrN or CrON interlayer. *J. Mater. Res.*, 23(**2**), 341–352.
3. Brodin, H., Eskner, M. (2004) The influence of oxidation on mechanical and fracture behavior of an air plasma-sprayed NiCoCrAlY bondcoat. *Surface Coat. Technol.*, **187**, 113–121.
4. Liang, J.J., Wei, H., Hou, G.C. et al. (2008) Thermal stability of phases in a NiCoCrAlY coating alloy. *J. Mater. Res.*, 23(**8**), 2264–2274.
5. (1995) *Superalloys II: High-temperature materials for aerospace and industrial power units*. Book 2. Moscow: Metallurgiya.
6. Samsonov, G.V., Dvorina, L.A., Rud, B.M. (1979) *Silicides*. Moscow: Metallurgiya.
7. Schapck, F. (1973) *Structure of binary alloys*. Moscow: Metallurgiya.

NEWS

EFFECTIVE APPLICATION OF LASER WELDING

At Chelyabinsk pipe rolling plant (OJSC «ChTPZ», Chelyabinsk region) a pilot welding of pipes of 530 × × 8 mm in size with use of a laser equipment was performed. The pipes were welded using two lasers of 8.3 kW total capacity with coincidence of two beams into one welding pool. Welding was performed using a filler wire Sv-08G2S of 1.2 mm diameter. Two pipe samples, welded by laser, were tested at the test grounds by supply of hydraulic pressure until fracture. The pipe fracture occurred at pressure of 203 atm: the weld withstood the pressure of 200 atm.

WELDING FABRICATION IN GAS TURBINE CONSTRUCTION (Review)*

V.V. ROMANOV and **Yu.V. BUTENKO**
SE «Zorya»–«Mashproekt», Nikolaev, Ukraine

The paper deals with modern developments of gas turbine units and commercial application of advanced welding and related technologies: electron beam welding, laser cutting, vacuum brazing, surfacing, etc.

Keywords: *welding technology, gas-turbine units, new materials, arc welding, laser cutting, electron beam welding, electroslag welding, plasma-powder surfacing, vacuum brazing*

Southern Turbine Plant (now called State Enterprise «Zorya»–«Mashproekt») was established at the start of 1950s with the purpose of development and batch production of gas turbine equipment for warships of the USSR Navy. At the start of 1979 the Enterprise mastered batch-production of gas turbines for pumping natural gas and producing power in mobile and stationary power plants.

«Zorya»–«Mashproekt» accumulated tremendous experience of development of various-purpose gas turbine units (GTU), namely for the drive of natural gas compressors, power engineering and navy power plants.

During more than fifty years of Enterprise operation, the design bureau developed 56 types and modifications of gas turbine engines (GTE), 38 types of different reduction gears, which were the basis for development of more than 70 types of GTU, which have been adopted and still are operated by the navy of CIS and a number of other foreign countries. More than 1700 navy GTE have been manufactured, which were used to equip more than 65 % of waterborne ships of USSR Navy by the start of 1990s. Total power of engines mounted on the ships is up to 17 mln hp, and their operation time is equal to 3 mln h.

At present more than 800 GTU produced by «Zorya»–«Mashproekt» are in operation at compressor stations, their total operation time being equal to 75 mln h. The Enterprise continues operating actively towards improvement of the currently available and development of promising GTU for gas-pumping units. Development of a regenerative cycle GTU of the rated power of 16 MW with more than 40 % efficiency for gas-pumping unit drive became one of the promising projects.

«Zorya»–«Mashproekt» is actively pursuing development of industrial type GTE for power engineering. The design features of such engines are two-support rotor design, absence of gas-dynamically isolated (free) generator turbine, high (up to 500–550 °C) gas temperature at the engine outlet, ability to maintain it in the partial regulation mode due to adjustment of air flow rate at engine inlet.

«Zorya»–«Mashproekt» developed industrial-type power GTU GTE-110 of nominal power of 110 MW with 36 % efficiency. This unit was the basis for development of projects of steam-gas plants (SGP) of the nominal power of 160 and 325 MW, with the efficiency of 50.2 and 51.5 %, respectively.

Samples of power units GTE-45(60) and UGT5000 of the nominal power of 60 and 5 MW, respectively, were made. GTE-45(60) unit is designed for use in «large-scale» power generation as part of GTU, and UGT5000 — as part of cogeneration units.

Compared to earlier developed units, UGT5000 has a number of fundamental differences. Therefore, designers, technologists and manufacturers are now solving the issues they have never faced before.

Different materials are used for manufacture of modern GTE (Figure 1), namely low- and high-alloyed (high temperature-resistant and high-strength) steels, titanium alloys, nickel wrought and cast dispersion-hardening alloys. Application of high-alloyed heat-resistant and high-temperature alloys, as well as wide use of welding and related technologies in engine manufacture, ensured high GTE performance at minimum weight and dimensions characteristics.

«Zorya»–«Mashproekt» has mastered modern technologies of laser cutting, electron beam welding (EBW) and electroslag welding (ESW), surfacing, vacuum brazing and other processes.

Laser cutting of sheet (up to 12 mm) material is performed by «Baystar-3015-3» laser system of «Baystronic» company, which consists of CO_2 laser with 3 kW output power with high-frequency pumping, gantry with high-speed drives, two replaceable working tables for sheets of 1.5 × 3.0 m size, computer unit for control of the process of cutting and monitoring the working mixture composition, gas bottle block for working mixture preparation, laser cooling unit with automatic maintenance of the set temperature, unit for aerosol suction from the cutting zone and feeding

*Published by the materials of the paper presented at scientific-technical conference held at the Admiral S.O. Makarov National Shipbuilding University on October 14–17, 2009.

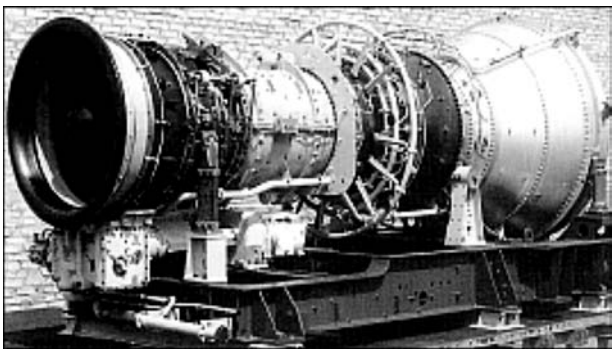

Figure 1. GTE DN-80 appearance

cleaned air back to the premises, unit for sheet loading and removal of cut out parts; it also incorporates a unit for cutting out shaped holes on pipes of up to 200 mm diameter.

Highest grade gases are used for laser radiation generation, namely commercial nitrogen, carbon dioxide gas and helium, and oxygen is used as cutting gas.

At present, the range of cut out parts includes many thousand part names. Parts cut out by the laser do not require and further machining.

EBW became the most widely accepted in fabrication of stator and rotor components. This is due primarily to the fact that this welding process combines a highly concentrated heat source and the most perfect means for molten metal protection, namely vacuum. The above EBW features allow welding alloyed, austenitic and martensitic steels, nickel and titanium alloys up to 100 mm thick with minimum deformations without edge preparation or filler wire application.

EBW sections were set up in the test and batch production facilities of «Zorya»–«Mashproekt» in cooperation with PWI. Vacuum chambers and displacement mechanisms were developed and manufactured by the enterprise staff. U-250A, ELA-15, ELA-30, ELA-60/60, ELA-60 power units are used for electron beam generation. A dimension-type series of the units has been developed, allowing welding stator components from blade units to large-sized components of 3.5 m diameter, as well as rotor shafts and drums.

Figure 2. Macrosection of EB-welded overlap joint of flue tube shells

Section of batch production is fitted with «Protok-10» device for demagnetizing the components before welding and with the required instrumentation. The above sections are located in immediate vicinity of each other, allowing quickly solving the arising problems.

At present EBW is used to perform about 70 % of welding operations on GTE components, and manufacturing of these engines is already unthinkable without it. This allowed gas turbine designers developing and introducing into batch production a number of fundamentally new welded structures, namely low- (LP) and high- (HP) pressures compressor rotors, central drive gears, HPC shafts from materials VT31, VT8, VT9, EP 609, EP 517.

Application of new materials (EP 609Sh, EP 866, EP 517) for manufacturing thick-walled components required a fundamental retrofitting of EBW techniques. Work has been performed in cooperation with PWI on development, mastering and introduction of beam control systems (SU-65, SU-29, SU-259). A new technology has been introduced, namely EBW with a horizontally located gun with electron beam rotation by a preset prgoram. All this allowed solving the problem of welding components with up to 70 mm wall thickness.

Flue tubes from EI 602 alloy of second generation engines (wall thickness δ = 2.5 mm) and from VZh 98 alloy of third generation engines (δ = 1.5 mm) are some of the most highly stressed elements, as they operate under the conditions of the impact of high thermal and vibration loads and determine the service life of the flue component. Attempts at making the joints using argon-arc welding (AAW) failed, as the weld root developed a brittle film, promoting initiation of longitudinal cracks. Investigations of overlap joints of thin-walled shells made by EBW, confirmed the effectiveness of this technology. A process of EBW of flue tubes with application of electron beam scanning by a specially designed generator was developed. Selection of amplitude, frequency and relative oscillation duration of the electron beam, allowed achieving a uniform penetration in the overlap joint of flue tube shells of up to 8 mm width (Figure 2). Figure 3 is the appearance of the flue tube, made with EBW application.

The fusion line metal structure does not have any oxide films or other defects. Transverse macrosections of the weld show that at EBW the length of the HAZ is equal to 1.5–2.5 mm, whereas at AAW it is equal to 10–12 mm. Width of the zone of heat contact of overlap joints increased 2–3 times. Flue tube EBW allowed item service life to be extended 4–6 times.

GTE nozzle vanes are particularly heavy-duty items, and are exposed to thermal and dynamic loads, bending moment and torque, as well as salt and sulfide

Figure 3. Appearance of flue tube (EI 602 alloy, δ = 2.5 mm) with five circumferential EB welds

corrosion; they are also exposed to erosion wear. It did not seem possible to produce sound joints of EP 539LM, ChS 70L, EK 9L, ChS 104 alloys applied for nozzle vanes of navy gas turbines, using arc welding processes, in view of the low technological strength of these alloys.

Proceeding from the results of experimental investigations, the ways of improvement of technological strength and main conditions of producing sound welds of vane units of nozzle blocks from EP 539LM, EK 9L alloys and other materials by EBW in forced modes with application of electron beam modulation were determined (Figure 4). Engine tests showed the high reliability of welded joints of nozzle block vane units.

Rotors of LP- and HP-compressors with speeds of 2000 rpm at high pressure are particularly critical compressor components. Rotor welded structure without closed cavities in the axial direction, in which the discs are connected not by pins, but by EBW, is more reliable in operation and adaptable to fabrication. As the discs come up for welding with finished slots, the difficulty of rotor fabrication consists in producing after welding the minimum radial and face runout of the component, not greater than 0.3 mm.

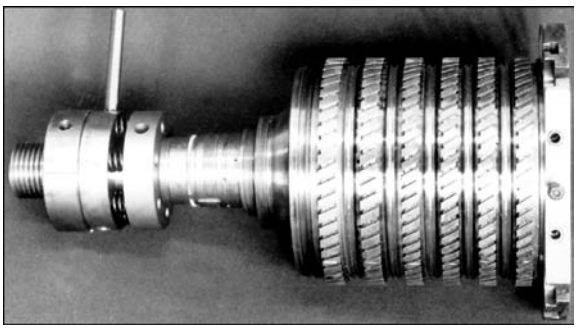

Figure 5. Appearance of all-welded HPC rotor from VT31 titanium alloy

In order to obtain a component of required dimensions, welding and subsequent heat fixation of rotors are performed in specially developed fixtures, which rigidly fasten each disc by its inner body diameter. Disc joining is performed on an aligning substrate 5–8 mm thick. After welding the component is heat-treated to relieve internal stresses and improve ductility properties of welded joints, and the substrate is cut off to remove defects in the weld root.

Manufacturing all-welded rotors of gas turbines from VT31, VT8, VT9 titanium alloys and EP 609, EP 517 alloys by EBW (Figure 5) is a considerable achievement of welding engineering. Tests of welded rotors conducted in rigs and engines showed their high performance.

Manufacturing of some GTE components requires materials, combining high strength and ductility, high temperature strength and heat resistance, hot hardness and thermal stability under operation conditions close to the limit ones. It is impossible to combine all these requirements in one material. Therefore, products are developed, the individual parts of which consist of various materials, the most suitable for operation conditions. Such dissimilar materials can be combined in one item using technologies of vacuum brazing or brazing in argon flow.

«Zorya»–«Mashproekt» has mastered the technology of vacuum brazing of air-cleaning and fuel filters, connector blocks, honeycomb and metal-ceramic seals, guide vane units, cages, igniter cases, torch device fittings, etc. Excellent results were obtained in repair of defects in castings from high-temperature nickel

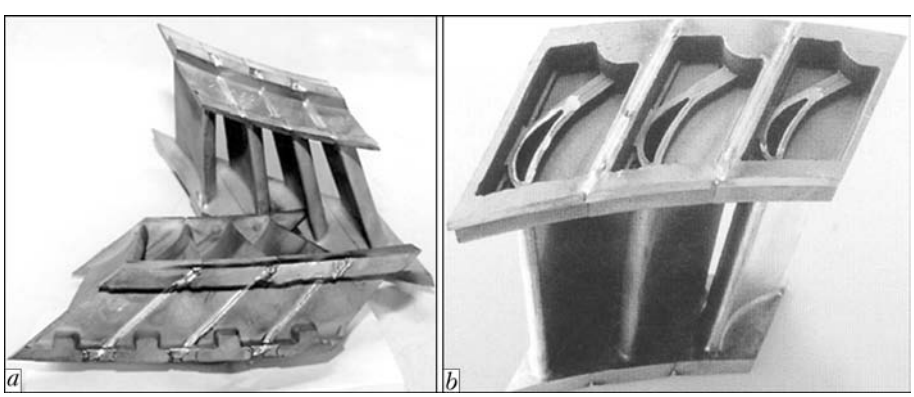

Figure 4. Vane units from EI 9L alloy of nozzle blocks of the 1st stage after EBW over small flange (*a*) and 2nd stage after EBW over large flange (*b*)

Figure 6. Appearance of brazed parts and products: *a* — air-cleaning and fuel filters, sensor connector blocks; *b* — nozzle unit vanes, variable vane cages, igniter cases; *c* — units and vanes of nozzle blocks after repair of surface casting defects; *d* — honeycomb and metal-ceramic seals

alloys by brazing, the technology of which was developed together with Admiral S.O. Makarov National Shipbuilding University (Figure 6).

High-temperature powder braze alloy VPr11-40N and proprietary braze alloys NS-12, NS-12A were used in production. Foil braze alloys VPr-4 and VPr-7 are applied in addition to powder braze alloys. Depending on braze alloy type brazing temperature is equal to 1050–1180 °C.

Both in full-scale and in pilot production specialized shop sections were set up, fitted with vacuum equipment, devices and fixtures.

In gas turbine construction it is also necessary to weld large cross-section parts. For instance, guide vane rings, LPC, HPC flanges are made of martensitic-ferritic class steels using forged semi-rings with cross-sectional area of up to 14,500 mm^2.

Practically all the components, using rings, operate at high loads and increased temperatures, thus requiring the semi-ring welded joints to have operational properties not lower than the level of those of the base metal.

Semi-rings from 20Kh13, EP 609Sh, EI 961Sh and other steel grades were produced by mechanized CO_2 welding by bath method. However, multiple repairs of weld defects enhance the cost of part manufacturing. In order to improve the quality of welding forged semi-rings, the Enterprise introduced ESW technology. Earlier, some ESW features did not permit application of this technology, as it was necessary to create a technological «pocket» for the start of electroslag process, mount run-off plates for welding on the «discard head» at the end of welding, apply copper water-cooled plates to form the weld side surfaces.

As a result of research it was possible to simplify the part preparation for welding. Application of preheating up to 500–600 °C allows moving over from the arc to electroslag process already in the second pass so that in the presence of allowances there is no need for the technological pocket.

Shrinkage looseness at the end of welding is achieved owing to an operation similar to crater welding up in arc welding. At the final stage the welding head is stopped. Welding current and wire feed are smoothly decreased to zero. Thus, there is no need for welding on the «discard head».

Copper forming plates requiring fitting of the edges to be welded in each concrete case were replaced by ceramic ones based on Al_2O_3. Such ceramics can stand the liquid pool temperature and does not go into the weld, owing to the presence of a thin layer of slag between it and liquid pool metal. Easy treatability of ceramic plates and ability to glue them in the butt zone by a mixture of liquid glass with alumina, make this material a convenient substitute of copper plates, particularly at a great difference in their thickness.

Welding of martensitic-ferritic steel is performed by EP 609Sh welding wire of 4 mm diameter, using AN-318A flux. Weld metal composition meets the requirements of TU 14-1-2412–78, mechanical properties of weld metal and HAZ are higher than similar base metal values.

Engine life is determined by the duration of operation of the «weakest» component or part. Components and parts of the high-temperature section operate under hard conditions. Turbine blades belong to the most heavy-duty parts, determining the life of modern GTE.

Nickel-based high-temperature alloys ChS 70, ChS 88VI, ChS 88U-VI, containing chromium, tungsten, molybdenum, titanium, aluminium, boron and other elements, are mainly used for GTE blades. They combine high high-temperature strength of the above alloys, which is due to presence of complex-alloyed solid solution and maximum content of the strengthening phase with satisfactory adaptibility to fabrication. An

alloy high-temperature properties are largely dependent on its structural states, grain size, shape and dispersity of the strengthening phases. Contact surfaces of blade flanges and edges wear during operation. Reduction of blade height promotes axial flowing over of gas with engine efficiency dropping by 1.5–3.5 %. Appearance of worn-out areas leads to formation of gaps and increase of the level of vibration loads, which may lead to blade fracture, and failure of the entire engine. The operating life of blades is determined by the degree of wear of contact surfaces of flanges and edges. However, despite the wear, the blade airfoil and root preserve their serviceability and after strengthening they can stand 3–4 operation life periods. In addition, worn earlier strengthened surfaces can be restored several times.

According to the earlier technology, strengthening of GTE blade edges and flanges was performed by nonconsumable electrode argon-arc hardfacing of stellite. The main disadvantages of this technology were cracking in the hardfacing zone (stellite–base metal) and non-uniform distribution of deposited stellite hardness over the area of the blade edge or flange.

Based on the new technology, trapezoidal electrodes (3 × 2 × 2 × 260 mm) are made from plasticized high-temperature material KBNKhL-2 in SNVE 1.3.1/16-IZ vacuum furnace. Surfacing with these electrodes was performed by oxygen-acetylene flame, using GO2 manual torch (#2 tip) and PV-200 flux. Edges of blades from ChS 70, ChS 88VI, ChS 88U-VI alloys are hardfaced.

Oxyacetylene hardfacing provides a high metal quality without external or internal defects with stable hardness *HRC* 60 over the entire area of blade edge or flange. At present the plasticized mixture of high-temperature material KBNKhL-2 is produced in the Enterprise.

Introduction of the technology of strengthening the edges and flanges of GTE blades by oxyacetylene hardfacing of high-temperature material KBNKhL-2 allowed eliminating rejects, which are caused by development of cracks and other defects. This technology was used for manufacturing more than 180 electrode sets and strengthening of edges and flanges on more than 1000 blades.

GTE design envisages fastening flue tubes by locators. The majority of the locators are made of martensitic-ferritic steels 14Kh17N2 and EI 961, and for newer and more powerful engines (for instance, DN-80), they are made of nickel-based austenitic alloy EP 648.

To improve wear resistance, locator working surfaces are hardfaced with stellite. Selection of hardfacing material is due to a high operating temperature of parts (450–600 °C), as well as presence of considerable contact loads on these surfaces. Main requirements made to the deposited layer are absence of cracks (LUMA control) and deposit hardness (*HRC* ≥ 40).

Earlier hardfacing was performed by manual AAW with cast rods of 3–4 mm diameter. This technology, however, has serious drawbacks. First, during hardfacing of 14Kh17N2 and EI 961 steels longitudinal cracks often form along the entire length of the deposit, propagating into the base metal. Stellite and martensitic-ferritic steel (for instance, 14Kh17N2) have different values of the coefficient of thermal expansion, so that cooling of the deposited part induces high stresses, and if the deposit has pores and inclusions, they become crack initiation sites. Secondly, part hardfacing is performed in two layers to ensure the required hardness of the deposited layer, as intensive mixing of stellite with the base metal takes place at AAW, which results in the hardness of the first layer not exceeding *HRC* 32–35. Two-layer hardfacing leads to extra consumption of expensive stellite and increase of labour consumption of part manufacture.

In this connection argon-arc hardfacing was replaced by plasma-powder hardfacing of cylindrical surfaces of tube locators in UPM-150D unit (Plasma-Master, Ltd.). Hardfacing is performed by high-temperature constricted arc, generated in a plasmatron with a non-consumable electrode. Range of adjustment of main arc current was equal to 25–150 A. Filler material is powder of Stellite 12 grade, the composition of which is identical to that of PRV-VZKR stellite. Argon was used as plasma, transporting and shielding gas. Design of drum type feeder ensures a uniform and precisely dosed powder feeding. In plasma-powder hardfacing of locators of 8 to 27 mm diameter, machining allowances can be smaller, which results in a good appearance of the deposit.

Introduction of the technology of plasma-powder hardfacing of stellite in the Enterprise improved the quality of the hardfaced parts and lowered the labour consumption in expensive part manufacture.

Technologies of electron beam spraying of heat-resistant and thermal-barrier coatings, plasma spraying and many other have also been mastered.

Thus, State Enterprise «Zorya»–«Mashproekt» has put into operation modern welding and related technologies, ensuring development and manufacturing of highly efficient GTU for various applications, competitive in the world market. The Enterprise welding production is currently capable of solving diverse technology tasks of any complexity.

STATE-OF-THE-ART OF DEVELOPMENT AND APPLICATION OF FLUX-CORED WIRES FOR WELDING OF CARBON AND LOW-ALLOYED STEELS

V.N. SHLEPAKOV, Yu.A. GAVRILYUK and **A.S. KOTELCHUK**
E.O. Paton Electric Welding Institute, NASU, Kiev, Ukraine

State-of-the-art in development of flux-cored wires for welding carbon and low-alloyed steels is considered. Main characteristics of flux-cored welding wires developed by the E.O. Paton Electric Welding Institute over the recent years, as well as properties of metal of the welds and welded joints made with these wires are presented. Recommended application field for these wires are listed.

Keywords: *arc welding, flux-cored wire, low-carbon and low-alloyed steels, state-of-the-art in development, application fields*

Mechanized and automatic flux-cored wire welding has become in the recent decade the main alternative to manual electrode arc welding and mechanized gas-shielded solid wire welding. Increase in consumption of flux-cored welding wires in the developed countries is explained by their evident engineering-and-economic advantages, such as high efficiency, excellent operating characteristics, consistent quality and guaranteed mechanical properties of the welds in welding of different-purpose steels. According to estimations, generalized indices of the volumes of production and application of flux-cored welding wires are at a level of 11 % in the Western Europe countries, 19 % in the USA, 27 % in Japan and more than 36 % in the Republic of Korea. The main areas of their application are shipbuilding, erection of drilling platforms, fabrication of structures and bridge construction, manufacture of tanks and vessels, and industrial and transport machine building.

Experts give the following estimates concerning distribution of the volumes of wires consumption by strength grades of steels. The share of wires for welding steels with yield strength of up to 500 MPa is 92 %, low-alloyed steels with yield strength above 500 MPa — 4 %, and steels designed for operation under low temperatures — around 2 %. The balance is a share of steels resistant to atmospheric corrosion, as well as other specialized steels. Consumption of flux-cored wires for welding of stainless steels is developing at an evident rate.

Development of an advanced technology for manufacture of flux-cored wires, meeting requirements of international quality standards, promoted progress in and increased application of flux-cored wire welding. The aim of the present article is to present the latest developments of domestic flux-cored wires, as well as areas of their effective application.

Metallurgical, technical and engineering-and-economic characteristics of flux-cored welding wires. Flux-cored wires are usually subdivided into classes, depending on the fact whether it is necessary to provide additional gas shielding of molten metal (gas-shielded) or there is no need in it (self-shielding). Respectively, according to the core composition, flux-cored wires are subdivided into gas-shielded, i.e. rutile, basic and metal-core (with metal type of the core), and self-shielding ones, i.e. carbonate- fluorite, oxide-fluoride, etc. As to their intended use, flux-cored wires are classified into wires of general and specialized application (in particular, wires for welding with forced weld formation).

Metallurgical advantages of flux-cored wires consist in a relatively easy and flexible adaptation of wire properties to composition and properties of steel being welded, as well as in providing the possibility of controlling heat input during welding. Utilization of special treatment of components of the wire core, wire surface treatment and deposition of protective coatings allow obtaining an invariably low level of the content of diffusible hydrogen in the weld metal below 5 $cm^3/100$ g [1].

Technological advantages of flux-cored wires are provided by a high arcing stability, low spattering of electrode metal and a convenient shape of the welds during welding in different spatial positions. Application of self-shielding flux-cored wires under field and erection conditions provides an easy welding process and flexibility, which are determined by the absence of the need to arrange additional shielding of molten metal. Besides, owing to a special sheath design and core composition, self-shielding flux-cores wires feature a higher efficiency of shielding of the molten metal during welding in open-air sites under the action of wind flows, compared with gas-shielded ones.

Engineering-and-economic advantages of flux-cored wires mainly lie in a high fusion efficiency provided by a high current density and extra filler material of the core (iron powder). The efficiency of fusion of flux-cored wires with a metal core amounts to 7.2–9.6 kg/h. An additional aspect is saving of power and heat, which are estimated to be at a level of 0.5–0.9 kW·h/kg of the deposited metal (Figure 1), if flux-cored wire welding is compared with solid wire welding. A more uniform radial penetration of metal [2–4] can be achieved when using flux-cored wires.

Hygienic and sanitary properties of modern flux-cored wires are at a level of those of solid wires (this applies, in particular, to flux-cored wires of rutile type and wires of metal-core type).

Classification requirements and properties of flux-cored wires for welding of different steel classes, as well as technical requirements to the flux-cored wires are unified in international standards ISO 17632:2004, ISO 17633:2004, ISO 18276:2005 and European standard EN 758, and in national standards AWS, DIN, JIS, GOST, DSTU, etc.

Most of the world producers use a technology of manufacture of the flux-cored wires from cold-rolled strips. In fact, the manufacture of wire is performed in one production line. It includes device for formation of the wire sheath (different designs) from a steel strip by continuously filling the formed profile with a mixture of powders and a multiple draw bench, where reducing of a wire to a finished size is carried out.

Advantages of such a technology include a small number of equipment pieces and personnel, low power consumption, and possibility of manufacturing a very wide range of wires with quick readjustment to a different wire type (high production flexibility). This technology was realized using different methods of reducing of billets and finishing treatment of the formed wire. The manufacture of wire from a tubular billet (seamless) requires a greater number of technological operations, this accordingly increasing production costs.

The complete technological cycle of manufacture of flux-cored wire with all the schemes includes a range of preparatory, intermediate, auxiliary and final operations, playing an important role in providing a quality product. Finished flux-cored wire is supplied in accordance with standardized methods of winding and packing (layer winding on spools or wire formers, or in containers of «Marathon» type according to EN 759). The quality assurance system (ISO standards) provides for the use of through inspection with accurate documentation of the procedures. This determines a wide application of up-to-date control technique, involving a qualified personnel and good analytic tooling of production. In particular, SE «Pilot Plant for Welding Consumables of the E.O. Paton Electric Welding Institute» uses devices for continuous control and monitoring of wire filling to realize inspection functions and documentation (Figure 2).

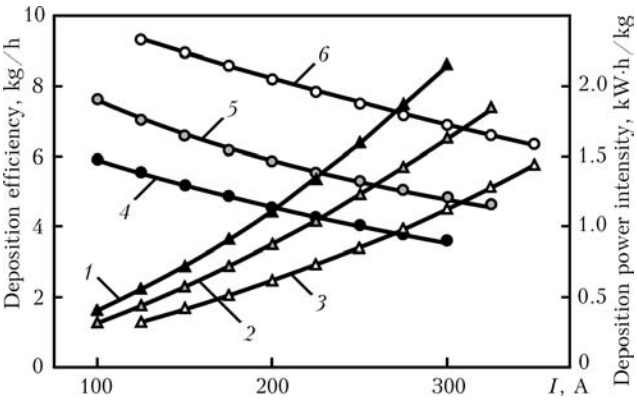

Figure 1. Typical indicators of deposition efficiency (*1–3*) and power intensity (*4–6*) in using flux-cored wires and solid wires 1.2 mm in diameter for mechanized welding: *1, 4* — flux-cored wire with metal core; *2, 5* — same with rutile core; *3, 6* — solid wire

Flux-cored wires for gas-shielded welding. New-generation flux-cored wires PP-AN59, PP-AN63 and PP-AN69 with a rutile core type, designed for welding of wide-application carbon and low-alloyed steels, and PP-AN61, PP-AN67 — for welding of high-strength low-alloyed steels were developed by the E.O. Paton Electric Welding Institute in the recent years according to European standard EN 758 and DSTU (GOST) 26271. These wires have a tubular design and are produced with diameters of 1.2 to 2.0 mm.

The wire world market is based on wires for CO_2 or Ar + CO_2 mixture welding of steels with yield strength of 400 to 500 MPa. Available are wires for welding of low-alloyed steels resistant to atmosphere corrosion and used at decreased temperatures. The scopes of application of wires for welding of steels

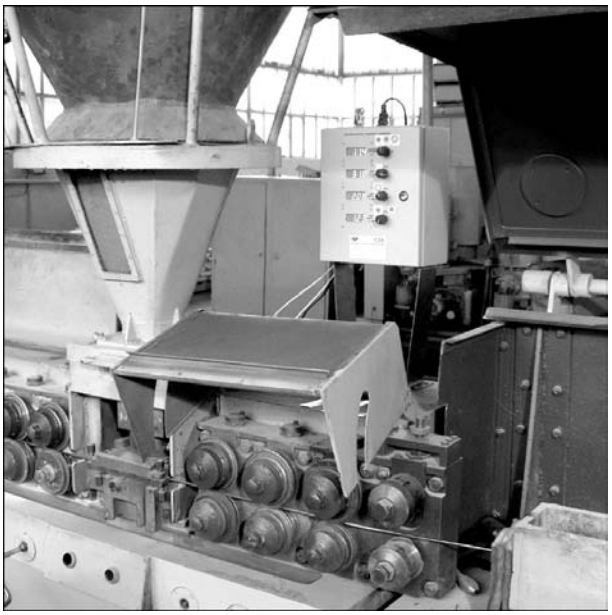

Figure 2. Device for monitoring of filling of the formed sheath of two-layer design flux-cored wire with a charge using a forming unit (SE «Pilot Plant for Welding Consumables of the E.O. Paton Electric Welding Institute»)

Table 1. Classification characteristics and properties of flux-cored wires for gas-shielded welding

Wire grade	Classification according to GOST 26271, EN 758 and AWS	Diameter, mm	Alloying system, wt.%	Guaranteed mechanical properties					
				σ_y, MPa	σ_t, MPa	δ, %	Correspondence to requirements for KCV_{min} = 35 J/cm^2 at temperature, °C		
							−20	−30	−40
PP-AN61	PG-49-A4U T46 4Z PCMI H5 E81T1-K2	1.2 1.4 1.6 2.0	0.06C 1.3Mn 0.4Si 1.6Ni	490	580	20			Yes
PP-AN63	PG-44-A2U T42 2PC1 H10 E71-T1	1.2 1.4 1.6 2.0	0.07C 1.3Mn 0.4Si	440	530	22	Yes		
PP-AN67	PG-59-A3V5 T59 3PC1 H5 E71-T1	1.2 1.4 1.6 2.0	0.08C 1.2Mn 0.4Si 1.2Ni 0.3Cr 0.3Mo	590	650	18		Yes	
PP-AN70M	PG-44-A3V T42 2MC3 H5 E71-T1	1.2 1.4 1.6 2.0	0.08C 1.4Mn 0.5Si	420	540	22	Yes		
PP-AN72	PG-48-A3V T48 5MC1 H5 E71-T1	1.2 1.4 1.6	0.08C 1.0Mn 0.3Si 2.2Ni	480	540	24			KCV_{min} = = 47 J/cm^2
PP-AN74	PG-59-A3V T59 5PC1 H10 E71-T1	1.2 1.4 1.6	0.06C 1.3Mn 0.4Si 2.5Ni 0.4Mo	590	680	24			Same

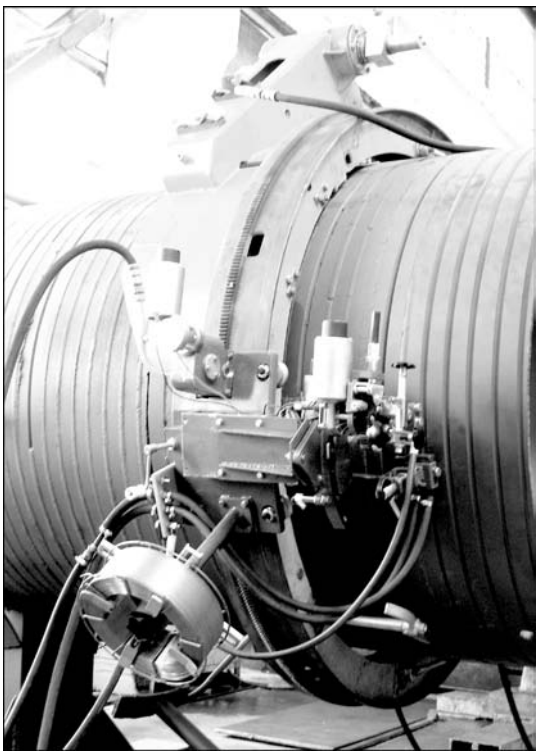

Figure 3. Welding machine of new-generation system «Styk» for automatic arc flux-cored wire position butt welding of large-diameter pipes with forced weld formation (manufacturer — OJSC «Kakhovka Plant of Electric Welding Equipment»)

with yield strength of up to 700 MPa increasing every year.

Widening of application of the metal-core wires relates to advancements in automated and robotic welding processes. The new wires providing good shape of the welds, low level of spattering and fumes can be used for welding in all spatial positions. Metal-core wires PP-AN70, PP-AN70M, PP-AN72 and PP-AN74, which demonstrate higher welding-technological properties than Sv-08G2S, were developed for automated and robotic welding in ship and machine building. Some characteristics of these flux-cored wires are given in Table 1. Manufacture of above flux-cored wires was mastered at SE «Pilot Plant for Welding Consumables of the E.O. Paton Electric Welding Institute».

Gas-shielded tubular-design flux-cored wires of the PP-AN61, PP-AN63, PP-AN72 and PP-AN74 grades are designed for semi-automatic welding, and the PP-AN70M grade wire, in addition, — for automatic (robotic) welding of low-carbon and low-alloyed steels. Wires of PP-AN70M, PP-AN72 and PP-AN74 grades are of a metal-core type. Ar + CO_2 (80 + + 20 %) gas mixture is recommended to for use as a shielding atmosphere for welding with these wires. CO_2 or Ar + CO_2 mixture can be used as a shielding

Table 2. Classification characteristics and properties of metal deposited with self-shielding flux-cored wires

Wire grade	Classification according to GOST 26271, EN 758 and AWS	Diameter, mm	Alloying system, wt.%	Guaranteed mechanical properties of deposited metal					
				σ_y, MPa	σ_t, MPa	δ, %	Correspondence to requirements of KCV_{min} = 35 J/cm^2 at temperature, °C		
							–20	–30	–40
PP-AN3	PS-44-A3N T42 3ZS3 H10 E70-TG	2.8 3.0	0.09C 1.2Mn 0.35Si	440	560	22		Yes	
PP-AN7	PS-44-A3V T42 3ZS3 H10 E71-TG	2.4	0.08C 1.1Mn 0.35Si	440	540	22		Same	
PP-AN60	PS-49-A3V T49 3ZS3 H10 E71-TG	1.2 1.4 1.6	0.08C 1.1Mn 1.3Ni 0.8Al	490	590	22			Yes

Table 3. Classification characteristics and properties of specialized self-shielding flux-cored wires

Wire grade	Classification according to GOST 26271, EN 758 and AWS	Diameter, mm	Alloying system, wt.%	Guaranteed mechanical properties of deposited metal					
				σ_y, MPa	σ_t, MPa	δ, %	Correspondence to requirements of KCV_{min} = 35 J/cm$_2$ at temperature, °C		
							–20	–30	–40
PP-AN19N	PS-39-A2(R)VP T42 2ZS3 H5 EG72-TG	2.4 3.0	0.09C 1.4Mn 0.4Si 0.5Ni	390	520	22	Yes		
PP-AN30	PS-54-AZUP — Corresponds to E81-TG	2.4	0.07C 1.7Mn 0.5Si 0.4Mo 0.07V	540	630	18			Yes
PP-AN30VS	PS-57-AZUP — Corresponds to E91-TG	2.0 2.4	0.07C 1.7Mn 0.5Si 0.6Ni 0.5Mo	570	690	18			KCV_{min} = = 47 J/cm^2

gas in welding with wires of the PP-AN61 and PP-AN63 grades.

The main areas of application of new-generation flux-cored wires for gas-shielded welding are as follows. The PP-AN61 grade wire is used in manufacture of railway cars, in machine building, manufacture of equipment designed for operation under conditions of high alternating loads and abrasive wear, welding of vessels and metal structures of different application, and in ship building; PP-AN63, PP-AN72 and PP-AN74 wires — for welding in all spatial positions in ship building, construction and fabrication of metal structures; PP-AN70M wire — for welding in flat position and on a horizontal plane in making filling welds for machine building and manufacture of vehicles and metal structures.

Self-shielding flux-cored wires. Primarily the USA and CIS countries were active in development and manufacture of flux-cored wires on commercial scales. The product line (quantity of grades) has been reduced in the last two decades as a result of decrease in output of wires with unreliable technological characteristics. An interest of the world market to this

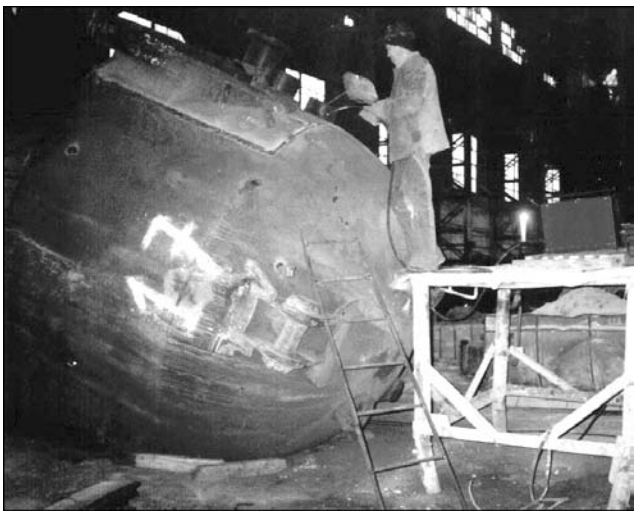

Figure 4. Repair welding of metallurgical equipment with flux-cored wire PP-AN7 at OJSC «F. Dzerzhinsky Dneprovsky Metallurgical Works, Dneprodzerzhinsk [5]

Figure 5. PP-AN9N flux-cored wire welding with forced formation of vertical butt joints on snap structures of Podolsko-Voskresensky Bridge over the Dnieper River in Kiev

class of the wires remains at a rather high level. In particular, this relates to building and erection operations (construction of pipelines, tanks, metallurgical units, bridges, industrial engineering and ship building). Wires for welding of steels with 400–500 MPa yield strength make the production basis. Wires for welding of pipelines make up a separate group. In addition to well-known wires of the two-layer design, self-shielding tubular flux-cored wires of small diameter with a core of fluoride-basic type were also developed by the E.O. Paton Electric Welding Institute. The core composition allows decreasing the silicon and aluminum content in the weld metal and provides the required value of impact toughness of welded joints at low temperatures.

Wires for welding with forced weld formation (electric gas welding) make an important subgroup of this class of wires. Growing demand for such wires in the CIS countries, in particular in Russia, is observed at present. The key customers are constructors of bridges, tanks and metallurgical facilities. Operation of new-generation pipe welding systems «Styk» (Figure 3) is being mastered.

Characteristics of some self-shielding flux-cored wires developed by the E.O. Paton Electric Welding Institute are given in Tables 2 and 3. PP-AN3 and PP-AN7 self-shielding flux-cored wires of a two-layer design are intended for semi-automatic welding of low-carbon and low-alloyed steels with thickness more than 5 mm. Wire PP-AN3 is applied for welding of road building machines, industrial equipment and building metal structures, and wire PP-AN7 — for welding of industrial equipment, in transport machine building, construction of off-shore structures and repair of industrial equipment (Figure 4).

Self-shielding tubular flux-cored wire PP-AN60 is recommended for semi-automatic welding in all spatial positions in manufacture of technological equipment, transport and hoisting devices, construction of drilling platforms and building structures.

PP-AN19N self-shielding flux-cored wire of a two-layer design is meant for automatic electric gas welding of low-carbon and low-alloyed steels with thickness of 8 up to 32 mm. It is mainly used with a process of welding of vertical butt joints by the downward method for construction of different metal structures, including vessels, ships, barges, span structures of bridges, tanks and bunkers (Figure 5).

PP-AN30 and PP-AN30VS self-shielding flux-cored wires of a two-layer design were developed for automatic erection welding of butt joints in pipes with 520 to 1420 mm diameter by using forced weld formation (electric gas process). Wire PP-AN30VS can be used for welding of butt joints in pipes of low-alloyed steels of the X80 strength class.

Ii should be noted in conclusion that rapid development of the market of consumption of flux-cored wires is an evidence of a high potential of arrangement of up-to-date productions for this type of welding consumables. Preference is given to production of wires with better operating characteristics, low metal losses for spattering and low emission of welding fumes. Structure of the world consumption, where small-diameter wires for welding of mass-application steels and increased-strength steels make the biggest shares, is to be taken into account in selection of production programs. Owing to successful accomplishment of the innovative project initiated by the National Academy of Sciences of Ukraine, SE «Pilot Plant for Welding Consumables of the E.O. Paton Electric Welding Institute» achieved the level of manufacture of flux-cored wires, which meets the up-to-date requirements for assurance of the quality of products, through upgrading of equipment and improvement of the technological process. Flux-cored wires of a new product line correspond to international standards and are competitive in the world market in their technical characteristics and quality. At the same time, the technology for their manufacture makes it possible to orient mainly to the raw materials base of Ukraine.

1. Pokhodnya, I.K. (2008) Metallurgy of arc welding of structural steels and welding consumables. *The Paton Welding J.*, **11**, 54–64.
2. Shlepakov, V.N. (2004) Current methods for investigation, prediction and estimation of properties of welding flux-cored wires. In: *Welding Consumables. Development. Technology. Manufacturing Quality:* Proc. of 3rd Int. Conf. on Welding Consumables of CIS countries. Dnepropetrovsk, 2004.
3. Shlepakov, V.N., Naumejko, S.M. (2005) Self-shielded flux-cored wires for welding low-alloy steels. *The Paton Welding J.*, **4**, 28–30.
4. Shlepakov, V.N., Kotelchuk, A.S., Naumejko, S.M. et al. (2005) Influence of the composition of flux-cored wire core and shielding gas on the stability of arc welding process. *Ibid.*, **6**, 16–20.
5. Shlepakov, V.M., Ignatyuk, V.M., Kotelchuk, O.S. et al. (2006) Mechanized repair flux-cored wire welding of units of metallurgical complex. In: *Problems of resource and safety service of structures, constructions and machines*. Kyiv: PWI.

FEATURES OF CONSUMABLE ELECTRODE PULSED-ARC WELDING OF ALUMINIUM ALLOYS WITHOUT APPLICATION OF FORMING BACKING ELEMENTS

V.S. MASHIN and **M.P. PASHULYA**
E.O. Paton Electric Welding Institute, NASU, Kiev, Ukraine

Technological features of automatic one-sided consumable electrode pulsed-arc welding in argon of butt joints of sheet aluminium alloys AMg6 and 1915T up to 3 mm thick without application of forming backing elements («gravity» welding) were studied. Influence of welding mode parameter modulation on the geometrical shape of welds and their macrostructure was shown. Recommendations on «gravity» welding technology are given.

Keywords: *consumable electrode welding, sheet aluminium alloys, pulsed arc, welding parameter modulation, butt joints, weld geometry, joint macrostructure*

It is known that consumable electrode pulsed-arc welding in inert gases of aluminium alloys compared to consumable electrode steady-arc welding allows improvement of weld formation, increasing the penetration depth of metal being welded, stabilizing the process of electrode metal drop transfer, burning out (evaporation) of low-boiling alloying elements from electrode wire and improvement of mechanical properties of welded joints [1–4].

Over the last decade welding machines, which include pulsed power sources with synergic control of the process of electrode metal drop transfer with maintenance of synchronous process of «one pulse — one drop» and push–pull type mechanisms have become widely accepted abroad for consumable electrode pulsed-arc welding [3–5]. Such power sources of the type of TransPulseSynergic (TPS) are designed for automated and robotic lines for consumable electrode pulsed-arc welding of various-purpose products and allow performance of single-pass welding of thin metal [5].

To prevent metal burn-through and for sound formation of weld back bead in consumable electrode steady-arc welding and consumable electrode pulsed-arc welding of aluminium alloy structures, removable forming backing elements (FBE) from stainless steel with grooves of various diameters of segment, rectangular or triangular shape are used [5, 7]. In case it is impossible to apply removable FBE from steel, permanent backing elements made from sheet material of composition close to that of the metal being welded are used. Such FBE are tack-welded to one of the sides of the abutted sheet and remain on the structure after lock welding.

Aluminium panels are used very often for fabrication of welded structures. In these extruded panels a «protrusion» having the function of remaining FBE, is already envisaged on one side [8]. However, not all the aluminium alloys can be extruded, and the extruded panels proper are much more expensive than the rolled sheet in terms of manufacturing cost. In addition, all the permanent FBE can essentially increase the weldment weight.

Consumable electrode pulsed-arc welding without FBE application («gravity» welding) can be regarded as an energy-saving technology, as it allows elimination of FBE material costs, time for its fabrication, as well as lowering the total power consumption. The main factor restraining the wide application of welding without FBE is the possibility of metal burns-through formation [9], because of absence of special electric welding equipment.

In this connection in most of the cases aluminium alloy joints produced in «gravity» position (particularly, at relatively large and extended gaps in the butts) are made by manual nonconsumable electrode argon-arc welding or semi-automatic consumable electrode steady-arc welding. The welder monitors shrinkage of weld pool liquid metal and makes the arc longer to lower welding current and/or increases the welding speed. Such manual manipulations keep the welding operator in continuous physical tension and do not always provide a satisfactory formation of welds in «gravity» welding.

In terms of thermal physics, joint burn-through in welding is determined by mobility of liquid metal, which depends on weld pool temperature and action of internal and external forces, namely pool metal gravity and welding arc pressure [10]. The only counteraction to liquid pool running out is the metal surface tension force and strength of oxide elastic film, formed from the weld root side. Its strength is inversely proportional to deformation and under certain conditions it is equal to zero, thus leading to burn-through formation [10, 11]. It is experimentally established that it is possible to select the necessary mode of automatic consumable electrode steady-arc welding, at which an equality of counteracting forces is observed. However, such an equilibrium condition is highly unstable because of the presence of gaps of different size in the abutted elements, and action of

random external disturbances. In practice, in order to improve the stability of welding process performed in the «gravity» position, forced oscillations (modulation) of its parameters, namely arc voltage (welding current) and welding speed, are most often applied. Periodical modulation of one of them leads to changes of weld pool temperature and dimensions, as well as arc pressure [10–13], thus allowing variation of heat input into the metal being welded, controlling the speed of pool metal solidification and, thus, performing welding without FBE application.

The simplest method to control heat input into the metal being welded is modulation of one of the parameters, namely power source output voltage U_a, welding speed v_w or electrode wire feed rate $v_{w.f}$ at other welding process parameters being constant [14].

Equipment with synergic control of the process of consumable electrode pulsed-arc welding is becoming widely accepted now. In this equipment the output parameters of the welding power unit and electrode wire feed rate are electrically interconnected by a synergic equation [4]. Interrelation of power source output voltage U_a with $v_{w.f}$ can allow a periodical transition from higher to lower welding mode, using an additional modulator, connected into the circuit of wire movement electric drive. A similar welding process can be achieved also, when using a current source and electric drive of welding wire feed, not connected electrically to each other, but synchronized by modulation.

Monitoring heat input into the metal being welded in welding without FBE application can be achieved also at a simultaneous variation of two or three parameters of the welding process, both when using synergic equipment, and regular equipment with separately operating functional components of the system for consumable electrode pulsed-arc welding. It should be noted that because of the presence of inertia links in the electric control circuits the modulated parameters of the welding process change not jump-like, but by an exponential law, taking into account the time constant of their electric circuits. The different rate of increase (decrease) of modulated parameters, which affects weld bead formation, requires preliminary lengthy adjustment of welding modes. Therefore, controlling three parameters of the welding process is irrational, if positive effect can be achieved at their smaller number. It should be noted that the process of consumable electrode steady-arc welding of sheet aluminium alloys proper is much more difficult to perform that the nonconsumable electrode welding process, and even more so in «gravity» welding of metal with relatively large gaps in the sheets being joined. Therefore, in keeping with GOST 14806–80, developed at the start of 1970s and still valid now, the process of consumable electrode steady-arc welding of aluminium alloys can be applied only for elements of not less than 3 mm thickness for butt and tee joints, and not less than 4 mm thickness for fillet and overlap joints.

The purpose of these investigations was improvement of the equipment and determination of the features of the technology of automatic one-sided consumable electrode pulsed-arc welding in argon without FBE application, allowing a satisfactory weld formation to be achieved in joints of aluminium alloys less than 3 mm thick.

Experimental procedure. Aluminum alloys AMg6 1.8 mm thick, 1915T 2.8 mm thick (GOST 4784–74) and welding wires SvAMg6 (GOST 7871–75) of 1.0, 1.2 and 1.6 mm diameters were used to conduct investigations. Highest grade argon was used as shielding gas. Consumable electrode pulsed-arc welding of butt joints was performed using Fronius TPS-450 power source on ASTV-2M welding head. Before welding plates of $400 \times 150 \times \delta$ mm size were subjected to chemical etching and scraping of the edges and

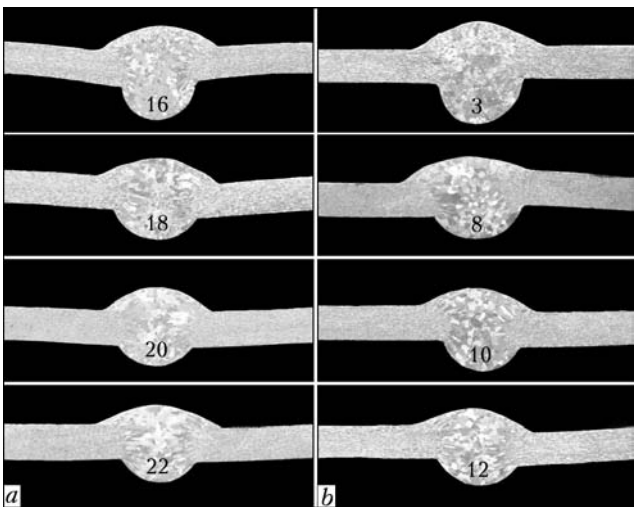

Figure 1. Macrostructure (×3) of welds, depending on modes of welding AMg6 alloy with 1.2 mm wire with $v_{w.f}$ (*a*) and v_w (*b*) modulation. Here and further the numbers on sections correspond to sample numbers

Table 1. Modes of welding AMg6 alloy with 1.2 mm wire with $v_{w.f}$ and v_w modulation

Sample #	I_w, A	U_a, V	v_w, m/h	$v_{w.f}$, m/min	$\bar{w}_{h.in}$, kJ/cm
$v_{w.f}$ modulation					
16	57–60	17.1–17.2	18	3.7–4.0	1.440
18	66–70	17.2–17.5	27	4.3–4.6	1.129
20	75–79	17.5–17.7	36	4.8–5.1	0.976
22	85–89	18.0–18.2	45	5.4–5.7	0.907
24	95–99	18.4–18.7	53	5.8–6.1	0.878
v_w modulation					
3	59	17.8	16–18	4.0	1.600
8	70	18.0	25–28	4.6	1.232
10	80	18.3	34–37	5.1	1.069
12	89	18.5	41–44	5.7	1.004
14	96	18.8	47–51	6.0	0.955

Table 2. Modes of welding AMg6 alloy with 1.0 mm wire with $v_{w.f}$ and v_w modulation

Sample #	I_w, A	U_a, V	v_w, m/h	$v_{w.f}$, m/min	$w_{h.in}$, kJ/cm
$v_{w.f}$ modulation					
28	56–61	15.4–15.7	20	5.0–5.3	1.175
30	72–78	16.7–17.0	40	6.5–7.0	0.816
31	84–89	17.1–17.5	50	7.5–7.9	0.776
32	94–99	17.6–17.9	60	8.3–8.7	0.742
v_w modulation					
34	61	15.6	19–22	5.3	1.203
35	71	16.6	29–32	6.2	1.002
36	77	17.0	40–43	7.0	0.818
37	89	17.4	48–52	7.9	0.803

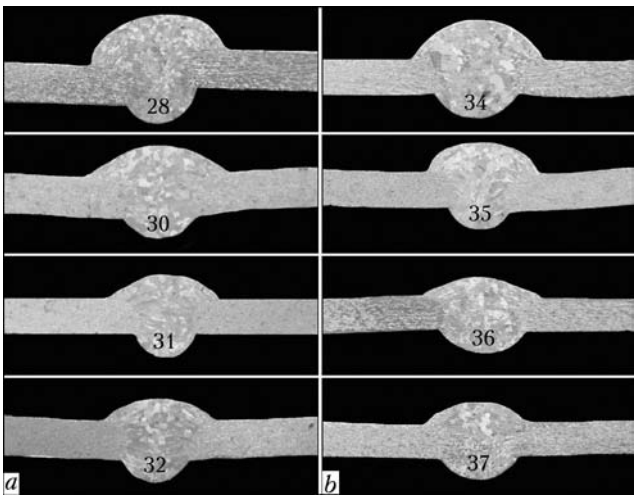

Figure 2. Macrostructure (×3) of welds, depending on modes of welding AMg6 alloy with 1.0 mm wire with $v_{w.f}$ (*a*) and v_w (*b*) modulation

HAZ from both sides. Abutted plates were tack-welded on the edges by manual nonconsumable electrode welding and a fixture with a groove of 50 × × 15 mm size was mounted, thus simulating «gravity» welding.

To study the influence of gaps on weld root formation in the plates, recesses of 0.25 × 90 and 0.5 × × 90 mm size were cut out in the metal from the side of abutted edges, this corresponding to the total gap in the assembled butt joint of 0.5 and 1.0 mm. Distance between the recesses was 50 mm. This eliminated considerable shrinking of the edges during welding and allowed maintaining a constant gap in the joints.

Angle of welding head inclination to the metal was 10–12°, distance between the torch nozzle and metal being welded was 10 mm, with argon flow rate of 15–20 l/min. Geometrical parameters of welds (width B and height H of weld reinforcement, as well as width b and height h of weld root) were determined on transverse macrosections with up to ±0.1 mm accuracy. Values of welding process heat input $w_{h.in}$ were calculated allowing for the fact that arc effective efficiency in argon is 0.72. Welding wire consumption P_{wire} in welding one running meter of weld was also determined.

To perform modulation of one or several parameters of the welding process, a device was proposed, allowing the necessary switching to be performed in electric control circuits of U_a, $v_{w.f}$ and v_w. This device was a programmable electronic time relay with an infinite cycle number and three-channel output. Each output was a key with a variable resistor connected to it in parallel, which was connected into the break of electric circuit in series with the main resistor — device controlling parameters U_a, $v_{w.f}$ and v_w, respectively. During performance of consumable electrode pulsed-arc welding of aluminium alloys without FBE, two programmable time relays RV-3 and RV-8 with three- or eight-channel output assembled by pulse–pair circuit were used. Continuous modulation period was 2.2 ± 0.2 s at 1.1 ± 0.1 s duration of increase or

Table 3. Modes of welding 1915T alloy with 1.0 mm wire with $v_{w.f}$ and v_w modulation

Sample #	I_w, A	U_a, V	v_w, m/h	$v_{w.f}$, m/min	$w_{h.in}$, kJ/cm
$v_{w.f}$ modulation					
120	72–76	17.1–17.3	20	2.5–2.8	1.650
130	87–92	17.0–17.8	30	2.8–3.1	1.346
140	101–106	17.9–18.1	40	3.4–3.5	1.207
150	115–119	18.5–18.7	49	3.7–3.8	1.151
160	126–130	19.5–19.6	57	4.1–4.2	1.135
v_w modulation					
220	77	17.3	20–22	2.8	1.644
230	92	17.5	30–32	3.2	1.346
240	106	18.4	40–43	3.5	1.218
250	119	18.7	49–52	4.0	1.142
260	131	19.2	54–57	4.2	1.174

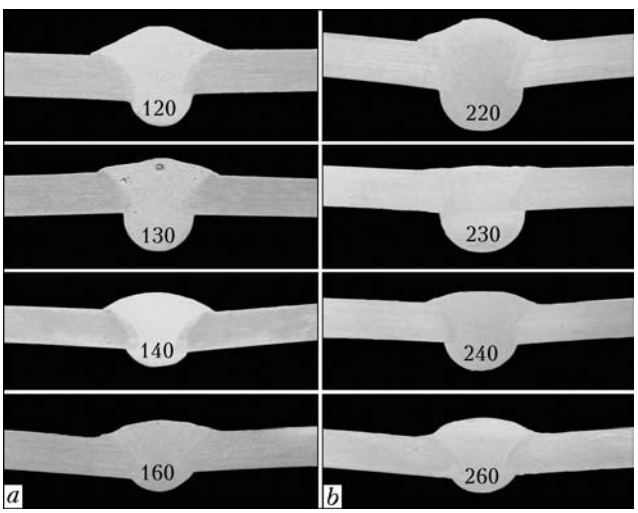

Figure 3. Macrostructure (×3) of welds, depending on modes of welding 1915T alloy with 1.6 mm wire with $v_{w.f}$ (*a*) and v_w (*b*) modulation

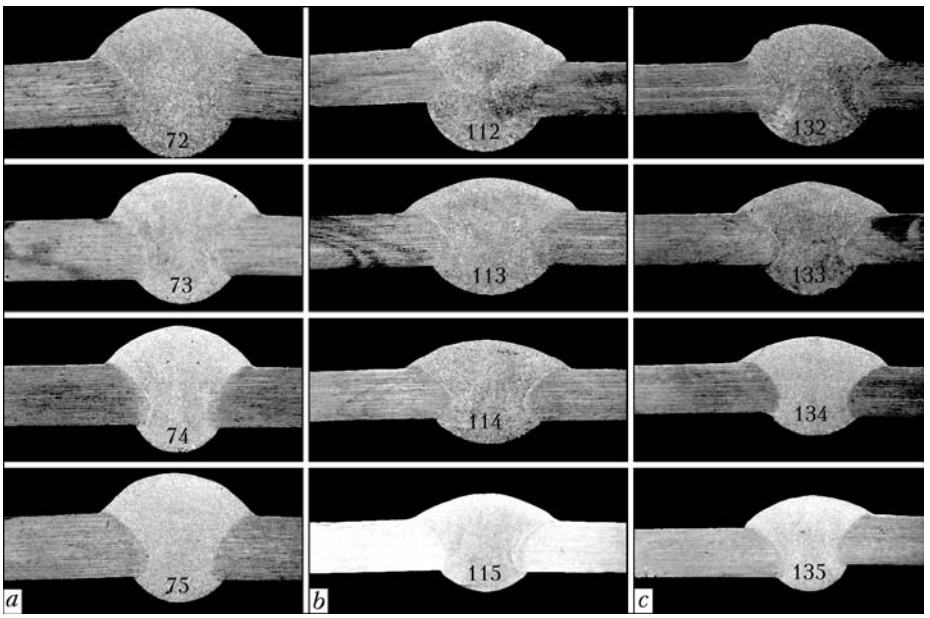

Figure 4. Macrostructure (×4) of welds, depending on modes of welding 1915T alloy with 1.2 mm wire with U_a modulation (*a*), with simultaneous $v_{w.f}$ and v_w modulation (*b*) and with simultaneous U_a, $v_{w.f}$ and v_w modulation (*c*)

decrease of modulated values. Frequency F_p of welding current pulses generated by TPS-450 machine corresponded to value $F_p = KI_w$, Hz, where K is the coefficient of proportionality, dependent on electrode wire grade and diameter and equal to 0.9–1.3 Hz/A for SvAMg6 wire of 1.2 mm diameter.

Experimental results. Table 1 gives the modes of consumable electrode pulsed-arc welding of AMg6 alloy with wire of 1.2 mm diameter with $v_{w.f}$ and v_w modulation, and Figure 1 gives the macrostructures of welds made in these welding modes. In the range of the above values of consumable electrode pulsed-arc welding modes change of $v_{w.f}$ by 0.3 m/min and of v_w by 3 ± 1 m/h (during modulation period of 2.2 ± ± 0.2 s) allows adjustment of the rate of metal solidification in the weld root part and producing joints without burns-through. Here, the most satisfactory weld formation on AMg6 alloy of 1.8 mm thickness can be achieved at $I_w > 85$ A and $v_w >> 45$ m/h.

Approximately the same dependencies are observed also at consumable electrode pulsed-arc welding of AMg6 alloy with 1.0 mm diameter wire (Table 2 and Figure 2) with modulation of $v_{w.f}$ (Figure 2, *a*) and v_w (Figure 2, *b*). Analysis of the data given in Tables 1, 2 and in Figures 1, 2 leads to the conclusion that in one modulation period increase of $v_{w.f}$ by 0.3–0.4 m/min leads to increase of I_w by 4–5 A and of U_a by 0.2–0.4 V. Irrespective of welding parameter, which is modulated, optimum formation of weld root is achieved at $w_{h.in} \le 0.8$ kJ/cm using 1.0 mm diameter wire.

Table 3 gives the modes of consumable electrode pulsed-arc welding of 1915T alloy with 1.6 mm wire without application of FBE and with modulation of $v_{w.f}$ and v_w, and Figure 3 gives the macrostructures of welds produced in these welding modes. In the entire range of the above modes of consumable elec-

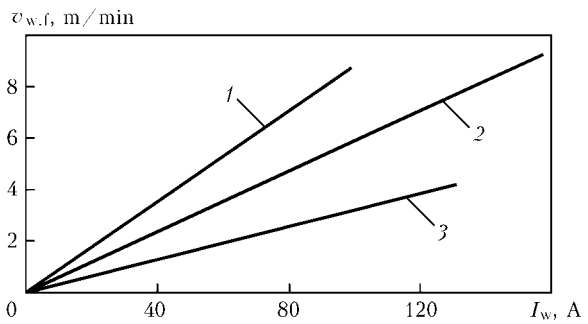

Figure 5. Interaction of values of welding current and feed rate of SvAMg6 electrode wire of 1.0 (*1*), 1.2 (*2*) and 1.6 (*3*) mm diameter

Table 4. Modes of welding 1915T alloy with 1.2 mm wire with U_a modulation, with simultaneous $v_{w.f}$ and v_w modulation and with simultaneous U_a, $v_{w.f}$ and v_w modulation

Sample #	I_w, A	U_a, V	v_w, m/h	$v_{w.f}$, m/min	$w_{h.in}$, kJ/cm
U_a modulation					
72	76–78	16.6–17.0	18	4.9	1.862
73	91–93	17.4–17.8	27	5.7	1.554
74	105–107	18.6–18.9	36	6.5	1.427
75	116–118	20.1–20.3	45	7.3	1.561
$v_{w.f}$ and v_w modulation					
112	75–79	17.6–17.8	15–18	4.6–4.9	2.141
113	88–92	18.5–18.7	23–27	5.3–5.6	1.736
114	101–105	19.3–19.4	36–41	6.1–6.4	1.338
115	115–118	20.1–20.3	47–49	6.9–7.2	1.265
U_a, $v_{w.f}$ and v_w modulation					
132	71–75	16.7–17.2	15–18	4.6–4.8	1.938
133	87–89	17.3–17.6	23–27	5.2–5.5	1.588
134	97–101	18.1–18.4	36–41	5.9–6.2	1.213
135	109–111	19.1–19.4	47–49	6.6–6.8	1.140

Table 5. Modes of welding 1915T alloy with 1.2 mm wire with $v_{w.f}$ modulation

Sample #	I_w, A	U_a, V	v_w, m/h	$v_{w.f}$, m/min	$w_{h.in}$, kJ/cm
320	76–79	17.9–18.1	18	4.8–5.1	1.996
330	87–91	18.6–18.8	27	5.4–5.7	1.580
340	101–105	20.0–20.3	36	6.2–6.5	1.490
350	111–115	20.3–20.6	45	6.8–7.1	1.328
360	122–126	21.2–21.4	53	7.3–7.6	1.292

Table 6. Modes of welding 1915T alloy with 1.2 mm wire with v_w modulation

Sample #	I_w, A	U_a, V	v_w, m/h	$v_{w.f}$, m/min	$w_{h.in}$, kJ/cm
420	77	18.3	16–18	5.1	2.148
430	88	19.0	24–27	5.7	1.700
440	102	19.5	33–36	6.3	1.497
450	115	20.6	42–45	7.1	1.411
460	132	21.5	51–53	8.0	1.415

trode pulsed-arc welding change of $v_{w.f}$ by 0.1–0.3 m/min and of v_w by 2–3 m/h allows achieving a satisfactory weld root formation without burns-through of the joints. Optimum geometrical dimensions of welds can be achieved at $I_w \geq 120$ A, $v_w \geq$ ≥ 45 m/h and $w_{h.in} < 1.15$ kJ/cm.

Table 4 gives the modes of consumable electrode pulsed-arc welding of 1915T alloy by 1.2 mm diameter wire with U_a modulation, with simultaneous modulation of two parameters ($v_{w.f}$ and v_w) and with simultaneous modulation of three parameters (U_a, $v_{w.f}$ and v_w), and Figure 4 gives macrostructures of welds

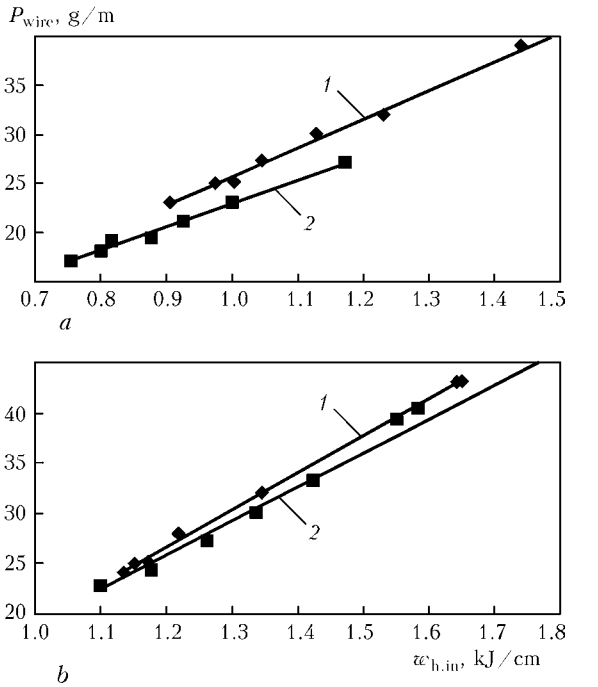

Figure 6. Influence of heat input of the welding process and electrode wire diameter on deposited metal consumption per one running meter of weld: *a* — AMg6 alloy, 1.2 (*1*) and 1.0 (*2*) mm wire; *b* — 1915T alloy, 1.6 (*1*) and 1.2 (*2*) mm wire

made in these modes. At continuous modulation of U_a within 0.2–0.4 V (as a result of changing the power source idle travel) value of I_w decreases only slightly, and arc length is increased, thus allowing a certain smoothing of the rippled surface of welds. At simultaneous modulation of two or three parameters, the process of weld formation is more stable. Irrespective of the number of parameters, which are simultaneously modulated, optimum formation of weld roots in 1915T alloy is observed at $w_{h.in} < 1.1$ kJ/cm.

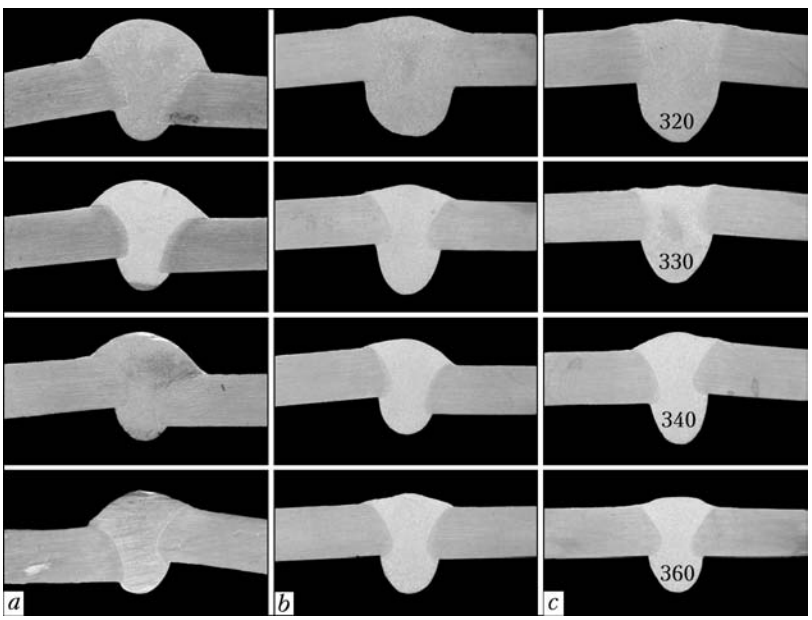

Figure 7. Weld formation, depending on modes of welding 1915T alloy with 1.2 mm wire with $v_{w.f}$ modulation in joints without a gap (*a*) and with 0.5 (*b*) and 1 (*c*) mm gap

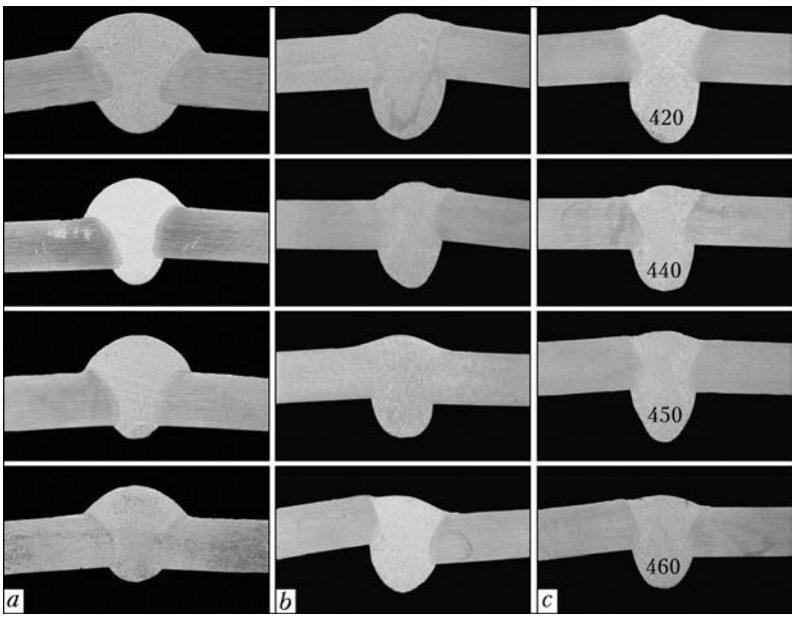

Figure 8. Weld formation, depending on the modes of welding 1915T alloy with 1.2 mm wire with v_w modulation in joints without a gap (*a*) and with 0.5 (*b*) and 1 (*c*) mm gap

Analysis of the modes of consumable electrode pulsed-arc welding of AMg6 and 1915T alloys given in Tables 1–4 showed that at any random disturbances of electrode wire feed rate, for instance, at abrupt increase of $v_{w.f}$ by 1 m/min, I_w value will change differently: for 1.0 mm diameter wire I_w will increase by 10 A, at 1.2 mm diameter — by 16 A, and at 1.6 mm diameter — by 30 A (Figure 5). The larger the diameter of wire of SvAMg6 grade, the greater I_w «jump» and the greater the probability of burn-through formation, which is one of the causes accounting for the rationality of application of small wire diameters in «gravity» welding.

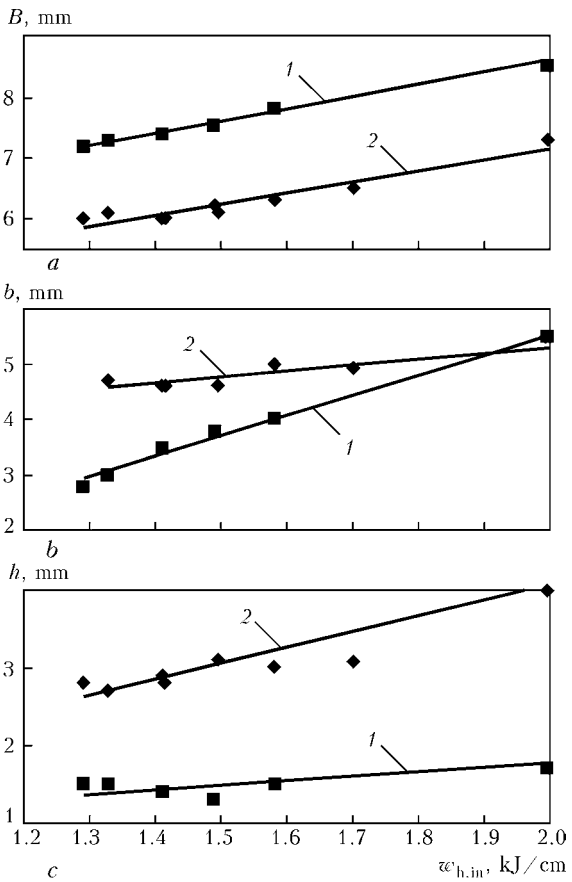

Figure 9. Influence of heat input of the process of welding 1915T alloy and gap (*1* — 0; *2* — 1 mm) in butt joints on the width of weld reinforcement (*a*), width (*b*) and height *h* of penetration root (*c*)

The cause for effectiveness of application of small diameter wires also is lowering of the weight of pool liquid metal and reduction of the time of metal solidification and of weld root «sagging» under the joint. Figure 6 shows welding wire consumption in consumable electrode welding of one running meter of the weld depending on $\varpi_{h.in}$ and wire diameter. At the same heat input into the metal being welded, the minimum pool mass forms, when 1.0 mm wire is used, and the higher $\varpi_{h.in}$ of the process of welding AMg6 alloy obtained at minimum values of I_w and v_w, the more noticeable is this difference.

Assessment of the influence of gap values in the abutted joints on stability of weld root formation and development of through-thickness burns-through of the metal is of special interest in consumable electrode pulsed-arc welding, particularly, of thinner sheet aluminium alloys. «Gravity» welding of 1915T alloy with wire of 1.2 mm diameter with modulation of $v_{w.f}$ (Table 5) and v_w (Table 6) was performed at the same modes at different width of artificially made gaps in the joints. Macrostructures of welds made with modulation of $v_{w.f}$ and v_w at different gaps are given in Figures 7 and 8. It is established that modulated control of the heat input allows at even relatively large gaps in the joints (more than 10 % of welded metal thickness) containing the liquid metal in the pool and prevents its flowing out of the weld root. Irrespective of $\varpi_{h.in}$ value gaps in the joints lead to reduction of the width and height of weld face reinforcement and greatly increase the width and height of its root part (Figure 9).

CONCLUSIONS

1. Modulation of the main parameters of the mode of consumable electrode pulsed-arc welding of sheet aluminium alloys allows periodically changing the heat input into the metal being welded, controlling the pool metal solidification and obtaining a reliable weld root formation without application of FBE at «gravity» welding.

2. Electronic devices additionally connected to systems of TransPulseSynergic type allow performing a separate or simultaneous modulation of consumable electrode pulsed-arc welding parameters, namely U_a, I_w, $v_{w.f}$ and v_w. Continuous modulation with the period of 2.2 ± 0.2 s allows performing automatic welding of butt joints in «gravity» position in case of extended (up to 90 mm) local gaps up to 1 mm wide.

3. In consumable electrode pulsed-arc welding without application of FBE it is rational to apply relatively thin electrode wires: 1.2 mm wire for 2.5–3.0 mm metal, and 1.0 mm diameter wire for less than 2.0 mm metal.

1. Mashin, V.S., Pavshuk, V.M., Dovbishchenko, I.V. et al. (1991) Influence of the conditions of pulsed-arc welding of AD0 aluminium on shape and porosity of welds. *Avtomatich. Svarka*, **4**, 57–60.
2. Zhernosekov, A.M., Andreev, V.V. (2007) Consumable electrode pulsed-arc welding (Review). *The Paton Welding J.*, **10**, 40–43.
3. Ishchenko, A.Ya., Mashin, V.S., Pashulya, M.P. (2005) Technological features of twin-arc consumable electrode pulsed welding of aluminium alloys. *Ibid.*, **1**, 10–14.
4. Voropaj, N.M., Ilyushenko, V.M., Lankin, Yu.N. (1999) Specifics of pulsed-arc welding with synergic control of parameters. *Avtomatich. Svarka*, **6**, 26–31.
5. Mashin, V.S., Pashulya, M.P., Shonin, V.A. et al. (2010) Consumable electrode pulsed-argonarc welding of thin-sheet aluminium alloys of 1–3 mm thickness (to be publ.).
6. Rabkin, D.M., Ignatiev, V.G., Dovbishchenko, I.V. (1982) *Arc welding of aluminium and its alloys*. Moscow: Mashinostroenie.
7. Zubrienko, G.L., Tenenbaum, F.Z., Petrovanov, V.M. et al. (1977) About some factors influencing the formation of oxide inclusions in welds of AMg6 alloy. *Svarochn. Proizvodstvo*, **5**, 24–27.
8. (2003) TIME TWIN as the highly efficient welding process. *Avtomatich. Svarka*, **4**, 39–42.
9. Shneerson, V.Ya. (2008) On the nature of burn-through of thin-sheet joints in welding. *Svarshchik*, **5**, 44–45.
10. Frolov, V.V. (1970) *Theoretical principles of welding*. Moscow: Vysshaya Shkola.
11. Yavorsky, B.M., Detlaf, A.A. (1980) *Reference book on physics*. Moscow: Nauka.
12. Ishchenko, A.Ya., Mashin, V.S., Dovbishchenko, I.V. et al. (1994) Mean temperature of electrode drop metal in inert-gas shielded welding. *Avtomatich. Svarka*, **1**, 48–49.
13. Ishchenko, A.Ya., Mashin, V.S., Dovbishchenko, I.V. et al. (1994) Mean temperature of weld pool metal in inert-gas shielded welding. *Avtomatich. Svarka*, **11**, 15–19.
14. Lebedev, V.A. (2007) Some peculiarities of mechanized arc welding of aluminium with controlled pulsed electrode wire feed. *Svarochn. Proizvodstvo*, **11**, 26–30.

NEWS

MACHINE MT-501 FOR SPOT RESISTANCE WELDING

The OJSC «Electric machine-building plant «SELMA company» has mastered the manufacture of machine MT-501, designed for AC resistance spot welding of products of low-carbon and low-alloy steels. Machine consists of a vertically-arranged casing with a power unit and system of pneumatic drive of welding electrode clamping, and also of an external control unit for control of resistance welding controller RKS-801M, designed for control of sequence of operation of the resistance spot welding machine. The system of pneumatic drive is equipped with a controller of electrode clamping force.

The principle of machine operation is based on passing the welding current through parts, clamped at a requited force during a preset time.

Main advantages of machine MT-501 (with a pneumatic drive):

- compactness and small size;
- control unit is made in the form of a small-size remote control panel of the resistance welding controller with a safe supply voltage;
- smooth adjustment of welding current passing duration;
- presence of thermal protection from overheating;
- adjustment of force of clamping and unclamping of electrodes;

- water cooling of electrodes;
- class of insulation H.

The machine can be used in a mass production for welding thin-sheet structures (casings, shells, linings) in machine building, in construction site (reinforcement welding), as well as repair-restoration works.

RESISTANCE SPOT WELDING WITH SPECIAL EDGE PREPARATION*

Yu.A. TSUMAREV
Belarusian-Russian University, Mogilyov, Republic of Belarus

It is shown that beveled edge preparation of the parts to be welded ensures an inclined position of the mating planes, promoting lowering of power in spot weld formation, reduction of harmful influence of bending on the load-carrying capacity of the welded joint in resistance spot welding, and lowering of the degree of non-uniformity of shear and tear force distribution across the cast nugget section.

Keywords: *resistance spot welding, edge preparation, inclined contact plane, force distribution, fracture force*

Resistance spot welding is widely used in modern industry, especially in auto- and aircraft engineering, owing to high labor efficiency, low power consumption, absence of filler materials and shielding atmospheres, as well as good hygienic conditions of work and relatively easy robotization of the process. Peculiarity of this welding method is utilization of only overlap joints at a comparatively big width of the overlap, which makes up from 7 to 12 thicknesses of the billets to be welded [1]. Resistance spot welding is usually used for joining of parts up to 6 mm thick, and sometimes this range widens to 10 mm. Bigger thicknesses involve serious difficulties related to substantial current bridging and decreased service life of electrodes [1]. Besides, the detrimental effect of bending moment on performance of welded joints increases. This is caused by increased eccentricity of longitudinal forces applied to the parts welded. Capacity of the equipment used for resistance spot welding is also increased with increase in thicknesses of the parts welded.

Strengthening with the help of an interlayer of glue introduced in the lap area between the parts welded is used to increase performance characteristics of spot welded joints, including their static and cyclic strength [2]. However, the efficiency of this approach falls with increase in thickness of the parts welded. While at thicknesses of 0.5 + 0.5 mm the presence of a glue interlayer increases static strength 5 times, at thicknesses of 2.5 + 2.5 mm the degree of strengthening is only 70 % [2, 3]. According to the data of study [2], static strength at plate thicknesses of more than 4 mm increases so insignificantly with introduction of the glue that its utilization becomes economically inexpedient. The authors of study [2] relate this fact to low strength of the glued welded joints when they are operated under conditions of non-uniform tear, taking place due to the presence of bending moment in the overlap type joint. The authors of study [3] even consider that the riveted joints are advantageous over the welded and glued-welded ones at thicknesses of the aluminum welded parts exceeding 2 mm.

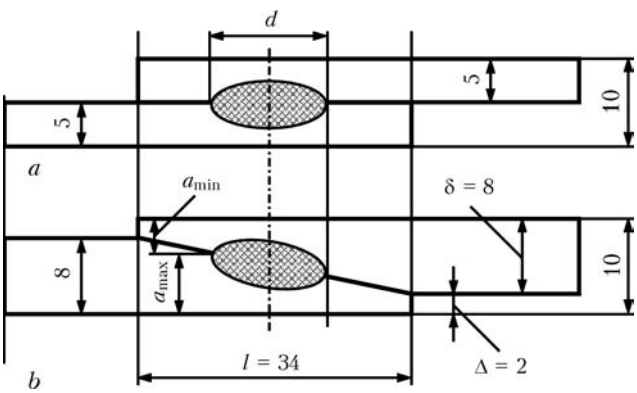

Figure 1. Schematics of welded joints made by resistance spot welding without (*a*) and with edge preparation (*b*)

It is suggested in the present study that special edge preparation in the form of bevels should be used over the entire overlap area to partially eliminate the detrimental effects related to increase in thickness of the parts welded by the resistance spot welding process. As a result, a spot joint acquires the form shown in Figure 1. Sizes of the known joint were taken from the recommendations of study [1] for the 5 + 5 mm thickness.

Geometry of the proposed joint (Figure 1, *b*) was chosen so that clearances between the electrode tips in both variants were similar, i.e. equal to 10 mm. It was assumed in this case that this choice of the geometry and sizes would allow performing resistance spot welding of the joints according to variant 1, *b* at the parameters recommended for welding of plates 5 + 5 mm thick with non-beveled weld edges.

In the proposed variant (see Figure 1, *b*), an inclined position of contact plane of the parts welded leads to violation of axial symmetry in formation of a welded joint during heating. First of all, this shows up in the fact that regions of the cast nugget adjacent to the lap ends form under the conditions of a significant difference in thicknesses of the elements being joined (minimum thickness designated in Figure 1, *b*

*In discussion.

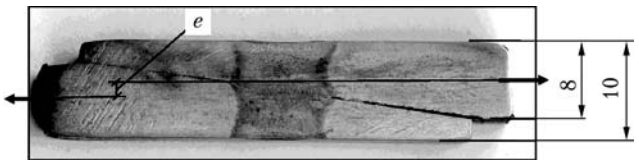

Figure 2. Macrosection (×1) of welded joint on 10kp (rimmer) steel parts with 8 + 8 mm thickness, having bevels on their mating surfaces

as a_{min} is not equal to maximum thickness a_{max}). At the same time, the central part of the cast nugget forms under the conditions characteristic of welding of parts of the same thickness. This leads to increase in the current density on a periphery of the weld spot due to spread of the current in a thicker element [1]. However, here no such phenomenon as a stronger inflow of heat to one of cooling electrodes takes place, as both electrodes are under the similar conditions. The difference in a_{min} and a_{max} thicknesses can be evaluated by using the following formulae:

$$a_{min} = \frac{\delta + \Delta}{2} - \frac{d}{2l}(\delta - \Delta), \quad (1)$$

$$a_{max} = \frac{\delta + \Delta}{2} + \frac{d}{2l}(\delta - \Delta), \quad (2)$$

where d, δ, Δ and l are the sizes of the joint shown in Figure 1, *b*.

Analysis of formulae (1) and (2) shows that $a_{max}/a_{min} = 2.5$, which is less than the three-fold value at which noticeable difficulties arise in formation of a full-valued cast nugget [1]. The experiments showed that resistance spot welding of low-carbon steel billets assembled in accordance with Figure 1, *b* involves, in fact, no difficulties related to the inclination of the contact plane. Examination of macrostructure (Figure 2) showed that the cast nugget extends along the contact plane of the billets, and the welded joint is free from any defects caused by the presence of bevels in the parts welded.

The difference between the a_{min} and a_{max} values will rise with an increase in diameter of the weld spot d or decrease in lap l. If this leads to difficulties in the process of formation of the required size and shape of the cast nugget, the electrodes with a non-round tip extended in a direction normal to size l can be recommended [4, 5]. In this case, the stress concentrator factor caused by closeness of force lines in the base metal over the spot [6] will decrease as well.

Owing to the proposed edge preparation of the parts welded, not only the clearance between the electrode tips is reduced, thus lowering the required power in welding, but also the conditions of formation of the welded joint are improved. This improvement is related to decrease in eccentricity e of the longitudinal forces applied to the parts. In a conventional variant of the welded joint, the value of eccentricity e is equal to thickness of each of the parts welded, while in the proposed variant $e = \Delta = 2$ mm. Thus, the four-fold decrease in eccentricity of the applied forces, as well

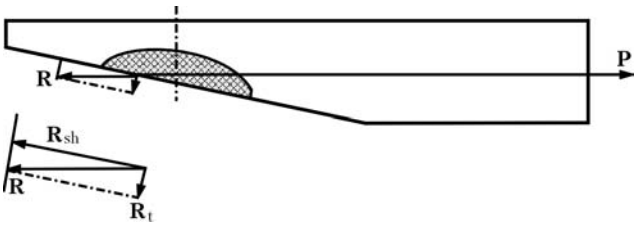

Figure 3. Schematic of equilibrium of one of the parts of the proposed welded joint

as a corresponding reduction of the effect of bending strains on performance of the parts are achieved in the proposed welded joint.

Equilibrium of one of the parts welded in the proposed welded joint is shown in Figure 3. According to the principle of rejection of bonds, instead of the rejected bond its reaction **R** is proposed, which, according to the theorem of two forces, can be reduced to a resultant. It is important that the resultant of the distributed forces making up reaction **R** is applied to a point lying on the line of action of applied force **P**. Therefore, its application point lies near to the center of gravity of weld spot section. Thus, it can be represented as a system of parallel forces distributed almost uniformly along the entire plane section of the spot.

Rejected bond reaction **R** can be expanded into constituents according to vector sum $\mathbf{R} = \mathbf{R}_{sh} + \mathbf{R}_t$, where $\mathbf{R}_{sh}$ and $\mathbf{R}_t$ are the resultants of shear and tear forces, respectively.

Vectors **R** and $\mathbf{R}_t$ were applied to one point. Hence, the degree of uniformity of distribution of the tear forces is as high as the degree of distribution of the forces making up a complete reaction.

Accordingly, the degree of uniformity of distribution for the system of parallel tear forces, forming complete reaction **R**, will also be high. Therefore, the proposed welded joint does not work under the conditions of a non-uniform tear, which deteriorate performance of the glued welds.

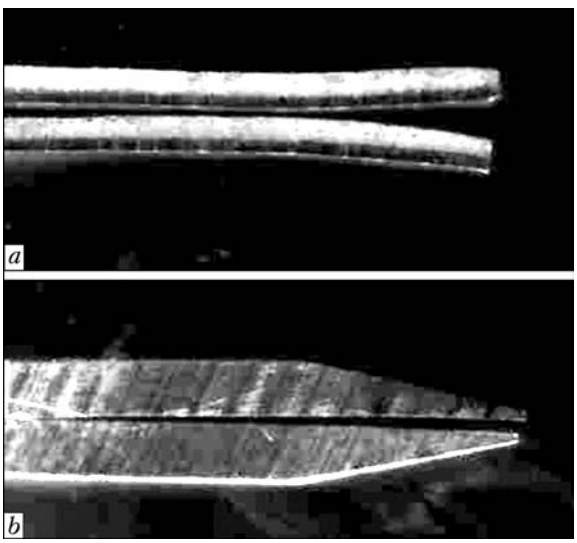

Figure 4. Appearances of specimens after mechanical tensile tests: *a* — traditional specimens; *b* — beveled specimens

In a traditional welded joint, the complete bond reaction cannot be reduced to the resultant, as any weld spot section lies aside from the line of action of the applied force. Therefore, the degree of non-uniformity of distribution of forces (including tear forces) will be much higher.

Experimental verification of the efficiency of the proposed technical solution was carried out through comparative statistical tensile tests of two batches of specimens, each batch comprising five specimens. Sizes and shapes of the specimens in both batches corresponded to the data shown in Figure 1. The first batch comprised specimens with 5 + 5 mm thickness (see Figure 1, *a*), and specimens of the second batch were beveled and had thickness of 8 + 8 mm (see Figure 1, *b*). The tests results showed that the average fracture force for specimens of the first batch was 21,950 kPa, and for specimens of the second batch it was 28,100 kPa. Therefore, strength of the second batch specimens, having the proposed edge preparation, was 28 % higher than that of the specimens made by the traditional scheme. Apparently, one of the reasons was a decreased bending effect due to eccentricity of the applied forces. Fragments of the specimen after the tests are shown in Figure 4. It can be seen from Figure 4, *a* that during testing the specimens of a conventional overlap welded joint acquired a bent shape, whereas the beveled specimens (Figure 4, *b*) remained straight.

It should be noted in conclusion that edge preparation in the form of bevels ensuring an inclined position of the mating planes reduces the equipment power consumption in formation of a weld spot, harmful influence of bending on the load-carrying capacity of the welded joint in resistance spot welding, and degree of non-uniformity of distribution of the shear and tear forces across the cast nugget section.

1. Orlov, B.D., Dmitriev, Yu.V., Chakalev, A.A. et al. (1975) *Technology and equipment for resistance welding*. Moscow: Mashinostroenie.
2. Shavyrin, V.N., Ryazantsev, V.I. (1981) *Glued-welded structures*. Moscow: Mashinostroenie.
3. Ryazantsev, V.I., Fedoseev, V.A., Abin, N.N. (1984) Technical-economical efficiency of application of welded, glued-welded and riveted joints. *Svarochn. Proizvodstvo*, **1**, 28–29.
4. Latypova, E.Yu., Tsumarev, Yu.A., Kuzmenko, I.M. et al. *Electrode for resistance spot welding*. Pat. 6379. BY. Publ. 30.09.2004.
5. Popkovsky, V.A., Latypova, E.Yu., Tsumarev, Yu.A. et al. *Electrode for resistance spot welding*. Pat. 6500. BY. Publ. 30.09.2004.
6. (1979) *Welding in machine-building*: Refer. Book. Ed. by V.A. Vinokurov. Vol. 3. Moscow: Mashinostroenie.

INFORMATION FOR CONTRIBUTORS TO
THE PATON WELDING JOURNAL

«The Paton Welding Journal» is an English translation of the monthly «Avtomaticheskaya Svarka» journal published in Russian since 1948.

THE PATON WELDING JOURNAL is a scientific journal publishing fundamental and applied papers and short notes in the area of:

- *weldability of structural materials*
- *welding different types of steels and cast irons*
- *welding non-ferrous metals, including aluminium, titanium, etc.*
- *joining dissimilar and composite materials*
- *welding refractory metals and alloys*
- *welding cryogenic materials*
- *arc welding*
- *flash-butt welding*
- *electron beam and laser welding*
- *explosion welding and cutting*
- *friction welding*
- *electroslag welding*
- *soldering and brazing*
- *advanced structural materials*
- *surfacing and coating deposition*
- *cutting*
- *computer technologies in welding*
- *strength of welded joints and structures*
- *residual stresses and strains*
- *calculation and design of welded joints and structures*
- *automation of welding fabrication*
- *estimation of residual life of welded structures*
- *welding for fabrication of unique structures*
- *welding and repair in thermal and nuclear power engineering*
- *advances in underwater welding, cutting and repair*

The journal accepts also advertisements and announcements of conferences and publications on related topics.

THE PATON WELDING JOURNAL is published monthly.

Subscription requests should be sent to the Editorial Office.

Manuscripts should be submitted in duplicate in English, and supplemented with a text file and figures on a diskette. An electronic copy may be submitted by e-mail.

The rules for submission of electronic copies are as follows:

- an electronic copy should be submitted on a diskette or by e-mail simultaneously with sending a hard copy of the manuscript;
- acceptable text formats: MSWord (rtf, doc);
- acceptable graphic formats for figures: EPS, TIFF, CDR. Figures created using software for mathematical and statistical calculations should be converted to one of these formats.

Manuscripts should be supplemented with:

- official letter signed by a chief manager of the institution where the work was performed. This rule does not apply to papers submitted by international groups of authors.

Title page:

- title of the paper and name(s) of the author(s);
- name of affiliated institution, full address, telephone and fax numbers, e-mail addresses (if available) for each author.

Abstract: up to 100 words, must be presented in English. Before the abstract text one should indicate in the same language: the paper title, surnames and initials of all authors.

Key words: their amount must not exceed eight word units. In the specific cases it is acceptible to use two- or three-word terms. These words must be placed under the abstract and written in the same language.

Text should be printed double-spaced on white paper (A4 format) with a 12-point font. Titles of the paper and sections should be typed with bold capitals.

Tables should be submitted on separate pages in the format of appropriate text processors, or in the text format (with columns separated by periods, commas, semicolons, or tabulation characters). Use of pseudo-graphic characters is not allowed.

List of references should be double-spaced, with references numbered in order of their appearance in the text.

Captions for figures and tables should be printed in the manuscript double-spaced after the list of references.

Pictures will be scanned for digital reproduction. Only high-quality pictures can be accepted. Inscriptions and symbols should be printed inside. Negatives, slides and transparencies are accepted.

Figures: each figure should be printed on a separate page of the manuscript and have a size not exceeding 160 × × 200 mm. For text in figures, use 10-point fonts. All figures are to be numbered in order of their appearance in the text, with sections denoted as (a), (b), etc. Placing figure numbers and captions inside figures is not allowed. On the back side, write with a pencil the paper title, author(s) name(s) and figure number, and mark the top side with an arrow.

Photographs should be submited as original prints.

Color printing is possible if its cost is covered by the authors.

For information about the rules and costs, contact the Executive Director.

No author's fee is provided for.

Publication in TPWJ is free of charge.

Manuscripts should be sent to:

Dr. Alexander T. Zelnichenko
Executive Director of
«The Paton Welding Journal»,
11, Bozhenko Str.,
03680, Kiev, Ukraine
International Association «Welding»
Tel.: (38044) 287 67 57, 529 26 23
Fax: (38044) 528 04 86
E-mail: journal@paton.kiev.ua
www.nas.gov.ua/pwj

SUBSCRIPTION
FOR «THE PATON WELDING JOURNAL»

If You are interested in making subscription directly via Editorial Board, fill, please, the coupon and send application by fax or e-mail.

The cost of annual subscription via Editorial Board is $324.

Telephones and faxes of Editorial Board of «The Paton Welding Journal»:

Tel.: (38044) 287 6302, 271 2403, 529 2623

Fax: (38044) 528 3484, 528 0486, 529 2623.

«The Paton Welding Journal» can be also subscribed worldwide from catalogues of subscription agency EBSCO.

SUBSCRIPTION COUPON
Address for journal delivery

Term of subscription since _____ **200** **till** _____ **200**
Name, initials _____
Affiliation _____
Position _____
Tel., Fax, E-mail _____

ADVERTISEMENT IN «THE PATON WELDING JOURNAL»
(DISTRIBUTED ALL OVER THE WORLD)

«AVTOMATICHESKAYA SVARKA»
RUSSIAN VERSION OF «THE PATON WELDING JOURNAL»
(DISTRIBUTED IN UKRAINE, RUSSIA AND OTHER CIS COUNTRIES)

External cover, fully-colored:
First page of cover (190×190 mm) – $700
Second page of cover (200×290 mm) – $550
Third page of cover (200×290 mm) – $500
Fourth page of cover (200×290 mm) – $600

Internal cover, fully-colored:
First page of cover (200×290 mm) – $400
Second page of cover (200×290 mm) – $400
Third page of cover (200×290 mm) – $400
Fourth page of cover (200×290 mm) – $400

Internal insert:
Fully-colored (200×290 mm) – $340
Fully-colored (double page A3) (400×290 mm) – $570
Fully-colored (200×145 mm) – $170

- Article in the form of advertising is 50 % of the cost of advertising area
- When the sum of advertising contracts exceeds $1000, a flexible system of discounts is envisaged

Technical requirement for the advertising materials:
- Size of journal after cutting is 200×290 mm
- In advertising layouts, the texts, logotypes and other elements should be located 5 mm from the module edge to prevent the loss of a part of information

All files in format IBM PC:
- Corell Draw, version up to 10.0
- Adobe Photoshop, version up to 7.0
- Quark, version up to 5.0
- Representations in format TIFF, color model CMYK, resolution 300 dpi
- Files should be added with a printed copy (makeups in WORD for are not accepted)